Ulm University Medical Center

Institute of Pharmacology of Natural Products and Clinical Pharmacology

Acting head of the institute: Prof. Dr. Oliver Zolk

Artemisia annua Herbal Preparations – Antitumor Activity, Analytical Characterization, and Identification of Potential Anticancer Ingredients

Dissertation submitted to obtain the doctoral degree of Human Biology of the Medical Faculty of Ulm University

Sophia Johanna Lang

born in Geislingen an der Steige

2019

Amtierender Dekan: Prof. Dr. Thomas Wirth

Erstgutachter: Prof. Dr. Thomas Simmet

Zweitgutachter: Prof. Dr. Lisa Wiesmüller

Tag der Promotion: 02.07.2020

Parts of this thesis have been published:

Journal articles:

1. **Lang, S.J.**, Schmiech, M., Hafner, S., Paetz, C., Steinborn, C., Huber, R., Gaafary, M.E., Werner, K., Schmidt, C.Q., Syrovets, T., Simmet, T., 2019. Antitumor activity of an *Artemisia annua* herbal preparation and identification of active ingredients. Phytomedicine 62: 152962. doi: 10.1016/j.phymed.2019.152962
2. Schmiech, M., **Lang, S.J.**, Syrovets, T., Simmet, T., 2019. Data on cytotoxic activity of an *Artemisia annua* herbal preparation and validation of the quantification method for active ingredient analysis. Data in Brief 27: 104635. doi: 10.1016/j.dib.2019.104635
3. **Lang, S.J.**, Schmiech, M., Hafner, S., Paetz, C., Werner K., El Gaafary, M., Schmidt, C.Q., Syrovets, T., Simmet, T., 2019. Chrysosplenol D, a flavonol from *Artemisia annua* induces ERK1/2-mediated apoptosis in triple negative human breast cancer cells. International Journal of Molecular Sciences 21: 4090. doi: 10.3390/ijms21114090
4. Schmiech, M., **Lang, S.J.**, Ulrich, J., Werner, K., Rashan, L.J., Syrovets, T., Simmet, T., 2019. Comparative investigation of frankincense nutraceuticals: Correlation of boswellic and lupeolic acid contents with cytokine release inhibition and toxicity against triple-negative breast cancer cells. Nutrients 11: 2341. doi: 10.3390/nu11102341
5. Schmiech, M., **Lang, S.J.**, Werner, K., Rashan, L.J., Syrovets, T., Simmet, T., 2019. Comparative analysis of pentacyclic triterpenic acid compositions in oleogum resins of different *Boswellia* species and their *in vitro* cytotoxicity against treatment-resistant human breast cancer cells. Molecules 24: E2153. doi: 10.3390/molecules24112153
6. El Gaafary, M., Ezzat, S.M., El Sayed, A.M., Sabry, O.M., Hafner, S., **Lang, S.**, Schmiech, M., Syrovets, T., Simmet, T., 2017. Acovenoside A induces mitotic catastrophe followed by apoptosis in non-small-cell lung cancer cells. J Nat Prod 80: 3203-3210. doi: 10.1021/acs.jnatprod.7b00546
7. El Gaafary, M., Hafner, S., **Lang, S.J.**, Jin, L., Sabry, O.M., Vogel, C.V., Vanderwal, C.D., Syrovets, T., Simmet, T., 2019. A novel polyhalogenated monoterpene induces cell cycle arrest and apoptosis in breast cancer cells. Mar Drugs 17: E437. doi: 10.3390/md17080437

Conference articles and contributions:

Experimental Biology, Orlando, FL, 2019

- **Lang, S.**, Schmiech, M., Hafner, S., Paetz, C., Schmidt, C.Q., Syrovets, T., Simmet, T., 2019. Constituents of *Artemisia annua* dietary supplements induce ROS elevation, ERK activation, and apoptosis in treatment-resistant triple negative human breast cancer cells. FASEB J 33, 816.816-816.816. doi: 10.1096/fasebj.2019.33.1_supplement.816.6

Annual Meeting of the German Pharmaceutical Society – DPhG, Hamburg, Germany, 2018

- **Lang, S.**, Schmiech, M., Hafner, S., Paetz, C., Schmidt, C.Q., Syrovets, T., Simmet, T., 2018. Ingredients of *Artemisia annua* dietary supplements are cytotoxic for highly metastatic triple negative human breast cancer cells. Abstract Book. Pharmaceutical Science: Structure, Function and Application. Annual Meeting of the German Pharmaceutical Society 2018 - DPhG

List of Content

Abbreviations

3D	3-Dimensional space
ADP	Adenosine diphosphate
ACN	Acetonitrile
AIF	Apoptosis-inducing factor
AKT/PKB	Protein kinase B
ALT	Alanine aminotransferase
APAF1	Apoptotic protease-activating factor 1
AST	Aspartate aminotransferase
ATCC	American Type Culture Collection
Atg proteins	Autophagy-related proteins
ATM	Ataxia telangiectasia mutated
ATR	Ataxia telangiectasia and Rad3-related
BAK	Bcl-2 antagonist/killer 1
BAX	Bcl-2 associated X protein
BCA	Bicinchonic acid
Bcl-2	B-cell lymphoma 2
BID	BH3 interacting-domain death agonist
BRCA	Breast cancer related antigen
BSA	Bovine serum albumin
C18-HD	Octadecyl modified silica phase with a high-density coverage
CAM	Chick chorioallantoic membrane
Cdc2	Cell division control protein 2
CDK	Cyclin-dependent kinase
c-FLIP	FLICE-like inhibitory protein
DAD	Diode-array detector
DCF	2', 7'–Dichlorofluorescein
Diablo	Diablo homolog (Smac)
DISC	Death-inducing signaling complex
DMEM	Dulbecco´s Modified Eagle Medium
DMSO	Dimethyl sulfoxide
DNA	Deoxyribonucleic acid
DNAse	Deoxyribonuclease
DTT	Dithiothreitol
DUSP	Dual-specificity phosphatase
dUTP	Deoxyuridine Triphosphate
EDTA	Ethylenediaminetetraacetic acid
EGFR	Epidermal growth factor receptor
ER	Estrogen receptor
ERK	Extracellular signal-regulated kinase

ESI	Electrospray ionization source
F12 K	Kaighn's Modification of Ham's F-12 Medium
FACS	Fluorescence-Activated Cell Sorting
FADD	Fas-associated death domain
FCS	Fetal calf serum
FITC	Fluorescein isothiocyanate
g	Gravitational acceleration, 9.80665 m/s²
GR_{50}	Half maximal growth rate inhibition
GTP	Guanosine triphosphate
h	Hour
H_2DCFDA	2',7'-dichlorodihydrofluorescein diacetate
HBSS	Hank's Balanced Salt Solution
HE	Hematoxylin and eosin staining
HEPES	4-(2-Hydroxyethyl)-1-piperazineethanesulfonic acid
HER2	Human epidermal growth factor receptor 2
HPLC	High-performance liquid chromatography
HPLC-MS	High-performance liquid chromatography-mass spectrometry
HPLC-MS/MS	High-performance liquid chromatography – tandem mass spectrometry
HP-β-CD	(2-Hydroxypropyl)-β-cyclodextrin
HRP	Horseradish peroxidase
i.p.	Intraperitoneal
IC_{50}	Half maximal inhibitory concentration
Ki-67	Cell proliferation marker
LC3	Microtubule-associated protein light chain 3
LOD	Limit of detection
LOQ	Limit of quantification
MAPK	Mitogen-activated protein kinase
MEGM	Mammary Epithelial Cell Growth Medium
MEK	Mitogen-activated protein kinase kinase (MAPKK)
MEM	Eagle′s minimum essential medium
MES	(2-(*N*-Morpholino)ethansulfonic acid-1-hydrat)
min	Minutes
MPT	Mitochondrial permeability transition
MRM	Multiple-reaction monitoring
MS	Mass spectrometry
mTOR	Mechanistic target of rapamycin
NMR	Nuclear magnetic resonance
NSCLC	Non-small cell lung cancer
PAGE	Polyacrylamide gel electrophoresis

PARP	Poly ADP ribose polymerase
PBMC	Peripheral blood mononuclear cells
PBS	Phosphate-buffered saline
pCR	Pathological complete response
PD-1	Programmed cell death protein 1
PD-L1	Programmed death ligand 1
PgR	Progesterone receptor
PI	Propidium iodide
PI3K	Phosphoinositide 3-kinase
PIP_2	Phosphatidylinositol (4,5)-bisphosphate
PIP_3	Phosphatidylinositol (3,4,5)-trisphosphate
PLK1	Polo-like kinase 1
PNPP	P-Nitrophenyl-phosphate disodium hexahydrate
PS	Phosphatidylserine
PTEN	Phosphatase and tensin homolog
PVDF	Polyvinylidenedifluoride
RB	Retinoblastoma protein
RIPA	Radioimmunoprecipitation assay buffer
RNAse	Ribonuclease
ROS	Reactive oxygen species
RP	Reversed phase
RPMI	Roswell Park Memorial Institute medium
RSD	Relative standard deviation
RT	Room temperature (20-25 °C)
RTK	Receptor tyrosine kinase
SD	Standard deviation
SDS	Sodium dodecyl sulfate
SEM	Standard error of the mean
SIM	Selected ion monitoring
SLB	Sample loading buffer
Smac	Second mitochondria-derived activator of caspases
tBID	Truncated BID
TBS	Tris-buffered saline
TBST	Tris-buffered saline containing Tween 20
TNBC	Triple negative human breast cancer
TNF	Tumor necrosis factor
TRADD	TNF receptor-associated death domain
TRAIL	TNF-related apoptosis-inducing ligand
Tris	2-Amino-2-(hydroxymethyl)propane-1,3-diol (Trometamol)
TUNEL	Terminal deoxynucleotidyl transferase dUTP nick end labeling

Tween 20	Polyoxyethylen(20)-sorbitan-monolaurat
UHPLC-MS/MS	Ultra high performance liquid chromatography - tandem mass spectrometry
US	United States
vs	versus
XTT	2,3-bis-(2-methoxy-4-nitro-5-sulfophenyl)-2H-tetrazolium-5-carboxanilide
β-ME	β-Mercaptoethanol
$\Delta\Psi_m$	Mitochondrial membrane potential

1 Introduction

1.1 *Artemisia annua* L.

The medicinal plant *Artemisia annua* L., belonging to the *Asteraceae* family (Figure 1) has been used since ancient times in form of decoctions and pressed juice for the treatment of malaria throughout Asia and Africa (Efferth, 2017b; van der Kooy and Sullivan, 2013). During the Vietnam War, the government of North Vietnam consulted China because high numbers of Vietnamese soldiers were infected with malaria. Tu Youyou, one of the 500 Chinese scientists who screened medicinal plants, identified *Artemisia annua* as herb with potential antimalarial activity. The sesquiterpene lactone artemisinin contained therein exhibits an endoperoxide moiety and generates reactive oxygen species (ROS) when reacting with ferrous ion (Efferth, 2017b). Ferrous iron is released, when the malaria parasites detoxify hemoglobin to hemozoin resulting in the generation of ROS, which are reported to be one of the mechanisms of action of artemisinin (Efferth, 2017b). In the past few years, artemisinin and in particular its semisynthetic derivatives (artemether, arteether, and artesunate) gained worldwide attention and combination therapy regimens based on artemisinin have been approved as standard therapeutics for malaria infections. For her excelling achievements, Tu Youyou was honored with the Nobel Prize for Medicine and Physiology in 2015.

Figure 1: **Leaves and florescence of *Artemisia annua*.**

However, *Artemisia annua* gained not only attention because of its antimalarial activity. In recent years, the medicinal plant and in particular artemisinin and its semisynthetic derivatives

with higher bioavailability were also analyzed for their potential anticancer efficacy (Efferth, 2017b). However, available evidence suggests, that beside artemisinin, *Artemisia annua* might contain further active ingredients with potential better anticancer activity (Efferth et al., 2011; Ferreira et al., 2010; van der Kooy and Sullivan, 2013). In the meantime, more than 600 secondary metabolites have been identified in *Artemisia annua* (Brown, 2010). The medicinal plant contains more than 50 different phenolic compounds (flavones, flavonols, coumarins, and phenolic acids) and *Artemisia annua* belongs to the four medicinal plants with the highest oxygen radical absorbance capacity (Brisibe et al., 2009; Ferreira et al., 2010). The presence of structurally diverse polymethoxylated flavonoids is a highly specific feature of *Artemisia annua* (Ferreira et al., 2010). Polymethoxylated flavonoids can enhance the bioavailability of artemisinin (Ferreira et al., 2010). Moreover they are reported to be more stable and exhibit better pharmacokinetics compared to their hydroxylated counterparts (Ferreira et al., 2010). Of note, the dietary flavonoid intake correlates inversely with later cancer occurrence (Ferreira et al., 2010). In line with that, available evidence demonstrates, that flavonoids might be cancer preventive and can help to delay or mend cancer (Ferreira et al., 2010; Rodriguez-Garcia et al., 2019).

Although some case reports about the successful application of *Artemisia annua* dietary supplements to patients and pets suffering from cancer are available (Breuer and Efferth, 2014; Efferth, 2017b), the anticancer activity of different extracts in general and of active ingredients beside the well-known artemisinin has only been insufficiently studied.

Natural products exhibit unique chemical structures selected by evolutionary pressure and are even today considered as an indispensable source for the identification of novel potential cancer therapeutics (Atanasov et al., 2015; Koehn and Carter, 2005). The unique structural and chemical diversity of natural products cannot be fully mimicked by synthetic small molecule libraries (Shen, 2015). For this reason, an *Artemisia annua* dietary supplement, lacking verifiable artemisinin (LOD = 0.2 ng/mg) but containing high amounts of methoxylated flavonols with high cytotoxicity, was analyzed for its anticancer efficacy and potentially responsible active ingredients. Whilst some studies demonstrated tubulin-binding and antiproliferative properties of casticin (Haidara et al., 2006; Liu et al., 2014), almost no data have been published about the structure-related chrysosplenol D.

1.2 Triple Negative Human Breast Cancer

Fighting cancer is still an unmet clinical challenge. Cancer is the second leading cause of death in the United States (Siegel et al., 2019). It is estimated, that breast cancer alone will account for 30 % of all new diagnosed cancers among females in 2019 (Siegel et al., 2019). After lung cancer, breast cancer is the second leading cause of cancer-related mortality in females worldwide (Diana et al., 2018; Siegel et al., 2019). In the United States, one out of eight women will develop breast cancer during a whole life time (Siegel et al., 2019).

Around 15 % of all breast cancers are triple negative breast cancer (TNBC) (Tao et al., 2015b). The highly aggressive TNBC molecular subtype is characterized by the lack of three receptors: estrogen receptor (ER), progesterone receptor (PgR), and human epidermal growth factor receptor 2 (HER2) (Denkert et al., 2017). All of these three receptors are molecular targets for therapeutic agents (Diana et al., 2018). The TNBC subtype is usually diagnosed in females younger than 50 years, with an incidence between 10 and 20 % and a higher one in African-American women (Diana et al., 2018; Siegel et al., 2019). Frequently, TNBC is associated with germline mutations of the BRCA genes. Compared with other subtypes of breast cancer, the TNBC subtype has the worst prognosis among all breast cancers (Diana et al., 2018; Jitariu et al., 2017). TNBC exhibits an aggressive clinical behavior, with a high tendency to develop visceral metastases, a high risk of relapse, and a lack of recognized molecular targets for therapy (Bianchini et al., 2016).

Chemotherapy remains the mainstay of TNBC treatment. Data from different studies over the past two decades demonstrate significant benefit of chemotherapy in TNBC patients when applied in adjuvant or neoadjuvant treatment regimens, and for treatment of the metastatic state (Bianchini et al., 2016; Cortazar et al., 2014; S3-Leitlinie-Mammakarzinom, 2018). Effective chemotherapeutic regimens are based on taxanes and anthracyclines, but even with optimal systemic therapy, fewer than 30 % of women with metastatic TNBC survive five years after diagnosis (Bianchini et al., 2016). Platinum salts increase the pathological complete response (pCR) in TNBC regardless of BRCA status (S3-Leitlinie-Mammakarzinom, 2018). However, the advantage of current chemotherapeutic regimens for progression-free survival and overall survival is not clear and substantially increased toxicity needs to be considered (S3-Leitlinie-Mammakarzinom, 2018).

On the basis of variations in gene expression, TNBC can be classified in different subtypes demonstrating the complexity and heterogeneity of the disease. Accordingly, new therapeutic approaches and trials targeting specific genetic alterations depending on the subtype are being explored. For this reason and because of frequently developed multidrug resistance, even after an initial good response, identification of targeted therapies got into the focus of intense research and clinical studies in the last few years (Diana et al., 2018). For example, such therapies for TNBC include androgen receptor therapy for the luminal androgen receptor subtype, poly ADP ribose polymerase (PARP) inhibitors for BRCA-deficient breast cancer, phosphoinositide 3-kinase (PI3K) and mechanistic target of rapamycin (mTOR) inhibitors for tumors with high PI3K pathway activation, MEK (mitogen-activated protein kinase kinase) inhibitors, immunotherapy targeting PD-1 and PD-L1, and antibody-drug conjugates for the selective delivery of chemotherapeutic agents (Denkert et al., 2017; Diana et al., 2018). The knowledge about TNBC has increased in the last 15 years but chemotherapy remains still the only validated therapy option for TNBC treatment in clinical practice (Denkert et al., 2017). Hence, new therapeutic agents for treatment and prevention of TNBC are urgently required.

1.3 Regulation of the Cell Cycle and Its Implication in Cancer

In healthy tissues, cell cycle progression and cell division are tightly controlled processes ensuring homeostasis of cell number and healthy tissue function (Hanahan and Weinberg, 2011). Dysregulation of the cell cycle and its checkpoint control mechanisms by mutations in genes encoding for the cell cycle proteins is a common feature of most neoplasias, resulting in uncontrolled proliferation and genomic and chromosomal instability (Malumbres and Barbacid, 2009). The critical dependency of cancer cells on altered cell cycle regulation to escape apoptosis and senescence makes cancer cells particularly sensitive to cell cycle inhibitors (Otto and Sicinski, 2017). Therefore, inhibition of the cell cycle progression became an important target for treatment strategies (Otto and Sicinski, 2017; Schwartz and Shah, 2005).

Briefly, during cell cycle progression, a cell proceeds through four phases: the first gap phase (G_1), DNA-synthesis phase (S), followed by the second gap phase (G_2), and finally mitosis (M-phase) (Lapenna and Giordano, 2009; Schwartz and Shah, 2005). This process is regulated by cyclins and CDK-inhibitors. Cyclins are transiently expressed according to growth signals regulating the activation of their associated cyclin-dependent kinases (CDK) (Lapenna and Giordano, 2009). Accurate cell cycle progression is controlled by checkpoints (Figure 2A), which initiate a halt of cell cycle progression, when defects in DNA-synthesis, DNA-damages, or failed segregation of chromosomes are recognized (Otto and Sicinski, 2017). Subsequently, a signaling pathway becomes activated, which inhibits the CDKs and induces cell cycle arrest till the DNA damage is repaired (Otto and Sicinski, 2017). According to the type of DNA-damage, the ataxia telangiectasia and Rad3-realted (ATR) or the ataxia telangiectasia mutated (ATM) kinases phosphorylate and activate the checkpoint kinase 1 (CHK1) (Otto and Sicinski, 2017). ATM kinases can also activate checkpoint kinase 2 (CHK2), which activates p53. The transcription factor p53 induces p21 expression inhibiting the cyclin E-CDK2 complex and inducing G_1-arrest (Otto and Sicinski, 2017). CHK1 is an indispensable inductor of S-phase and G_2-phase arrest caused by DNA-damage, especially in p53-deficient cancer cells (Otto and Sicinski, 2017). Activated CHK1, induces S-phase and G_2-phase arrest by inhibitory phosphorylation of CDC25. Thus, the CDC25 phosphatase is unable to dephosphorylate CDK1 and CDK2, keeping these kinases inactive and inducing cell cycle arrest in the G_2-phase. CHK1 also phosphorylates and activates the kinase WEE1, which subsequently phosphorylates and inhibits CDK2 and CDK1 (Otto and Sicinski, 2017). If DNA-repair is unsuccessful, the cell undergoes senescence or apoptosis (Malumbres and Barbacid, 2009).

When cells from the quiescent (G_0) phase enter in G_1-phase, CDK4 and CDK6 become activated by D-type cyclins resulting in phosphorylation of the retinoblastoma protein (RB1) and other 'pocket' protein family members (Lapenna and Giordano, 2009). By phosphorylation, their function as suppressors of transcription becomes inactivated. In the late G_1-phase, the activating cyclin E-CDK2 complexes amplify phosphorylation of additional sites on RB1, resulting in dissociation and complete activation of E2F transcription factors (Figure 2B). Then, the S-phase gene expression program is irreversibly activated (Giacinti and Giordano, 2006; Lapenna and

Giordano, 2009; Schwartz and Shah, 2005). Progression through S-phase is governed by the cyclin A-CDK2 complex, followed by formation of the complex cyclin A-CDK1 (cdc2) important for proceeding G_2-phase. At least, the CDC25 phosphatase dephosphorylates and activates the cyclin B-CDK1 complex necessary to initiate mitosis (Figure 2) (Aarts et al., 2013; Schwartz and Shah, 2005). CDK1 activation and entry into mitosis activates the anaphase-promoting complex, inducing sister chromatid separation and inactivating CDK1 completely thereby enabling mitotic exit and reentry of the cell into G_1-phase (Rhind and Russell, 2012). Moreover, proceeding through mitosis is controlled by Aurora kinases (AURKA, B, C) regulating important mitotic events such as centrosome function, spindle formation, activation of Polo-like kinase 1(PLK1), and cytokinesis (Dominguez-Brauer et al., 2015). Aneuploidy and cytokinesis failure can be a result of abnormal AURK activity (Dominguez-Brauer et al., 2015). Proper PLK1 function is also required for mitotic entry, maturation of the centrosome, spindle formation, anaphase-promoting complex/cyclosome (APC/C) regulation, and finally cytokinesis (Figure 2) (Aarts et al., 2013; Dominguez-Brauer et al., 2015).

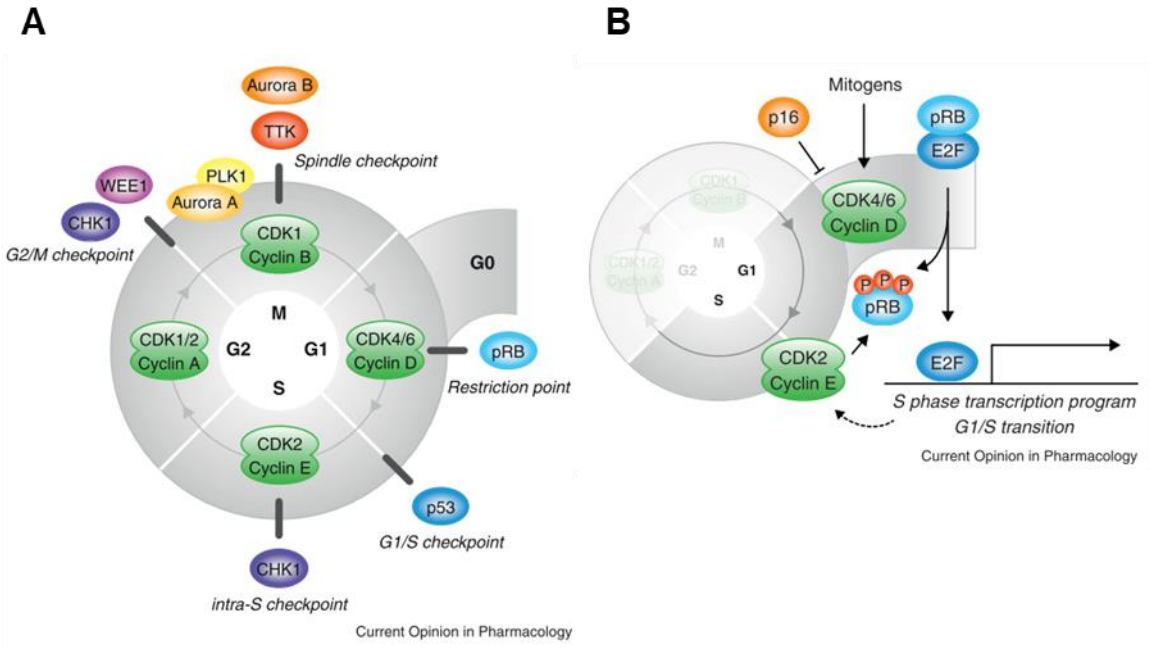

Figure 2: **Schematic overview of the regulation of the cell cycle progression.** (A) The cell cycle progression is regulated by transient cyclin-CDK activity. Several cell cycle checkpoints can interrupt the cell cycle progression and induce an arrest in different phases. (B) Mitogenic signals induce activation of cyclin D-CDK4 activity phosphorylating pRB. Cyclin E-CDK2 also phosphorylates pRB inducing the entire release of E2F and enabling transcription of S-phase proteins. Reprinted from (Aarts et al., 2013), page 530, with permission from Elsevier, © 2013 Elsevier.

1.4 Types of Cell Death

The controlled destruction of a cell is an important physiological process, essential for maintaining the physiologic balance between cell death and cell growth. Defects in cell-death pathways often contribute to cancer development as well as to resistance to cancer therapy (Koff et al., 2015). Resistance to apoptosis is frequently related to tumorigenesis, but tumor cell death can also be induced by non-apoptotic mechanisms like mitotic catastrophe, senescence, autophagy, and necrosis. Being the cause of the problem, reactivation or activation of the cell death machinery has become an important treatment strategy for malignant diseases (Okada and Mak, 2004; Wong, 2011).

1.4.1 Apoptosis

The most common form of cell death is the physiological 'suicide' program of a cell, termed apoptosis (type I cell death) (Okada and Mak, 2004). Apoptosis can occur in physiological but also pathological conditions (Wong, 2011). Many diseases are characterized by a dysbalance, when either too much (e.g. Parkinson's, Alzheimer's, spinal muscular atrophy) or too little apoptosis (e.g. cancer or autoimmune diseases) occurs (Lawen, 2003). Cell death by apoptosis is a highly regulated, active process ensuring neighboring structures to remain unaffected. A family of cysteine proteases named caspases orchestrate these events (Taylor et al., 2008). After the controlled destruction of the cell, cellular debris can be removed by phagocytes.

Typical morphological signs of apoptosis are condensation of chromatin and fragmentation of the nucleus (Ouyang et al., 2012; Taylor et al., 2008). Reduction of the cellular volume (pyknosis), shrinkage and loosing contact to neighboring cells, rounding up and retraction of pseudopods are further morphological changes (Lawen, 2003; Wong, 2011). Membrane integrity remains intact throughout the whole process. At later stages, membrane blebbing, alterations of cytoplasmic organelles, and damaged membrane integrity can be observed. Usually cells undergoing apoptosis are engulfed by phagocytes before formation of apoptotic bodies occurs (Wong, 2011).

Biochemical hallmarks of apoptosis are activation of caspases, DNA- and protein fragmentation, and plasma membrane alterations. An early event is the phosphatidylserine exposure to the outer leaflet of the cell membrane for recognition by macrophages, followed by characteristic DNA-fragmentation down to 180 to 200 base pairs. Active caspases cleave vital cellular proteins after aspartic acid residues resulting in breakup of the cytoskeleton and the nuclear scaffold. Furthermore, activated caspases recruit DNAses, which induce the degradation of DNA (Hengartner, 2000; Wong, 2011).

Mechanistically, one can distinguish three caspase-activating pathways:

a) Extrinsic apoptotic pathway

Extracellular signals, e.g. Fas ligand (Fas-L), TNF-related apoptosis-inducing ligand (TRAIL), and tumor necrosis factor (TNF) target the death receptors of the TNF family and recruit adaptor proteins (Figure 3). Such adaptor proteins are the Fas-associated death domain (FADD) protein and the TNF receptor-associated death domain (TRADD), which subsequently recruit and aggregate procaspase 8 and 10 molecules resulting in formation of the death-inducing signaling complex (DISC) (Pfeffer and Singh, 2018; Taylor et al., 2008). DISC formation activates the initiator procaspases 8 and 10, which further activate the executioner caspases 3, 6, and 7 initiating further caspase activation and which culminate in proteolysis and cell death. c-FLIP can inhibit DISC thereby regulating its activity. The extrinsic pathway and the intrinsic pathway concur when caspase 8 becomes activated. Caspase 8 cleaves the BH3 interacting-domain death agonist (BID). The resulting truncated BID (tBID) in turn activates and oligomerizes BAX and BAK promoting mitochondrial cytochrome c release and assembly of the apoptosome and the intrinsic pathway proceeds (Figure 3) (Pfeffer and Singh, 2018; Taylor et al., 2008).

b) Intrinsic apoptotic pathway

The intracellular, mitochondrial pathway becomes activated in response to extracellular stresses and internal insults such as DNA damage, oncogene induction, growth-factor withdrawal, and hypoxia (Hengartner, 2000; Okada and Mak, 2004). Signals in response to these stresses affect mainly mitochondria (Okada and Mak, 2004). Typically, one or more members of the BH3-only protein family become activated. Activation of BH3-only proteins above a critical threshold induces the assembly of BAK-BAX oligomers in the outer mitochondrial membrane by overcoming the inhibitory effect of anti-apoptotic B-cell lymphoma-2 (BCL-2) family proteins (Taylor et al., 2008). BAK-BAX oligomers enable mitochondrial membrane permeabilization and release of cytochrome c and further pro-apoptotic molecules (e.g. Smac/Diablo, AIF) into the cytosol resulting in the formation of the apoptosome. When cytochrome c is released, the caspases downstream are irreversibly activated (Lawen, 2003; Okada and Mak, 2004). The apoptosome is a large protein complex containing cytochrome c, apoptotic protease-activating factor 1 (APAF1), and caspase 9 homodimers and propagates a proteolytic cascade activating further caspases (Figure 3) (Okada and Mak, 2004; Taylor et al., 2008).

c) Granzyme B pathway

A further caspase activating pathway, worth of mentioning is the granzyme B pathway. Cytotoxic T lymphocytes and natural killer cells release the protease granzyme B. The released granules contain perforin, a pore-forming protein oligomerizing in the membrane of the target cell thereby enabling entry of granzyme B. Granzyme B in turn cleaves its substrates after an aspartic acid residue and can activate BID as well as caspase 3 and caspase 7 (Taylor et al., 2008).

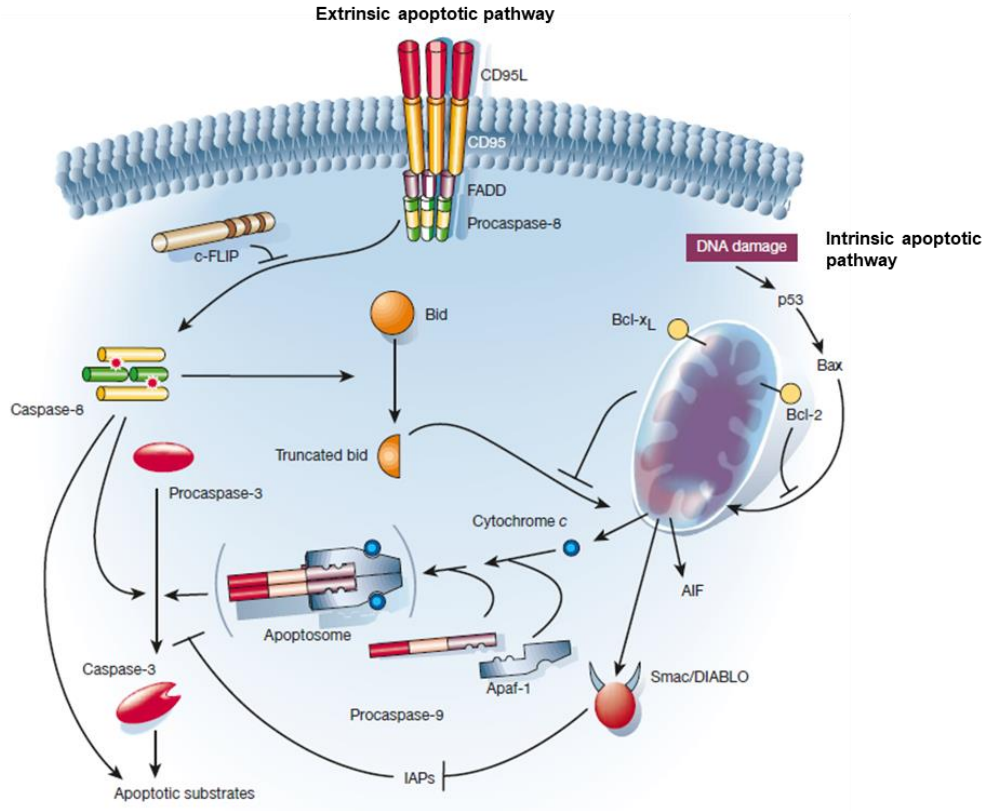

Figure 3: **Schematic overview of the extrinsic (receptor-mediated) and intrinsic (mitochondrial) pathway of apoptosis.** Adapted by permission from Springer Nature Customer Service Centre GmbH: Springer Nature (Hengartner, 2000), page 773, © 2000, Springer Nature.

1.4.2 Mitotic Catastrophe

Mitotic catastrophe is a type of cell death, which is caused by mitotic failure resulting in the formation of giant micro- and multinucleated cells (Vitale et al., 2011). Mitotic catastrophe is described to be morphologically distinct from apoptosis, necrosis, and autophagy (Okada and Mak, 2004), but mitotic catastrophe is also described to be rather a pre-stage of cell death and the final outcome of the cell depends on the molecular profile (Okada and Mak, 2004; Vitale et al., 2011). Nevertheless, the most important attributes are briefly outlined in this section. Cell death through mitotic catastrophe is considered to be an oncosuppressive mechanism, for the maintenance of genomic stability (Vitale et al., 2011) and different outcomes have been described:

- cells can die without accomplishing mitosis,
- cells can proceed to G_1-phase of the cell cycle and are then subjected to cell death and,
- cells can proceed to G_1-phase and are subjected to senescence (Vitale et al., 2011).

Another feasible scenario is mitotic slippage resulting in tetraploid cells. Cells exit from mitosis, but anaphase and cytokinesis is not initiated (Lens and Medema, 2019). Then the cells can enter

the cell cycle again and may be subjected to mitotic catastrophe (Portugal et al., 2009). Mitotic catastrophe can be initialized by a very heterogenous group of different stimuli. DNA-damaging agents can induce mitotic arrest, especially when the G_2-checkpoint is weakened, often in the absence of TP53 (Vitale et al., 2011). Furthermore, tubulin-binding agents can induce mitotic arrest, by disrupting the mitotic spindle (Vitale et al., 2011). Mitotic catastrophe caused by the microtubular poison paclitaxel is often attended by abnormally prolonged CDK1 activity, circumventing cytokinesis to proceed (Okada and Mak, 2004). Inhibitors, e.g. of the CHK1, PLK1, AURKB, survivin, and of components of the chromosomal passenger complex can selectively cause mitotic catastrophe (Vitale et al., 2011). The same is reported for the inhibition of proteins necessitated for centrosome clustering (Vitale et al., 2011). Interestingly, cancer cells are more sensitive to mitotic catastrophe compared to their healthy analogues revealing a 'therapeutic window' for possible therapeutic agents (Vitale et al., 2011).

1.4.3 Autophagy

Autophagy (type II cell death), in contrast to apoptosis, can have pro-survival as well as pro-death functions (Ouyang et al., 2012). The catabolic process of self-digestion through autophagic vacuoles is primarily important for the cell as a quality control mechanism, for survival under nutrient deprivation and also for degradation of misfolded proteins, damaged cell organelles, and intracellular pathogens (Denton et al., 2012; Glick et al., 2010). Typical morphological characteristics are vacuolization, degradation of cell organelles, and slight chromatin condensation, but no DNA-laddering. In contrast to apoptosis, autophagy may lead to a caspase-independent form of cell death characterized by high lysosomal activity (Fink and Cookson, 2005; Okada and Mak, 2004). Cell death by autophagy is also a highly regulated process without induction of inflammation (Fink and Cookson, 2005). When type II cell death is initiated, autophagosomes encapsulate the respective cell organelles and protein aggregates, followed by fusion with lysosomes. The autophagy signaling pathway involves PI3K and mTOR signaling. The activity of PI3K is important for autophagosome formation in the early stage and mTOR negatively regulates autophagy initiation (Denton et al., 2012; Okada and Mak, 2004). Briefly, autophagy starts with the formation of the phagophore, conjugation of Atg5 and Atg12, followed by interaction with Atg16L, multimerization, and recruitment to the phagophore (Glick et al., 2010). Two ubiquitin-like conjugation systems regulate the conjugation of Atg5 to Atg12 and LC3-I to LC3-II, the phosphatidylethanolamine-conjugated form (Liu and Levine, 2015). Then LC3-II inserts into the membrane of the autophagosome initiating fusion with the lysosome for degradation of lysosomal contents by proteases (Denton et al., 2012; Liu and Levine, 2015).

1.4.4 Necrosis

Necrotic cell death (type III cell death) is in contrast to apoptotic cell death an unregulated process and generally a consequence of pathological conditions, e.g. infections, inflammation, ischaemia, or traumatic cell destruction (Okada and Mak, 2004). Membrane integrity rapidly

gets lost and intracellular components are released to the extracellular space damaging contiguous cells and triggering inflammation (Taylor et al., 2008). Typical morphological alterations are cell membrane swelling and rupture, increased vacuolization, degradation of cell organelles as well as nuclear DNA, and mitochondrial swelling (Okada and Mak, 2004).

1.5 Reactive Oxygen Species (ROS) and Their Implication in Cancer and Apoptosis

Reactive oxygen species (ROS) are highly reactive molecules and exhibit important biological functions, for instance cell growth and differentiation, signal transduction, regulation of transcription factors, and modulation of gene function (Trachootham et al., 2009). However, high levels of ROS can also alter the function of biomolecules by damaging proteins, lipids, and DNA (Trachootham et al., 2009). Cancer cells exhibit persistently increased levels of ROS compared to their healthy counterparts and deregulations of the redox homeostasis are common features of malignant cells (Panieri and Santoro, 2016). It was previously shown that oncogenes such as *Ras* can directly increase superoxide anion level (Behrend et al., 2003). Loss of tumor suppressor genes like p53 can also increase ROS stress (Trachootham et al., 2009). ROS can drive tumor progression by activation of pro-tumorigenic signaling and promote DNA damage as well as genetic instability (Moloney and Cotter, 2018). On the other hand, an increase of ROS can also mediate cell death caused by oxidative stress (Moloney and Cotter, 2018). Due to selective pressure exerted by the persistently heightened ROS levels, cancer cells have adapted to these conditions by ROS detoxification mechanisms allowing cancer cells to survive under pro-oxidizing conditions (Panieri and Santoro, 2016). However, this dependency on antioxidant systems makes cancer cells specifically vulnerable towards increased ROS (Panieri and Santoro, 2016). Thus, considerable efforts focus on induction of cancer cell apoptosis by agents increasing ROS generation above a critical threshold (Redza-Dutordoir and Averill-Bates, 2016; Sabharwal and Schumacker, 2014; Trachootham et al., 2009). Worth of mentioning is the involvement of ROS in ERK1/2 (extracellular signal-regulated kinases 1 and 2) mediated cell death (Cagnol et al., 2006). Several studies demonstrate that ERK1/2-mediated cell death could depend on ROS (Cagnol and Chambard, 2010; Lee et al., 2005; Nabeyrat et al., 2003; Son et al., 2011). One possible reason is that ERK1/2 specific phosphatases (DUSP) can be inhibited by ROS and provoke the activation of ERK1/2 (Cagnol and Chambard, 2010).

1.6 Ras/Raf/MEK/ERK and PI3K/AKT Signaling and Their Involvement in Apoptosis

The two isoforms, ERK1 and ERK2, are serine/threonine kinases belonging to the family of mitogen-activated protein kinases (MAPKs) and are a part of the pro-oncogenic Ras/Raf/MEK/ERK signaling pathway (Asati et al., 2016; Cagnol and Chambard, 2010). In particular activating mutations in *Ras* and *B-Raf* genes are frequently observed in human cancers

(De Luca et al., 2012). Receptor tyrosine kinases (RTKs), e.g. epidermal growth factor receptors (EGFRs), are phosphorylated and activated in the presence of growth factors. Then, adaptor proteins and exchange factors induce activation of Ras. GTP-loaded Ras proteins recruit Raf kinases, which in turn phosphorylate and activate the MAPK kinases (MAPKK), MEK 1 and MEK 2. Activated MEK subsequently phosphorylate and activate ERK1/2 by tandem phosphorylation on threonine-202/tyrosine-204 and threonine-185/tyrosine-187 (Cagnol and Chambard, 2010; De Luca et al., 2012). Activated ERK1/2 kinases translocate to the nucleus and induce changes in gene expression, controlling many transcription factors and proteins with important biological functions (Figure 4) (Asati et al., 2016; Cagnol and Chambard, 2010). Interestingly, ERK1/2 kinases do not only regulate cell cycle progression and cell survival (De Luca et al., 2012). Paradoxically, ERK1/2 might also trigger different tumor suppressor pathways (Deschenes-Simard et al., 2014). A huge number of studies suggest ERK1/2-mediated apoptotic cell death, senescence and autophagy (Cagnol and Chambard, 2010). These uncommon effects depend on sustained ERK1/2 activity and might be dependent on increased cellular ROS levels (Cagnol and Chambard, 2010). Interestingly, the pro-apoptotic activity of this pathway is well documented for commonly used agents inducing DNA-damage such as doxorubicin, etoposide, and cisplatin, but is also well documented for natural compounds like resveratrol, quercetin, betulinic acid, or apigenin (Cagnol and Chambard, 2010).

ERK1/2 can induce apoptosis through caspase 8 activation, even though by direct activation, and by induction of *de novo* gene expression (Cagnol and Chambard, 2010; Cagnol et al., 2006). Furthermore, ERK1/2 was reported to activate intrinsic apoptosis by targeting mitochondria or by modulation of pro-apoptotic protein expression such as the Bcl-2 family, tightly associated with p53 activity. Upregulation and stabilization of the tumor suppressor gene p53 is a further important mechanism that might be targeted by activated ERK1/2 kinase (Cagnol and Chambard, 2010). However, the final cellular outcome depends on ERK1/2 signaling intensity, negative feedback loops, which control the RaS/Raf/MEK/ERK signaling, and crosstalk with alternative pathways (Figure 4) (Deschenes-Simard et al., 2014).

The PI3K/AKT/mTOR signaling pathway is activated by stimulation with growth factors of the RTKs initiating binding of the regulatory subunit of PI3K to the activated RTK. The PI3K heterodimer is recruited to the plasma membrane and induces phosphorylation of PIP_2 (phosphatidylinositol (4,5)-bisphosphate). Activated Ras can also stimulate PI3K (Figure 4). The phosphatase PTEN (phosphatase and tensin homolog) dephosphorylates PIP_3 and hence negatively regulates PI3K. PIP_3 promotes activation of several signaling molecules beneath the AKT kinase, which is recruited to the plasma membrane and is phosphorylated by the 3-phosphoinositide-dependent kinase 1 (PDK1) and the second mTOR complex (mTORC2) (Figure 4) (De Luca et al., 2012). Activated AKT promotes cellular survival in particular transcription, progression of the cell cycle, apoptotic cell death, autophagy, and metabolism (Asati et al., 2016). The PI3K/AKT pathway genes are frequently mutated in human cancers (Mayer and Arteaga, 2016).

The Ras/Raf/MEK/ERK and PI3K/AKT/mTOR pathways are not only regulated by feedback mechanisms but also by complex crosstalk mechanism. Compensatory loops can induce activation of one pathway whilst inhibiting the other pathway (Figure 4) (De Luca et al., 2012).

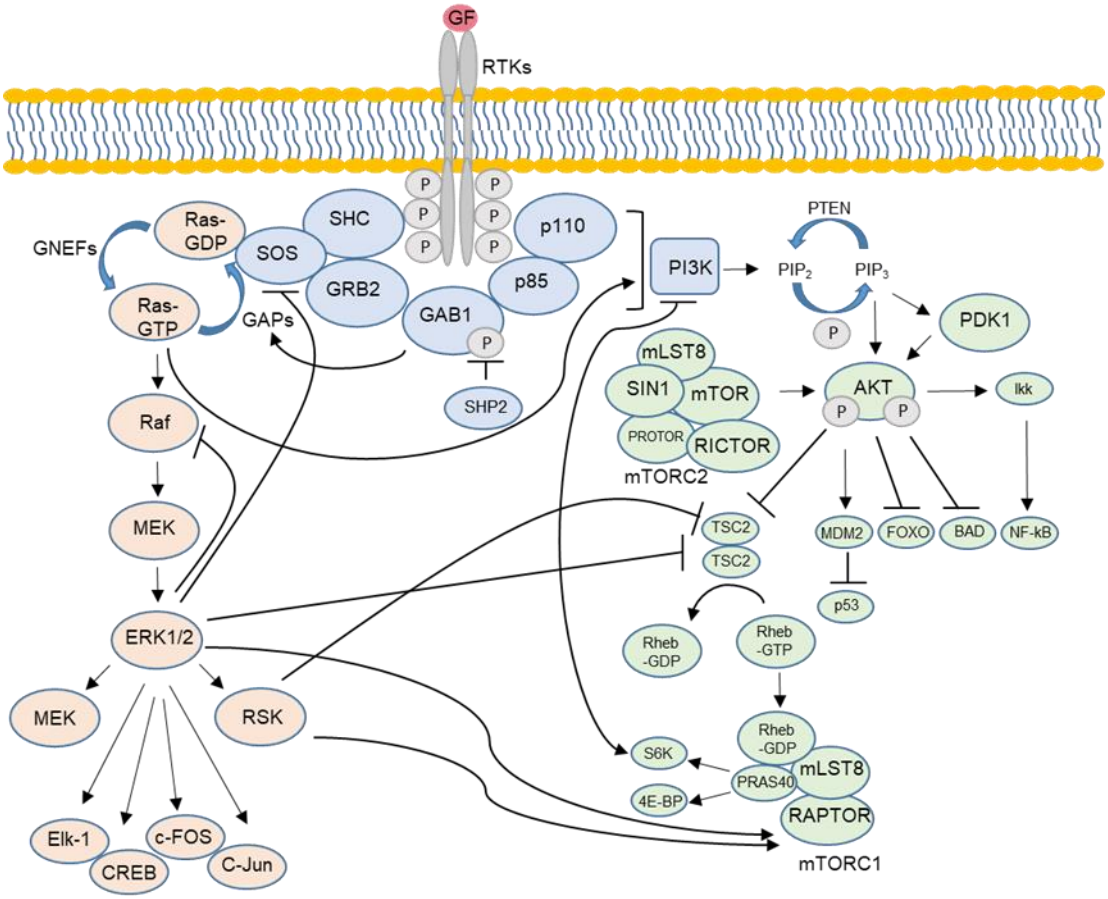

Figure 4: **Schematic overview of the Ras/Raf/MEK/ERK and the PI3K/AKT/mTOR signaling pathways and crosstalk mechanisms.** According to (De Luca et al., 2012).

1.7 Aim of the Thesis

This work was originated as a part of the projects of the Academic Center for Complementary and Integrative Medicine (AZKIM), State Ministry of Baden-Württemberg for Sciences, Research and Arts. Dietary supplements frequently applied in therapy regimens of complementary medicine, are widely accepted and used by 52 % of adults in the U.S. (Cowan et al., 2018). However, their efficacy, safety, and benefit are at large insufficiently studied. This is also one of the reasons why complementary medicine is often seen as one opposing the academic western medicine. AZKIM was founded to investigate the efficacy and safety of complementary and integrative medicine with strict scientific methods. In the focus are, among other topics, the molecular mechanisms of action of potentially active herbal ingredients.

The aim of the study was to identify biologically active ingredients of *Artemisia annua* in addition to artemisinin using an *Artemisia annua* extract marketed as a dietary supplement. Thus, the *Artemisia annua* extract should be fractionated and chemically characterized, and the most abundant extract components should be identified. Furthermore, the activity of the *Artemisia annua* extract against TNBC and other chemoresistant cancer cell lines should be investigated. Finally, the identified active ingredients should be further analyzed for potential antiproliferative and apoptosis-inducing properties. Hence, the study should provide scientific evidence for potential therapeutic efficacy of distinct *Artemisia annua* extracts marketed as dietary supplement and of its individual ingredients.

2 Material and Methods

2.1 Materials

2.1.1 Reagents

Compound / Material / Kit	Supplier
(2-(*N*-Morpholino)ethansulfonic acid 1-hydrat) (MES)	Fluka, Sigma-Aldrich, St. Louis, MO, USA
(2-Hydroxypropyl)-β-cyclodextrin (HP-β-CD)	Sigma-Aldrich, St. Louis, MO, USA
2',7'-Dichlorodihydrofluorescein diacetate (H_2DCFDA)	Molecular Probes, San Diego, CA, USA
Annexin V-FITC	BD Biosciences, Heidelberg, Germany
BCA Protein Assay Kit Pierce™	Thermo Fisher Scientific, Waltham, MA, USA
Bovine serum albumin (Fraction V)	AppliChem, Merck, Darmstadt, Germany
Calcium chloride ($CaCl_2$)	Merck, Darmstadt, Germany
Caspase 3/7 substrate (Z-DEVD-R110)	Bachem, Bubendorf, Switzerland
Cell Proliferation Assay XTT	Roche, Basel, Switzerland
Coomassie Brilliant Blue G250	Sigma-Aldrich, St. Louis, MO, USA
Dithiothreitol (DTT)	Sigma-Aldrich, St. Louis, MO, USA
D-luciferin	Biomol, Hamburg, Germany
ECL prime substrate	GE Healthcare, Buckinghamshire, UK
Ethylene diaminetetracetic acid (EDTA)	AppliChem, Merck, Darmstadt, Germany
Glycerol	Sigma-Aldrich, St. Louis, MO, USA
Glycine	AppliChem, Merck, Darmstadt, Germany
Hank's balanced salt solution (HBSS)	Gibco Life Technologies, Carlsbad, CA, USA
HEPES	Gibco Life Technologies, Carlsbad, CA, USA
Hoechst 33342	Sigma-Aldrich, St. Louis, MO, USA
Igepal CA-630	Sigma-Aldrich, St. Louis, MO, USA)
JC-1	Molecular Probes, San Diego, CA, USA
Matrigel	BD Biosciences, San Jose, CA, USA
MitoSOX™ Red	Molecular Probes, San Diego, CA, USA
Non-fat dry milk	AppliChem, Merck, Darmstadt, Germany
NuPAGE™ 4-12 % Bis-Tris Protein Gel, 1.5 mm, (Invitrogen™)	Invitrogen, Thermo Fisher Scientific, Waltham, MA, USA

PageRuler™ Prestained Protein Ladder	Thermo Fisher Scientific, Waltham, MA, USA
Paraformaldehyde	Sigma-Aldrich, St. Louis, MO, USA
P-Nitrophenyl-phosphate (PNPP)	Sigma-Aldrich, St. Louis, MO, USA
Propidium iodide	Sigma-Aldrich, St. Louis, MO, USA
Protease-inhibitor-mix	Merck, Darmstadt, Germany
Proteome Profiler™ Human Phospho-Kinase Array	R&D Systems, Minneapolis, MN, USA
RNAse A	Sigma-Aldrich, St. Louis, MO, USA
Sodium chloride (NaCl)	AppliChem, Merck, Darmstadt, Germany
Sodium chloride, 0.9 % (NaCl, 0.9 %)	B. Braun Melsungen AG, Meslungen, Germany
Sodium deoxycholate	Sigma-Aldrich, St. Louis, MO, USA
Sodium dodecyl sulfate (SDS)	Sigma-Aldrich, St. Louis, MO, USA
Sodium fluoride (NaF)	Sigma-Aldrich, St. Louis, MO, USA
Sodium hydrogen phosphate (Na_2HPO_4)	Merck, Darmstadt, Germany
Sodium orthovanadate (Na_3VO_4)	Sigma-Aldrich, St. Louis, MO, USA
Sterofundin	B. Braun Melsungen AG, Melsungen, Germany
Tris base	USB Corporation, Cleveland, OH, USA
Tris-HCl	AppliChem, Merck, Darmstadt, Germany
Triton X-100	Sigma-Aldrich, St. Louis, MO, USA
TUNEL Kit	Roche, Basel, Switzerland
Tween 20	AppliChem, Merck, Darmstadt, Germany
β-Glycerophosphate	Calbiochem, Merck, Darmstadt, Germany
β-Mercaptoethanol (β-ME)	Fluka, Sigma-Aldrich, St. Louis, MO, USA

2.1.2 Equipment and Software

Equipment / Software	Supplier
AB API 2000 triple quadrupole mass spectrometer	Applied Biosystems, Foster City, CA, USA
Amersham™ Imager 680	GE Healthcare, Chicago, IL, USA
Analyst 1.6.1 software	Ab Sciex, Framingham, MA, USA
Automatic sample injector Aspec XL	Abimed, Langenfeld, Germany
Axio Lab.A1 microscope	Carl Zeiss, Göttingen, Germany
BD FACSVerse flow cytometer	BD, Heidelberg, Germany
BD Vacutainer, NH 170 I.U.	BD, Plymouth, UK
Chromeleon software version 6.6	Dionex, Idstein, Germany
Column oven IWN CH100	Junedis, Gröbenzell, Germany

EDTA tubes	Kabe Labortechnik GmbH, Nürnbrecht-Elsenroth, Germany
Falcon 6-well Clear Flat Bottom TC-treated Multiwell Cell Culture Plate	Corning Life Sciences, Durham, NC, USA
Falcon 96-well Clear Flat Bottom TC-treated Culture Microplate	Corning Life Sciences, Durham, NC, USA
FlowJo software	FlowJo LLC, Ashland, OR, USA
Fraction collector	Gilson, Limburg-Offheim, Germany
HPLC 1260 Infinity system	Agilent, Santa Clara, CA, USA
HPLC column ReproSil-Pur Basic C18-HD, 3 µm, 125x3 mm	Dr. Maisch HPLC GmbH, Ammerbuch, Germany
HPLC column ReproSil-Pur Basic-C18, 1.9 µm, 75 x 2 mm	Dr. Maisch HPLC GmbH, Ammerbuch, Germany
HPLC column ReproSil-Pur Universal RP, 5 µm, 10x4 mm	Dr. Maisch HPLC GmbH, Ammerbuch, Germany
HPLC column, SecurityGuard, C18, 4x3 mm	Phenomenex, Aschaffenburg, Germany
HPLC column, Synergi Hydro-RP, 4 µm, 80 Å, 250x10 mm	Phenomenex, Aschaffenburg, Germany
Invitrogen™ Novex™ XCell SureLock® Mini-Cell electrophoresis apparatus	Fisher Scientific, Leicestershire, UK
IVIS *in vivo* Imaging System	PerkinElmer, Waltham, MA, USA
LC-9A Shimadzu pump	Shimadzu, Kyoto, Japan
M1000 PRO Tecan plate reader	Tecan Group Ltd., Männedorf, Switzerland
Microscopy chamber, µ-slide 8 well	Ibidi GmbH, Martinsried, Germany
Milli-Q station	Millipore, Eschborn, Germany
Photodiode array detector UVD 340U	Dionex, Idstein, Germany
Polyvinylidene difluoride membrane (PVDF), 0.2 µm	Schleicher & Schuell Bioscience GmbH, Dassel, Germany
Primaria™ Cell culture dish (100 × 20 mm)	Corning Life Sciences, Durham, NC, USA
Progres Gryphax software	Carl Zeiss, Göttingen, Germany
SigmaPlot Software	Systat Software GmbH, Erkrath, Germany
Tecan D300e digital dispenser	Tecan Group Ltd., Männedorf, Switzerland
Ti-E inverse fluorescence microscope	Nikon, Düsseldorf, Germany
Trans-Blot Turbo Transfer System	Bio-Rad Laboratories GmbH, Munich, Germany
Valoo software	Applica, Bremen, Germany
Whatman papers	GE Healthcare, Buckinghamshire, UK
Zeiss 2/3" CMOS-camera	Carl Zeiss, Göttingen, Germany

2.1.3 Compounds and Extracts

Compound / Extract	Supplier
6,7-Dimethoxycoumarin	Extrasynthese, Genay cedex, France
Arteannuic acid	Carbosynth, Berkshire, UK
Arteannuin B	Carbosynth, Berkshire, UK
Casticin	Extrasynthese, Genay cedex, France
Chrysosplenol D	ChemFaces, Wuhan, Hubei, China
Doxorubicin	Sigma-Aldrich, St. Louis, MO, USA
Momundo	MoMundo GmbH, Bad Emstal, Germany
Paclitaxel	Sigma-Aldrich, St. Louis, MO, USA
U0124	Bio-Techne, Minneapolis, MN, USA
U0126	Biomol, Hamburg, Germany

2.1.4 Antibodies

Antibody	Catalog number	Supplier
Actin	# MAB1501	Merck Millipore, Darmstadt, Germany
AKT-1	# 2967L	Cell Signaling Technology, Danvers, MA, USA
Alexa Fluor® 488 α-tubulin antibody	# 5063	Cell Signaling Technology, Danvers, MA, USA
ECL™ Anti-mouse IgG, Horseradish Peroxidase linked F(ab')$_2$ fragment	# NA9310V	GE Healthcare, Buckinghamshire, UK
ECL™ Anti-rabbit IgG, Horseradish Peroxidase linked F(ab')$_2$ fragment	# NA9340V	GE Healthcare, Buckinghamshire, UK
ERK 1/2	# 9102	Cell Signaling Technology, Danvers, MA, USA
Ki-67	# M7240	Dako, Glostrup, Denmark
P-AKT (S473)	# 4058S	Cell Signaling Technology, Danvers, MA, USA
P-ERK (T202/Y402)	# 4376	Cell Signaling Technology, Danvers, MA, USA

2.2 Preparation of *Artemisia annua* Extracts

The Momundo extract, commercially available as a dietary supplement was prepared by dissolving of the capsule content directly in dimethyl sulfoxide (DMSO). For Momundo-ACN extract preparation, the Momundo capsule content was macerated in acetonitrile (ACN) for 1 h at RT during consecutive stirring. After centrifugation, the supernatant was transferred into a new vessel and the ACN solvent was evaporated under a stream of nitrogen. The yielded dry extract (Momundo-ACN) was dissolved in DMSO for further biological experiments (Figure 5) (Lang et al., 2019).

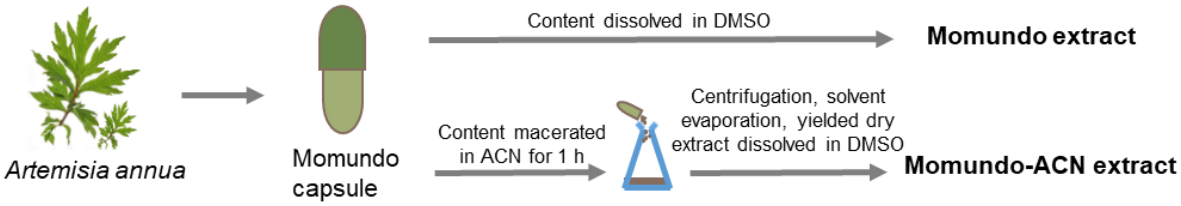

Figure 5: **Schematic presentation of *Artemisia annua* extract preparation.** Preparation of Momundo and Momundo-ACN extract. Momundo extract was prepared by solvation of the capsule content in DMSO. The Momundo-ACN extract was prepared by maceration of the Momundo capsule content in ACN. After centrifugation, the solvent was evaporated under a stream of nitrogen to yield the Momundo-ACN dry extract. Figure adapted with permission from our own publication (Lang et al., 2019), page 2, © 2019 The Authors, under a creative commons license, CC BY-NC-ND 4.0, creativecommons.org/licenses/by-nc-nd/4.0/.

2.3 General Experimental Procedures

All stock solutions were prepared in DMSO. For the biological experiments, the DMSO stock solutions were further diluted with medium containing 1 % FCS. The final DMSO concentration was 0.5 % DMSO in all biological experiments.

For xenograft treatment in mice, HP-β-CD complexes with the Momundo extract were prepared. For this purpose, the Momundo *Artemisia annua* extract was dissolved in ethanol/water (1:1, v/v). HP-β-CD was dissolved in ethanol. The obtained solutions were mixed in a mass ratio 1:11 during continuous shaking for 2.5 h, followed by vacuum concentration and lyophilization. The resulting water-soluble complexes were dissolved in in 0.9 % NaCl and used for *i.p.* application of the Momundo extract *in vivo* (Lang et al., 2019).

2.4 Analytical Characterization of *Artemisia annua* Dietary Supplements

2.4.1 Determination of Artemisinin Content by HPLC-MS/MS

The HPLC-MS/MS analysis was carried out on an Agilent 1260 Infinity system, coupled with an AB API 2000 triple quadrupole mass spectrometer via an electrospray ionization source (ESI). The data were analyzed with Analyst 1.6.1 software. An analytical HPLC column (Dr. Maisch ReproSil-Pur Basic C18-HD, 3 µm, 125x3 mm) with a precolumn (Dr. Maisch ReproSil-Pur Universal RP, 5 µm, 10x4 mm) was used for the separation.

Samples were prepared as follows: 30 mg Momundo capsule content was suspended in 1.5 ml ACN and extracted for 1 h at RT whilst continuously stirring. After centrifugation (16,000 g, 10 min) of the suspension, 1 ml supernatant was added to 1 ml water, followed by filtration through regenerated cellulose (0.45 µm). The resulting sample concentration was 10 mg/ml and was analyzed in triplicates.

Chromatographic separation was performed with a flow rate of 600 µl/min and an injection volume of 70 µl. Constitution of the mobile phase was eluent A (deionized, ultrapure water + 0.1 % acetic acid and 10 mM ammonium acetate) and eluent B (acetonitrile + 0.1 % acetic acid). Chromatographic separation started with 60 % eluent A and 40 % eluent B. Then, a linear gradient followed till 90 % eluent B for 10 min and then, 90 % of eluent B till 13 min. Thereafter, the linear gradient was set to initial conditions until 15 min. Then re-equilibration followed until 20 min. To stabilize the chromatographic system, the column temperature was constantly kept at 28 °C.

The MS/MS analysis was accomplished in the positive atmospheric pressure ESI and multiple-reaction monitoring (MRM) detection modes. For the quantification of artemisinin the precursor ion at m/z 300.2 ($[M + NH_4]^+$) and the product ion of highest intensity at m/z 151.2 were selected. To obtain linearity and to specify the limit of detection (LOD) and limit of quantification (LOQ), six levels of standard solutions in the range from 7.5 ng/ml to 100 ng/ml were analyzed, each in triplicates. To evaluate the accuracy of the method, the recovery was determined using the method of standard addition. Therefore, a real sample was spiked at six levels and extraction was performed as described above for sample preparation. Analysis was performed in triplicates. To determine the precision of the method, a reference sample with six replicates was analyzed at four different days (Lang et al., 2019).

2.4.2 Fractionation of Momundo Extract by Semipreparative HPLC-DAD Analysis

For the identification of potential anticancer ingredients contained in Momundo, the extract was fractionated. The fingerprint characterization and the *Artemisia annua* extract fractionation was accomplished by semipreparative HPLC. The HPLC system consisted of a low gradient LC-9A Shimadzu pump, an automatic sample injector Aspec XL, a column oven IWN CH100, a photodiode array detector UVD 340U, and a fraction collector connected to a computer running

Chromeleon Software version 6.6. A precolumn (Phenomenex, SecurityGuard, C18, 4x3 mm) with a semi-preparative column (Phenomenex, Synergi Hydro-RP, 4 µm, 80 Å, 250x10 mm) were used for the extract separation and fractionation (Lang et al., 2019).

For sample preparation, 100 mg/ml Momundo-ACN extract (extraction procedure is described in section 2.2) was dissolved in DMSO and was filtered through a membrane filter with a pore size of 0.45 µm. Then, the automatic sample injector was loaded with 200 µl of the prepared extract. The flow rate was adjusted to 5,000 µl/min. Absorbance was traced by the photodiode-array detector at 210 nm. The elution gradient consisted of eluent A (deionized ultrapure water + 0.05 % formic acid) and eluent B (acetonitrile + 0.05 % formic acid) starting with 30 % acetonitrile and 70 % water, followed by linear gradient till 18 min to 95 % eluent B for 6 min. After 24 min, the system was returning in 1 min to initial conditions for further 5 min. For acquiring the chromatograms, the photodiode array detector was set at 210 nm (Lang et al., 2019).

The fractions of the major peaks a, b, c, d, e (Figure 7A), were collected and the solvent was removed with a rotary evaporator. Structure determination was accomplished by HPLC-MS/MS. The retention times, mass spectra, and fragmentation mass spectra were compared with reference standards. Peak b (chrysosplenol D) was additionally analyzed by ^{1}H- and ^{13}C-NMR spectroscopy using a Bruker DRX 500 NMR spectrometer. For the HPLC-MS/MS analysis the Agilent 1260 Infinity HPLC system connected with an AB API 2000 triple quadrupole mass spectrometer through an ESI source was used. For data analysis Analyst 1.6.1 software was used (Lang et al., 2019).

2.4.3 Quantification of the Major Ingredients in Momundo Extract

For quantification of the most abundant compounds, identified in Momundo extract, an UHPLC-MS/MS method was developed. The chromatographic system, described previously in section 2.4.1, was equipped with an analytical UHPLC column (Dr. Maisch ReproSil-Pur Basic-C18, 1.9 µm, 75 x 2 mm) and a precolumn (Phenomenex, SecurityGuard, C18, 4 x 2 mm). Flow rate was set to 350 µl/min and the injection volume was 2 µl. The mobile phase consisted of eluent A (ultrapure water + 0.05 % formic acid) and eluent B (acetonitrile + 0.05 % formic acid). Gradient elution started with 70 % eluent A and 30 % eluent B. Then, a linear gradient followed to 95 % eluent B for 6.5 min, thereafter, 95 % eluent B until 9.1 min. Then, a linear gradient was applied to starting conditions until 9.5 min, followed by re-equilibration until 12.5 min. For stabilization of the chromatographic system, the column temperature was kept at 28 °C. The MS/MS analysis was accomplished in the positive atmospheric pressure ESI mode and multiple-reaction monitoring (MRM) detection mode. For analysis of 6,7-dimethoxycoumarin, the precursor ion at m/z 207.1 and the product ion of highest intensity at m/z 151.1 were selected. For chrysosplenol D the ions at m/z 361.3 and 327.8 were used and for casticin m/z 375.4 and 342.0. Similarly, the ions at m/z 249.3 and 142.9 were used for arteannuin B. The analysis of arteannuic acid was accomplished in the negative ionization mode and the selected ion monitoring (SIM)

detection mode at m/z 233.2. The compounds were quantified by external calibration (Lang et al., 2019).

The quantification method was validated in terms of linearity, precision, accuracy, limit of detection, and limit of quantification as described (Lang et al., 2019). Triplicates of the standard solutions in the range from 10 ng/ml to 5,000 ng/ml (nine levels) were analyzed to obtain the linearity and to define the limit of detection (LOD) and the limit of quantification (LOQ). On the basis of the standardization criteria of DIN 32645, the regression, the LOD and LOQ were determined with Valoo software. Using the method of standard addition, the recovery and accuracy of the method were calculated. For the evaluation of the precision of the method, standards (two levels) were analyzed with six replicates on four different days to determine the intraday and interday variation data (Lang et al., 2019).

2.5 Cell Culture

Cell lines and reagents	Supplier
A549 cells (non-small cell lung cancer cells)	ATCC, Rockville, MD, USA
Biocoll separating solution	Biochrom GmbH, Berlin, Germany
DMEM medium (high glucose)	Gibco, Life Technologies, Carlsbad, CA, USA
F12 K medium	Gibco, Life Technologies, Carlsbad, CA, USA
FCS (fetal calf serum)	Gibco, Life Technologies, Carlsbad, CA, USA
hTERT-HME1 cells (normal human breast epithelial cells)	ATCC, Rockville, MD, USA
L-glutamine	Life Technologies, Carlsbad, CA
MCF-7 cells (estrogen responsive breast cancer cells)	ATCC, Rockville, MD, USA
MDA-MB-231/Luc cells (triple negative breast cancer cells, stably expressing firefly luciferase)	Cell Biolabs, San Diego, CA, USA
MEGM medium	Lonza, Basel, Switzerland
MEM non-essential amino acids	Biochrom GmbH, Berlin, Germany
MIA PaCa-2 cells (pancreatic cancer cells)	ATCC, Rockville, MD, USA
PBS (phosphate buffered saline)	Gibco, Life Technologies, Carlsbad, CA, USA
PC-3 (androgen independent prostate cancer cells)	ATCC, Rockville, MD, USA
Penicillin/Streptomycin	Gibco, Life Technologies, Carlsbad, CA, USA
RPMI 1640 medium	Gibco, Life Technologies, Carlsbad, CA, USA
Trypsin/EDTA (1×) 0.05 %/0.02 % in PBS	PAN-Biotech, Aidenbach, Germany

Cell lines	Growth medium
A549	RPMI 1640, 10 % FCS, 2 mM L-glutamine, 100 U/ml penicillin, 100 mg/ml streptomycin
hTERT-HME1	MEGM medium
MCF-7	DMEM, 4.5 g/l glucose, 10 % FCS, 0.1 mM MEM non-essential amino acids, 2 mM L-glutamine, 100 U/ml penicillin, 100 mg/ml streptomycin
MDA-MB-231/Luc	DMEM, 4.5 g/l glucose, 10 % FCS, 0.1 mM MEM non-essential amino acids, 2 mM L-glutamine, 100 U/ml penicillin, 100 mg/ml streptomycin
MIA PaCa-2	DMEM, 4.5 g/l glucose, 10 % FCS, 100 U/ml penicillin, 100 mg/ml streptomycin
PC-3	F12 K, 10 % FCS, 100 U/ml penicillin, 100 mg/ml streptomycin

2.5.1 Subculturing

Cells were cultured in a humidified atmosphere at 37 °C and 5 % CO_2. Every three to four days, when cells reached 80 % confluence, they were subcultured according to the suppliers' recommendations. Briefly, the medium was removed, cells were rinsed with PBS followed by incubation with trypsin for approximately 5 min. Trypsin was neutralized with medium containing 10 % FCS. A small aliquot for determination of cell number with a Neubauer's counting chamber was taken. Cells were centrifuged at 150 - 400 g (depending on the cell line) for 5 min at RT. Then supernatant was removed and cells were cultured for further three to four days in fresh medium.

2.5.2 Freezing and Thawing

Cells were aliquoted in cryovials (2×10^6 cells) in freezing medium containing 5 - 10 % DMSO, followed by slowly freezing in an appropriate freezing container at - 70 °C for > 4 h, and were then stored in the vapor phase of liquid nitrogen. For thawing, the cryovial was quickly thawed at 37 °C, cells were suspended in prewarmed medium and were centrifuged at 150 - 400 g for 5 min at RT to remove excess of DMSO.

2.5.3 Isolation of Peripheral Blood Mononuclear Cells (PBMC)

All experiments using human blood cells have been approved by the Institutional Ethics Committee (reference number 177/18). PBMC were isolated from whole blood samples of healthy donors, collected in lithium-heparin tubes. Whole blood was mixed with an equal volume of PBS, followed by density gradient centrifugation using Biocoll separating solution at 400 g for

30 min at RT without brake. The whitish buffy coat (PBMC) from the interphase was carefully aspirated and mixed with three times of their volume with PBS and centrifuged at 200 g for additional 15 min. The resulting pellet was washed in PBS containing 2 mM EDTA (pH 7.2-7.3) and centrifuged for 10 min at 200 g. Subsequently, the PBMC were maintained in RPMI 1640 supplemented with 10 % FCS and 100 U/ml penicillin, 100 mg/ml streptomycin.

2.6 Analysis of Cell Viability

Reagent	Compound solution
XTT sodium salt	2,3-bis-(2-methoxy-4-nitro-5-sulfophenyl)-2H-tetrazolium-5-carboxanilide, 1 mg/ml in PBS
Electron-coupling reagent (phenazine methosulfate)	(N-methyl dibenzopyrazine methyl sulfate), 0.383 mg/ml (1.25 mM) in PBS

Cell viability was analyzed by XTT-assay as described (Schmiech et al., 2019). In metabolic active cells, the tetrazolium salt is reduced by mitochondrial dehydrogenases forming a water soluble orange formazan dye. Cells were plated in 96-well plates and were treated the next day with different concentrations of the extracts or compounds for 24 h, 48 h or 72 h. In some experiments, MDA-MB-231 cells were pretreated for 1 h with the MEK-inhibitor U0126 (5 µM) or its inactive analogue U0124 (5 µM). Subsequently, cells were treated with chrysosplenol D or casticin (both at 10 µM) for further 48 h. The final DMSO concentration was 0.5 %. Then, 50 µl of XTT labeling mixture consisting of XTT sodium salt and electron coupling reagent (51:1) was added, followed by incubation for 4 h at 37 °C. Absorbance was measured using the Infinite M1000 PRO Tecan plate reader at 450 nm with a 639 nm reference filter. Viability was quantified by subtraction of the blank-values (medium containing respective concentrations of extract/compounds) and normalization to the vehicle control (0.5 % DMSO) (Lang et al., 2019; Lang et al., 2020).

2.7 Analysis of Cell Cycle Progression

2.7.1 Tubulin and Hoechst Staining

Reagent	Solution
Blocking solution	2 % bovine serum albumin in PBS

MDA-MB-231 cells were seeded in 8-well µ-slides from Ibidi and treated the next day with the respective compounds for 24 h, followed by one washing step with PBS and fixation with 4 % paraformaldehyde for 20 min at 4 °C. Subsequently, the cells were washed with PBS three times

and were permeabilized with 0.3 % Triton X-100 in PBS for 5 min at RT. After three washing steps with PBS, blocking solution was added for 20 min at RT to prevent unspecific binding of the antibody. Staining was performed, protected from light, for 1 h at RT with Alexa Fluor® 488 α-tubulin antibody (1:100 in PBS) and Hoechst 33342 (1 µg/ml in PBS). The cells were washed again for three times and imaged with a Ti-E inverse fluorescence microscope using x40 objective (El Gaafary et al., 2017).

2.7.2 Propidium Iodide Staining

Reagent	Solution
DNA-extraction buffer	pH 7.8 0.2 M Na_2HPO_4 Triton X-100 0.1 % (v/v)
Propidium iodide staining solution	PBS 1× 40 µg/ml DNAse free RNAse A 40 µg/ml propidium iodide

0.1×10^6 MDA-MB-231 cells per well were seeded in 6-well plates and were treated the next day with the respective concentrations of extracts or compounds for 24 h or 48 h. After treatment, the cells were harvested by trypsinization and fixed with 70 % ice-cold ethanol at - 20 °C overnight. After permeabilization with DNA-extraction buffer, DNA was stained for 1 h with propidium iodide staining solution at RT. Samples were analyzed by flow cytometry using the linear scale for cell cycle analysis and logarithmic scale for analysis of cells with DNA content ≥ 8N as established previously (El Gaafary et al., 2019). Quantification was accomplished by FlowJo software.

2.8 Analysis of Apoptosis

2.8.1 Analysis of Active Caspase 3

Caspase 3 activity was analyzed as established (El Gaafary et al., 2017). 0.1×10^6 MDA-MB-231 cells per well were seeded in 6-well plates, followed by treatment with Momundo extract for 48 h. After treatment, the cells were harvested by trypsinization, rinsed with PBS and were incubated with the fluorogenic caspase 3/7 substrate (Z-DEVD-R110, 100 µM) in PBS protected from light for 1 h at 37 °C. The cleavage of the substrate by active caspase 3 was analyzed flow cytometrically.

2.8.2 Analysis of Phosphatidylserine Exposure

Reagent	Solution
Annexin V binding buffer	Sterofundin 500 ml 1 M HEPES 5 ml 40 mM $CaCl_2$

Early apoptotic cells were analyzed by Annexin V-FITC and propidium iodide double staining. 0.1×10^6 MDA-MB-231 cells per well were seeded in 6-well plates and were treated the next day with different concentrations of the extracts and compounds for 24 h or 48 h. The cells were harvested by trypsinization and were incubated for 15 min in 0.5 ml growth medium (10 % FCS) for regeneration of the cell membrane at 37 °C. Subsequently, the cells were rinsed with Annexin V binding buffer containing 40 mM $CaCl_2$. Afterwards, staining was performed with FITC-labeled Annexin V (1:100 v/v in Annexin V binding buffer containing 40 mM $CaCl_2$) for 30 min at RT in the dark. Propidium iodide (0.5 µg/ml end concentration) was added 1 min before the measurement. After appropriate compensation by unstained and single stained samples, early apoptotic (Annexin V^+/PI^-) cells were analyzed by flow cytometry.

2.8.3 Analysis of DNA-Fragmentation

MDA-MB-231 were treated as described in section 2.7.2. The percentage of cells with hypodiploid DNA-content (subG_1-peak) was determined by flow cytometry using the logarithmic scale.

2.9 Analysis of Cell Proliferation and Apoptosis *In Vivo*

2.9.1 Chick Chorioallantoic Membrane (CAM) Assay

MDA-MB-231/Luc cells were xenotransplanted on the chorioallantoic membrane (CAM) of fertilized chick eggs seven days after fertilization. 1×10^6 cells in medium/matrigel (1:1) for experiments with Momundo extracts and 0.75×10^6 cells per egg for experiments with the pure compounds. The next three consecutive days, the cells were treated topically with 20 µl of the respective extract or compound dissolved in 0.9 % NaCl (vehicle control: 0.5 % DMSO) (El Gaafary et al., 2019; Syrovets et al., 2005). Momundo and Momundo-ACN were used in concentrations of 10 and 100 µg/ml, casticin and chrysosplenol D were used in concentrations of 30 µM and doxorubicin at 1 µM. On day four after treatment initiation, bioluminescence of MDA-MB-231 xenografts was measured after application of D-luciferin (20 µl of 0.75 mg/ml in PBS per egg) using an IVIS *in vivo* Imaging System. Afterwards, tumors were collected, imaged, fixed, and paraffin embedded for analysis by immunohistochemistry. 5 µm-slices of the collected tumors were stained for analysis of proliferation using antibodies against Ki-67.

For analysis of apoptotic cell death *in vivo*, DNA strand breaks were visualized. For this purpose, deoxynucleotidyl transferase dUTP nick end labeling (TUNEL) was performed according to the manufacturer's recommendations. Images were recorded with an Axio Lab. A1 microscope and a Zeiss 2/3" CMOS-camera using Progres Gryphax software. The tumor volume (mm^3) was assessed with the formula (Lang et al., 2019):

$$Tumor\ volume\ (mm^3) = \ length\ (m\text{m}) \times width^2\ (mm^2)\ \times \frac{\pi}{6}$$

2.9.2 Mouse Xenografts

The experiments with mice were approved by the ethics committee on September 19th, 2018 (reference number: 1408) with the short name "Pharmakologisch-toxikologische Untersuchung von Naturstoffen zur Behandlung maligner, orthotoper Brustkrebs-Xenotransplantate an Mäusen". During the whole study, the health conditions of the mice were monitored daily by using an appropriate score sheet.

For analysis of tumor growth and toxicity *in vivo*, an orthotopic xenograft nude mouse model was used. After two weeks of acclimatization in the animal research center of Ulm University, 0.5×10^6 MDA-MB-231/Luc breast cancer cells in 50 µl PBS were orthotopically xenografted into the mammary gland of female NMRI-*Foxn1*$^{nu/nu}$ mice (Janvier, Le Genest-St.-Isle, France). The mice were eight to nine weeks old, with a body weight between 24.0 and 30.3 g at treatment initiation. On day eight after xenotransplantation, mouse cages were randomly distributed in three groups (eight mice/group) and intraperitoneal treatment was initiated with 100 mg kg^{-1} day^{-1} Momundo-HP-β-CD, 2 mg kg^{-1} $week^{-1}$ doxorubicin, or 1000 mg kg^{-1} day^{-1} solvent (HP-β-CD) in 0.9 % NaCl for three weeks (Figure 17A).

Once a week the body weight was monitored and the tumor volumes were calculated according to the formula:

$$Tumor\ volume\ (mm^3) = \ 0.5\ \times length\ (m\text{m}) \times width\ (m\text{m}) \times thickness\ (m\text{m})$$

On day 22 after treatment initiation, mice were sacrificed by inhalation of carbon dioxide and blood was collected by cardiac puncture. Blood samples were analyzed by the university hospital's clinical chemistry laboratory for alterations of plasma levels of the liver enzymes aspartate aminotransferase AST and alanine aminotransferase ALT using standard methods (Lang et al., 2019).

2.10 Analysis of ROS Levels

To monitor cellular ROS production, the cell permeable 2',7'-dichlorodihydrofluorescein diacetate (H_2DCFDA) dye was used (El Gaafary et al., 2017). After cell permeabilization, H_2DCFDA is deacetylated by cellular esterases and oxidized in the presence of ROS into 2',7'–dichlorofluorescein (DCF), a fluorescent compound with absorption/emission maxima at ~

495/529 nm. Superoxide anions were determined by MitoSOX™ Red staining. MitoSOX™ Red specifically targets mitochondria. Oxidation by superoxide anions produces a fluorescent product with absorption/emission maxima at ~510/580 nm.

0.1×10^6 MDA-MB-231 cells per well were seeded into 6-well plates and were treated the next day for 1.5 h, 5 h, 24 h, and 48 h with 30 µM of the respective compounds or with 100 µM H_2O_2 for 5 h, serving as a positive control. After treatment, cells were stained with 10 µM H_2DCFDA or 5 µM MitoSOX™ for 20 min at RT and were washed with HBSS two times.

Cells with increased fluorescence compared to untreated control cells indicating increased ROS or superoxide levels, were quantified by flow cytometry and FlowJo software.

2.11 Analysis of the Mitochondrial Membrane Potential

Monitoring the mitochondrial membrane potential (ΔΨm) had previously been established (El Gaafary et al., 2019). For this purpose the membrane permeable JC-1 mitochondrial potential sensor was used. JC-1 is a lipophilic cationic dye accumulating in mitochondria in a potential-dependent manner. In intact mitochondria, JC-1 forms multimeric J-aggregates, which emit red fluorescence at 590 nm. Due to the leakage of damaged mitochondria, the monomeric form of the dye accumulates in the cytosol and exhibits absorption/emission maxima at 490/527 nm.

For the analysis of mitochondrial integrity, 0.1×10^6 MDA-MB-231 cells per well were plated in 6-well plates and were treated the next day with Momundo (10 µg/ml), chrysosplenol D (10 µM), casticin (1 µM), or paclitaxel (100 nM) for 24 and 48 h. Afterwards, the cells were incubated with 10 µg/ml JC-dye in DMEM medium without supplements at 37 °C. Cells with decreased red to green fluorescence intensity ratio demonstrating loss of ΔΨm, were quantified by flow cytometry and FlowJo software.

2.12 Quantification of Sample Protein Concentration

The protein concentration in the samples was determined by Pierce™ BCA Protein Assay Kit. The first step of the reaction is the copper chelation with protein in an alkaline environment forming a light blue complex (biuret reaction). Thereby, Cu^{3+} is reduced to Cu^{2+}, which reacts in the second step with bicinchonic acid (BCA). The chelation of two molecules BCA with one cuprous ion results in the violet colored reaction product of which the optical density can be measured photometrically. The complex of copper and BCA exhibits a strong linear absorbance at 562 nm with increasing protein concentrations. For quantification of the lysates, BSA-standards were prepared in concentrations of 0.1 mg/ml till 0.0312 mg/ml in water/10 % cell lysis buffer. The cell lysates were diluted 1:10 in H_2O and 100 µl BCA working solution was added according to the manufacturer's instructions. After 1 h at 37 °C, absorbance at 562 nm was measured with the Infinite M1000 PRO Tecan plate reader.

2.13 Human Phospho-Kinase Array

For analysis of the phosphorylation profiles of kinases and their protein substrates, the Proteome Profiler™ Human Phospho-Kinase Array from R&D Systems was used. This array provides an economical, rapid, and sensitive tool for the simultaneous analysis of the relative phosphorylation levels of 43 kinases and two related proteins (R&D Systems). Membranes, spotted in duplicates with capture and control antibodies, were incubated with the cell lysates overnight followed by washing steps to remove unbound protein and incubation with a cocktail of biotinylated detection antibodies. A signal corresponding to the amount of bound phosphorylated protein can be obtained after adding streptavidin-HRP and chemiluminescent detection reagents (R&D Systems).

0.8×10^6 MDA-MB-231 cells per cell culture dish (100 × 20 mm) were plated overnight, followed by serum starvation for 12 h. Then the cells were treated with casticin and chrysosplenol D (both 30 µM) for 3 h and were collected by scraping.

2.13.1 Preparation of Whole Cell Lysates

Cell lysates were prepared by solubilizing the cells for 30 min on ice in lysis buffer containing protease- and phosphatase-inhibitor-mix (1:100 and 1:50). Cell lysates were rocked and resuspended gently during this time. After centrifugation at 14,000 g for 5 min at 4 °, the supernatants were transferred to clean test tubes. 5 µl of the supernatants were taken for determination of sample protein concentration by Pierce™ BCA Protein Assay.

2.13.2 Quantification of Sample Protein Concentration

Protein concentration in the samples was determined by Pierce™ BCA Protein Assay Kit as described in 2.12.

2.13.3 Array procedure

Nitrocellulose membranes were blocked with Array Buffer 1 (contained in the array kit) for 1 h on a rocking platform shaker. Cell lysates were diluted with Array Buffer 1 to get the recommended protein concentration, which should be between 200-600 µg per array set and the membranes were incubated with 1 ml of cell lysates at 2-8 °C overnight. The next day, membranes were washed 3 times for 10 min with 20 ml wash buffer per dish. Then, the Detection Antibody Cocktail A for part A membranes and Cocktail B for part B membranes were added and the membranes were incubated for 2 h at RT on a rocking platform shaker. Next, the membranes were washed again for 10 min and three times followed by incubation for 30 min at RT with 1.0 ml of Streptavidin-HRP diluted with Array Buffer 2/3. A third washing step as described previously followed and the luminescent signal was detected after application of the chemiluminescent reagent mix using an Amersham™ Imager 680. The Kinase Array was performed for two times (Lang et al., 2020).

2.14 Western Immunoblotting

2.14.1 Preparation of Whole Cell Lysates

Reagent	Solution
RIPA buffer (Radioimmunoprecipitation assay buffer)	1 x PBS 1.0 % Igepal CA-630 0.5 % Sodium deoxycholate 0.1 % Sodium dodecyl sulfate (SDS) Directly before use: 1:50 protease inhibitor cocktail and 1:100 phosphatase inhibitor cocktail
Protease Inhibitor Cocktail Set III	Calbiochem
50x Phosphatase Inhibitor Cocktail	312.6 mM NaF (Natriumfluorid) 625 mM β-Glycerophosphate 62,5 mM Na_3VO_4 (Sodium orthovanadate) 625 mM PNPP (p-Nitrophenyl-phosphate) Compounds were solved in deionized water, heated to 50 °C for 5 min and aliquots were stored at - 20 °C.

Cells were serum starved for 12 h. Then, MDA-MB-231 cells were treated for 3 h with the respective compounds in medium containing 1 % FCS.

For analysis of differences in protein phosphorylation between different cell lines, untreated cells were serum starved for 12 h. Subsequently, medium containing 10 % FCS was added to the cells for 3 h and differences in the activation of ERK and AKT kinases were analyzed.

Cells were harvested by scraping in medium at 4 °C, collected in 15 ml tubes, centrifuged at 800 g for 5 min at 4 °C, and washed with ice-cold PBS. 100 µl RIPA buffer was added and left on ice for 15 min whilst vortexing every 5 min, followed by sonication for 15 min in an ice bath. Cell lysates were centrifuged again at 21,000 g for 10 min at 4 °C and supernatants were collected.

2.14.2 Quantification of Total Protein Content

Sample protein content was quantified by Pierce™ BCA Protein Assay Kit as described in section 2.12.

2.14.3 Sodium Dodecyl Sulfate-Polyacrylamide Gel Electrophoresis (SDS-PAGE)

Reagent	Solution
3x SLB (sample loading buffer)	150 mM Tris-HCl, pH 6.8 36 % Glycerol 12 % Sodium dodecyl sulfate (SDS) 4.65 % DTT (Dithiothreitol) 0.02 % Coomassie Brilliant Blue G250 Directly before use: 6 % β-Mercaptoethanol
1x MES buffer	50 mM (2-(*N*-Morpholino)ethansulfonic acid 1-hydrat) (MES) 50 mM Tris base 0.1 % Sodium dodecyl sulfate (SDS) 1 mM EDTA

Before SDS-PAGE, samples were boiled for 5 min with 3x sample loading buffer (SLB) containing β-mercaptoethanol (β-ME) at 95 °C. During this process, the proteins' disulfide bridges are cleaved by the reducing β-ME and secondary and tertiary structures are lost. The anionic detergent SDS binds and solubilizes the proteins. The primary protein structure remains reserved. SDS confers a high negative charge to the solubilized proteins, which is proportional to the size of the protein and covers the charges, which the proteins carry by themselves. Then, the proteins are separated by an electric field, based on the pore size of the polyacrylamide gel.

30 µg protein per sample and 6 µl of the molecular weight marker (PageRuler™ Prestained Protein Ladder,10 to 180 kDa) were loaded on a NuPAGE 4-12 % Bis-Tris Protein Gel, 1.5 mm, using a vertical Mini-Cell electrophoresis apparatus. The electrophoresis chamber system was filled with 1x MES buffer and the electrophoresis was run at 200 V for 45 min.

2.14.4 Western Blotting and Protein Detection

Reagent	Solution
Blotting Buffer	192 mM Glycine 25 mM Tris-HCl (pH 8.3) 10 % Methanol
TBS (10x)	0.2 mM Tris-HCl (pH 7.6) 1.4 M NaCl
TBST	1× TBS 0.05 % Tween 20
Blocking buffer	5 % not-fat dry milk powder in TBS-T

After SDS-PAGE, the separated protein bands were transferred onto a polyvinylidene difluoride (PVDF) membrane using a Trans-Blot Turbo Transfer System from BioRad. For this purpose, the polyacrylamide gel was equilibrated for 15 min in blotting buffer and the polyvinylidene difluoride membrane was activated for 1 min in methanol followed by equilibration in blotting buffer for 3 min. The Whatman papers were soaked with blotting buffer and all constituents were assembled for the semidry blot in the BioRad Box as follows, starting from the bottom of the chamber: five Whatman papers, the PVDF membrane, acrylamide gel and five Whatman papers. Western blotting was carried out by the semi-dry western blot system and the 1.5 mm gel transfer protocol for 60 min from Bio-Rad.

After protein transfer, the membranes were blocked for 1 h in blocking buffer at RT, followed by incubation with the 1st antibody at 4 °C overnight with gentle agitation. The next day, membranes were washed three times for 10 min in TBST and the appropriate 2nd antibody, coupled with horseradish peroxidase, was added for further 45 min at RT. After incubation, the membranes were washed again three times for 10 min with TBST and once with TBS. The proteins were visualized with ECL prime substrate (GE Healthcare) using an AmershamTM imager 600 from GE Healthcare Life Sciences (Lang et al., 2020).

Antibody	Supplier	Catalog number	Target molecular weight (kDa)	Species	Dilution
Actin	Millipore	# MAB1501	42	Mouse	1:5000 in 5 % milk in TBST
AKT-1	Cell Signaling Technology	# 2967L	60	Mouse	1:1000 in 5 % milk in TBST
ERK1/2	Cell Signaling Technology	# 9102	42, 44	Rabbit	1:1000 in 5 % BSA in TBST
P-AKT (S473)	Cell Signaling Technology	# 4058S	60	Rabbit	1:1000 in 5 % BSA in TBST
P-ERK (T202/Y402)	Cell Signaling Technology	# 4376	42, 44	Rabbit	1:1000 in 5 % BSA in TBST
ECL^{TM} Anti-mouse IgG, Horseradish Peroxidase linked F(ab')$_2$ fragment	GE Healthcare	# NA9310V	-	-	1:10.000 in 5 % milk in TBST
ECL^{TM} Anti-rabbit IgG, Horse-	GE Healthcare	# NA9340V	-	-	1:7000 in 5 % milk in TBST

radish Peroxi-dase linked $F(ab')_2$ fragment					

2.15 Statistical Analysis

For the statistical analysis Sigmaplot software was used. If not indicated otherwise in the figure captions, quantitative results are shown as mean ± standard error of the mean (SEM) of at least three independent experiments. Two-group comparisons of normally distributed data, were accomplished with the two-tailed Student's t-test. For parametric data multi-group analysis was performed with the one-way analysis of variance followed by the Newman-Keuls post hoc test. Multi-group analysis of non-parametric data was accomplished by the Kruskal-Wallis test, followed by the Dunn's post hoc test. Significance levels were set at $*p < 0.05$, $**p < 0.01$, $***p < 0.001$. Statistical details are described in the captions of the figures.

3 Results

3.1 Analytical Characterization of *Artemisia annua* Dietary Supplements

3.1.1 Quantification of Artemisinin in *Artemisia annua* Dietary Supplements

To identify new compounds with anticancer activity beside the well-known artemisinin (Efferth, 2017a, b), Momundo *Artemisia annua* extracts were investigated for potential active ingredients. HPLC-MS/MS analysis indicates that the Momundo *Artemisia annua* extracts contain verifiable no artemisinin. The analysis indicates that the content of artemisinin in Momundo *Artemisia annua* dietary supplements is below the LOD. The LOD of the HPLC-MS/MS quantification method was 0.2 ng/mg extract and LOQ 0.8 ng/mg (Figure 6). The recovery was 94.8 % (± 9.6 % SD). Analysis of the precision of the method revealed an intraday variation of 1.5 % (RSD) and an interday variation of 1.8 % (RSD) (Lang et al., 2019).

A

	Artemisinin content, ng/mg extract
Momundo	≤ 0.2, (LOD = 0.2 ng/mg)
Momundo-ACN	≤ 0.2, (LOD = 0.2 ng/mg)

B

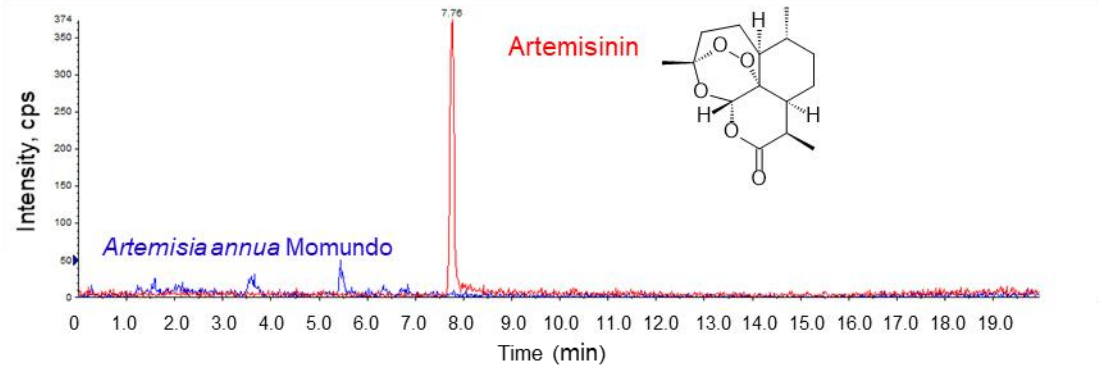

Figure 6: **Momundo extracts do not contain any detectable artemisinin.** (A) No detectable artemisinin was identified in the Momundo extracts as analyzed by HPLC-MS/MS analysis (LOD = 0.2 ng/mg). (B) HPLC-MS/MS (MRM) chromatograms of Momundo extract (blue) and the artemisinin reference standard solution (red) indicate that Momundo extract does not contain any detectable amount of artemisinin (LOD = 0.2 ng/mg). Figure adapted with permission from our own publication (Lang et al., 2019), page 2, © 2019 The Authors, under a creative commons license, CC BY-NC-ND 4.0, creativecommons.org/licenses/by-nc-nd/4.0/.

3.1.2 Fractionation and Chemical Characterization of Momundo Extracts

With the intention to identify new active ingredients in the extract, the most abundant extract components were isolated by semipreparative HPLC-DAD. The isolated fractions were further analyzed by HPLC-DAD-MS and comparison of retention times and mass spectra of the respective reference substances. The fraction, which contained chrysosplenol D, was additionally analyzed by ^{1}H- and ^{13}C-NMR spectroscopy. 6,7-Dimethoxycoumarin (a), chrysosplenol D (b), casticin (c), arteannuin B (d) and arteannuic acid (e) were identified to be the most abundant compounds in the Momundo *Artemisia annua* dietary supplement (Figure 7). The extract and the identified pure compounds were further investigated concerning their potential cytotoxicity and antitumor efficacy.

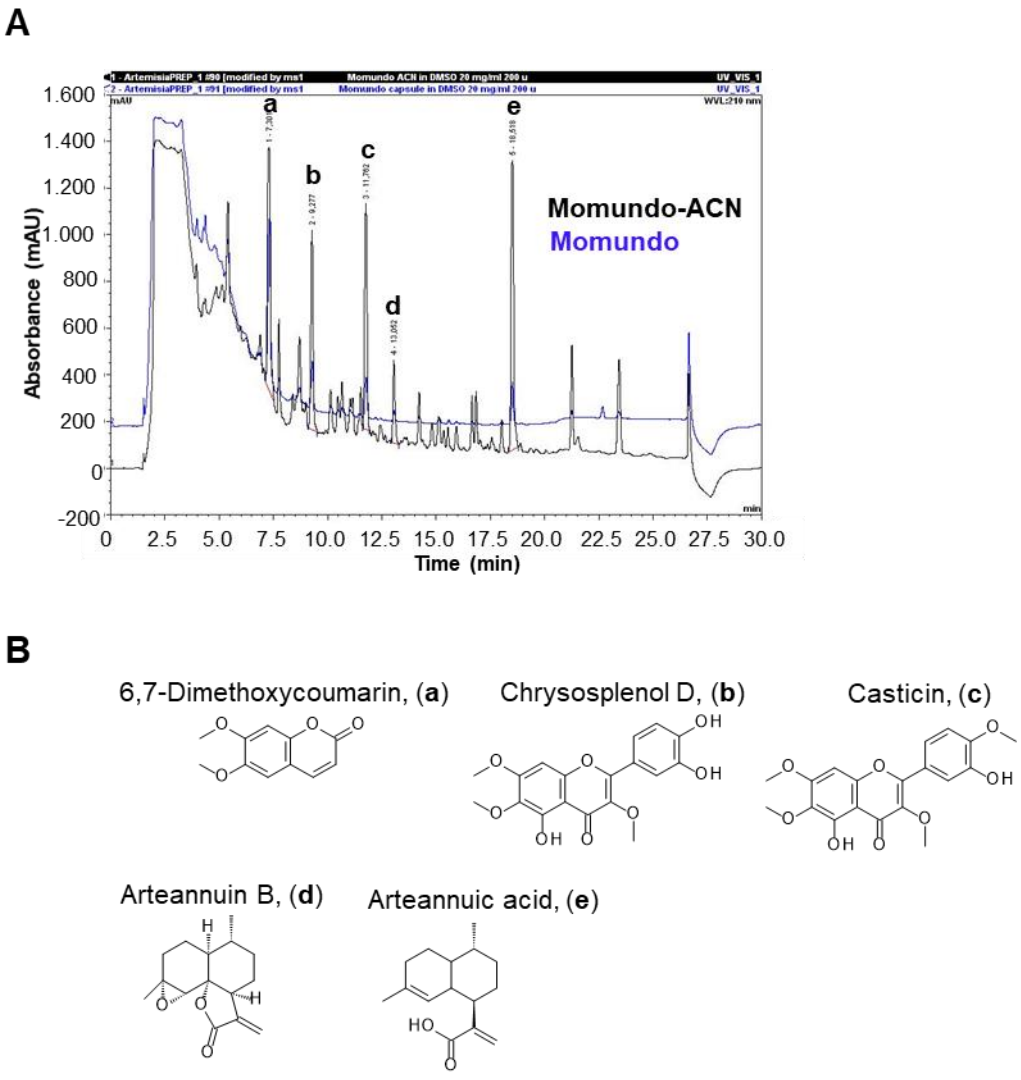

Figure 7: **Fractionation of Momundo *Artemisia annua* extract and identification of the most abundant compounds.** (A) HPLC-DAD fingerprint of the Momundo and Momundo-ACN extracts at 210 nm.

(B) Chemical structures of the identified compounds. Figure adapted with permission from our own publication (Lang et al., 2019), page 2, © 2019 The Authors, under a creative commons license, CC BY-NC-ND 4.0, creativecommons.org/licenses/by-nc-nd/4.0/.

The most abundant compounds of Momundo extracts were quantified by UHPLC-MS/MS, demonstrating that maceration of the Momundo capsule contents in ACN as described in section 2.2 resulted in enrichment of the identified lipophilic components (Figure 7A and Table 1). Data regarding the validation of the quantification method are shown in Table 2 (Lang et al., 2019).

***Table 1*: Quantification of the isolated ingredients of the Momundo *Artemisia annua* extract.** Contents of the individual compounds identified in the extracts as quantified by UHPLC-MS/MS. Data are mean ± SD, $n = 3$. Table adapted with permission from our own publication (Lang et al., 2019), page 2, © 2019 The Authors, under a creative commons license, CC BY-NC-ND 4.0, creativecommons.org/licenses/by-nc-nd/4.0/.

Fraction	Substance	Retention time t_R, min	Content µg/mg extract, mean ± SD	
			Momundo	Momundo-ACN
a	6,7-Dimethoxycoumarin	7.3	0.79 ± 0.02	4.30 ± 0.13
b	Chrysosplenol D	9.3	1.42 ± 0.08	8.17 ± 0.15
c	Casticin	11.8	0.53 ± 0.01	4.32 ± 0.03
d	Arteannuin B	13.1	0.42 ± 0.02	1.82 ± 0.04
e	Arteannuic acid	18.5	3.30 ± 0.17	50.58 ± 1.72

3.2 Antitumor Activity of the Momundo *Artemisia annua* Extracts

3.2.1 Momundo Extracts Selectively Inhibit the Viability of Cancer Cells

Momundo *Artemisia annua* extracts inhibited the viability of highly metastatic TNBC MDA-MB-231 breast cancer cells in a concentration- and time-dependent manner. Doxorubicin was used as a positive control. The cytotoxicity of Momundo-ACN was considerably higher exhibiting an IC_{50} value of 18 µg/ml compared to Momundo extract, which exhibited an $IC_{50} > 100$ µg/ml after 48 h (Figure 8A). These data demonstrate that the maceration with ACN as described in section 2.2 resulted in enrichment of lipophilic cytotoxic compounds (Lang et al., 2019).

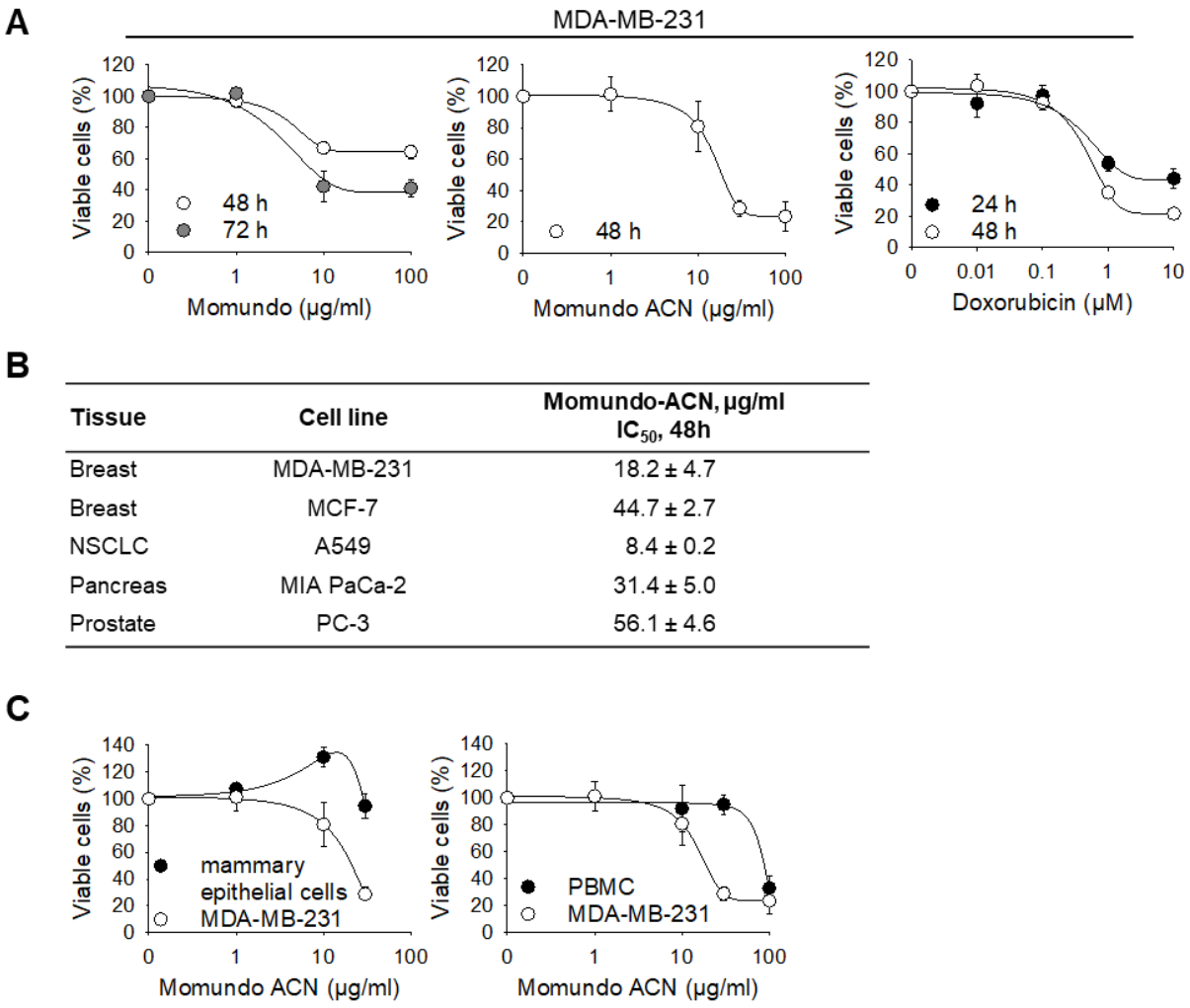

Tissue	Cell line	Momundo-ACN, µg/ml IC_{50}, 48h
Breast	MDA-MB-231	18.2 ± 4.7
Breast	MCF-7	44.7 ± 2.7
NSCLC	A549	8.4 ± 0.2
Pancreas	MIA PaCa-2	31.4 ± 5.0
Prostate	PC-3	56.1 ± 4.6

Figure 8: **Momundo *Artemisia annua* extracts are selectively cytotoxic towards a variety of different cancer cells.** (A) The viability of MDA-MB-231 breast cancer cells is effectively reduced by treatment with Momundo *Artemisia annua* extracts; doxorubicin served as positive control. Viability was analyzed by XTT. (B) Momundo-ACN extract exhibits cytotoxicity towards various treatment-resistant cancer cell lines of different origin. The viability was analyzed as in (A). (C) After 48 h of Momundo-ACN treatment, normal mammary epithelial cells and PBMC are relatively resistant. All data are mean ± SEM, n = 3 - 5. Figure adapted with permission from our own publication (Lang et al., 2019), page 5, © 2019 The Authors, under a creative commons license, CC BY-NC-ND 4.0, creativecommons.org/licenses/by-nc-nd/4.0/.

The *Artemisia annua* extract Momundo-ACN exhibited a similar cytotoxicity towards a variety of treatment-resistant cancer cell lines. These data reveal no cancer specificity of Momundo-ACN and the lack of dependency on hormone receptor expression, because the viabilities of both, the TNBC MDA-MB-231 and the estrogen responsive MCF-7 cell lines, were inhibited. Among the cell lines tested, the NSCLC A549 cells were the most sensitive cells to Momundo-ACN extract treatment with an IC_{50} of 8 µg/ml. The PC-3 prostate carcinoma cells are androgen-

independent and exhibited the highest resistance to Momundo-ACN with an IC_{50} of 56 µg/ml (Figure 8B). Noteworthy, the highly cytotoxic Momundo-ACN extract demonstrates selectivity towards cancer cells because at concentrations of 30 µg/ml the viability of MDA-MB-231 cells was inhibited by around 72 %, whereas the viability of normal mammary epithelial cells (hTERT-HME1) and PBMC remained unaffected (Figure 8C) (Lang et al., 2019). Of note, we also observed similar selective cytotoxicity for other herbal extracts. For example, a *Boswellia sacra* extract showed an IC_{50} of 8 µg/ml on MDA-MB-231 cells after 72 h of treatment, whereas it exhibited no toxicity on PBMC at this concentration (Schmiech et al., 2019).

3.2.2 Momundo Extracts Inhibit the Progression of the Cancer Cell Cycle

Treatment with Momundo or Momundo-ACN extract for 24 h, followed by morphological analysis by fluorescence microscopy demonstrated that the extracts, especially Momundo-ACN, induced formation of multinucleated cells, in particular 4N cells (Figure 9). The cell morphology after Momundo-ACN treatment revealed similar effects as after treatment with 100 nM paclitaxel (Figure 9) (Lang et al., 2019).

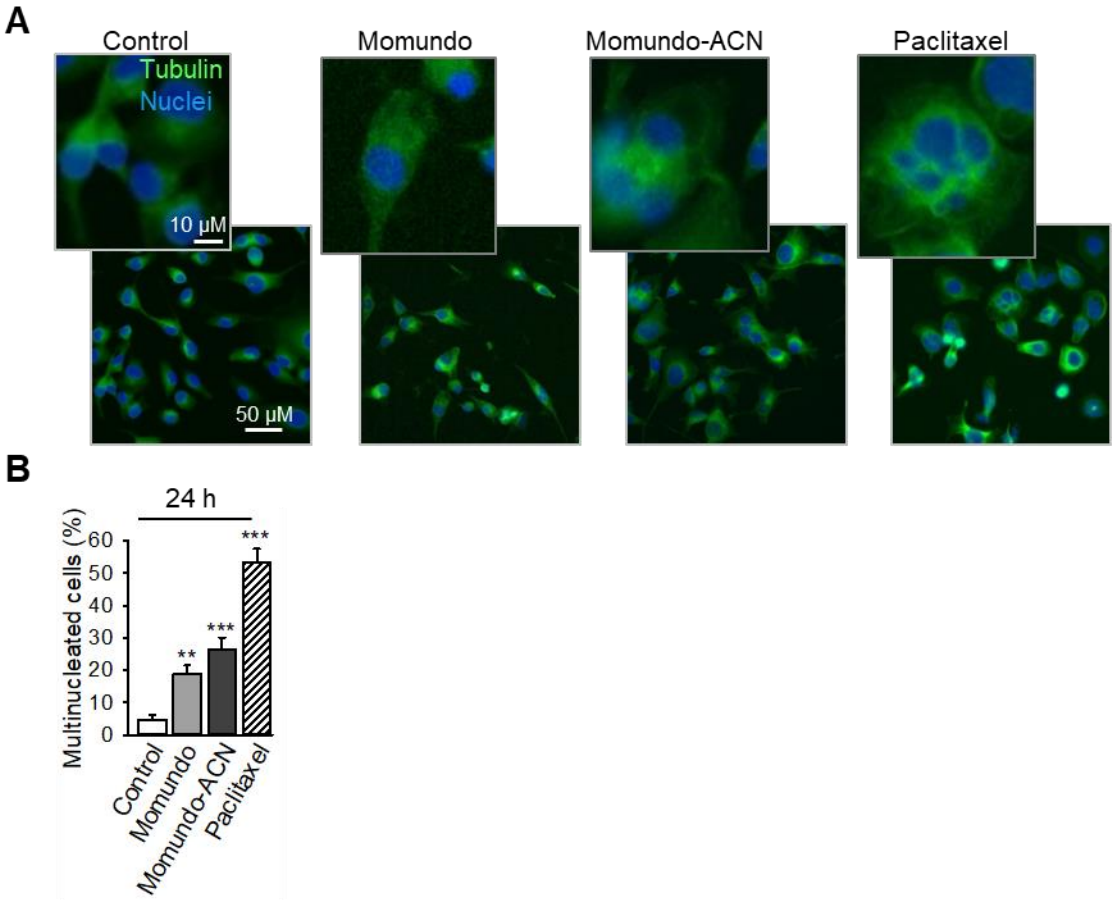

Figure 9: **Treatment with Momundo *Artemisia annua* extracts induces the formation of multinucleated cancer cells.** (A) MDA-MB-231 cells were treated with 100 µg/ml Momundo, 30 µg/ml Momundo-ACN, or 100 nM paclitaxel for 24 h followed by staining with the fluorescence-labeled anti-

tubulin antibody and Hoechst 33342. Cells were analyzed by fluorescence microscopy. (B) Quantification of multinucleated cells. Cells were quantified in at least five randomly chosen fields. $^{**}p < 0.01$, $^{***}p < 0.001$ Figure adapted with permission from our own publication (Lang et al., 2019), page 4, © 2019 The Authors, under a creative commons license, CC BY-NC-ND 4.0, creativecommons.org/licenses/by-nc-nd/4.0/.

DNA-staining confirmed that after 24 h of treatment with Momundo extracts the number of polyploid (≥ 8N) cells was increased and was even heightened after 48 h. Interestingly, after 24 h of treatment, no dramatic increase of apoptotic sub-G_1 cells was observed (Figure 10) (Lang et al., 2019). Similarly, the inhibition of the cell cycle progression and the induction of polyploid cells was also observed in A549 cells, treated with the cardenolide glycoside acovenoside A, and in MDA-MB-231 cells, treated with a bromochlorinated monoterpene, a synthetic analogue of halogenated monoterpenes from *Plocamium* red algae (El Gaafary et al., 2017; El Gaafary et al., 2019).

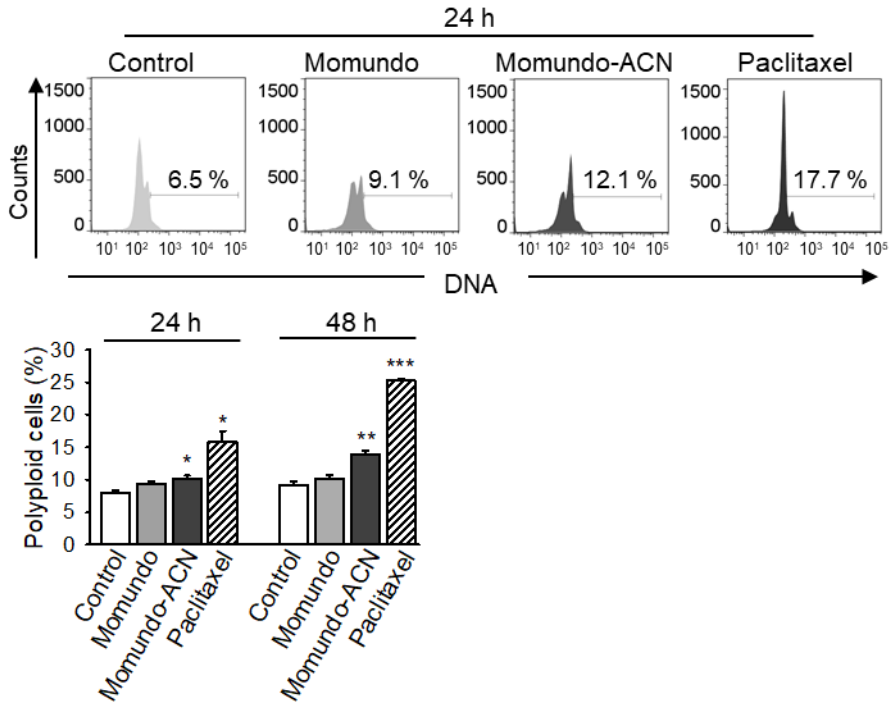

Figure 10: **Momundo *Artemisia annua* extracts arrest the cancer cell cycle and induce formation of polyploid cells (≥ 8N).** MDA-MB-231 breast cancer cells were treated with 100 µg/ml Momundo, 30 µg/ml Momundo-ACN, or 100 nM paclitaxel for 24 and 48 h, followed by DNA-staining with propidium iodide and analysis by flow cytometry. Data are mean ± SEM, $n = 3$, $^{*}p < 0.05$, $^{**}p < 0.01$, $^{***}p < 0.001$. Figure adapted with permission from our own publication (Lang et al., 2019), page 4, © 2019 The Authors, under a creative commons license, CC BY-NC-ND 4.0, creativecommons.org/licenses/by-nc-nd/4.0/.

Paclitaxel is a well-known inductor of mitotic arrest (Flores et al., 2012; Morris and Fornier, 2008). Due to morphological similarities between cells after extract and paclitaxel treatment (Figure 9 and Figure 10), the cell cycle progression of MDA-MB-231 cells after extract treatment was precisely analyzed. Cell cycle analysis demonstrated that the populations of MDA-MB-231 cells in S-phase and G_2/M-phase were concentration-dependently increased and the number of cells in G_0/G_1-phase were respectively reduced. The increase of cells in the S-phase might be a result of accumulated G_2- or M-phase cells undergoing apoptosis (Figure 11) (Lang et al., 2019).

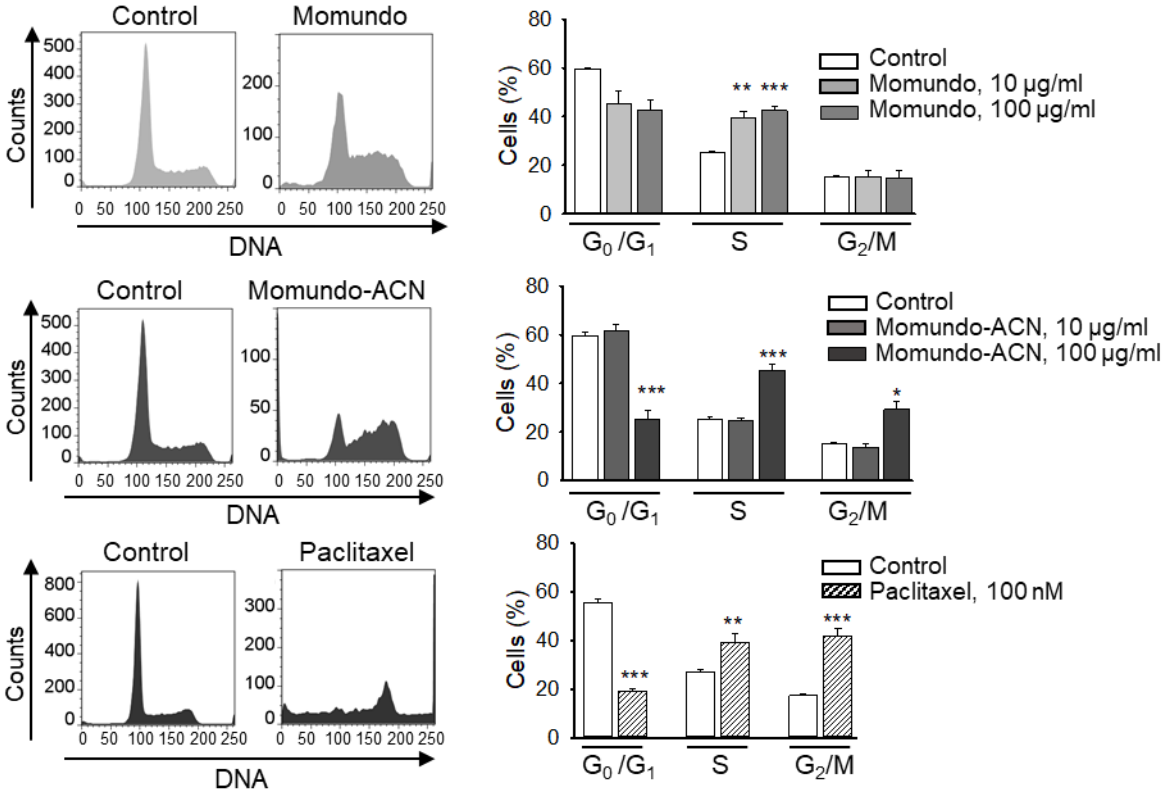

***Figure 11: Artemisia annua* extracts inhibit the cancer cell cycle progression.** MDA-MB-231 cells were treated with 10 and 100 µg/ml Momundo or Momundo-ACN extract, or 100 nM paclitaxel for 48 h. DNA-staining was performed with propidium iodide and the cell cycle progression was analyzed by flow cytometry. Data are mean ± SEM, $n = 3$, $*p < 0.05$, $**p < 0.01$, $***p < 0.001$. Figure adapted with permission from our own publication (Lang et al., 2019), page 4, © 2019 The Authors, under a creative commons license, CC BY-NC-ND 4.0, creativecommons.org/licenses/by-nc-nd/4.0

3.2.3 Momundo Extracts Induce Apoptosis in Breast Cancer Cells *In Vitro*

To analyze if Momundo extracts induce cell death by apoptosis, different characteristic parameters of apoptotic cell death were examined.

One characteristic feature of apoptotic cell death is the fragmentation of the nucleus and formation of apoptotic bodies (Okada and Mak, 2004). The number of cells with hypodiploid DNA-content was significantly increased after treatment with Momundo (10 and 100 µg/ml) from 9.9 % to 16.2 % and 25.1 % as well as with Momundo-ACN from 4.7 % to 11.7 % and 22.3 % after 48 h demonstrating DNA-fragmentation and apoptotic body formation. Paclitaxel served as positive control and a similar increase from 6.8 % to 29.4 % of the hypodiploid subG$_1$ cell population was observed (Figure 12) (Lang et al., 2019).

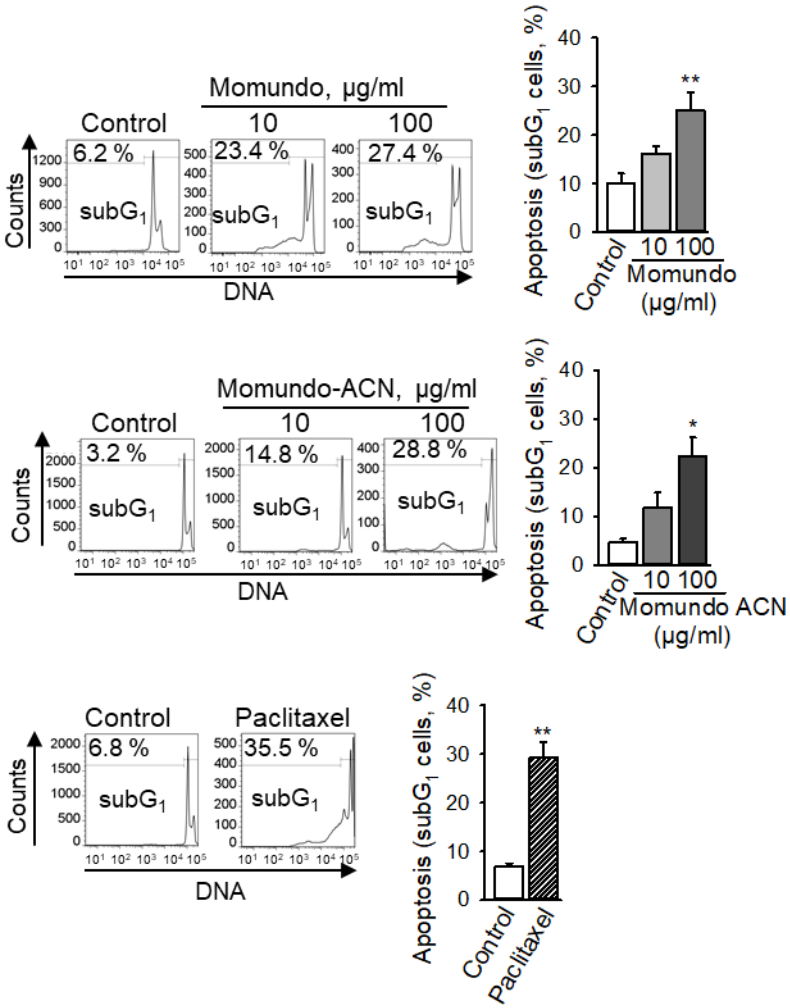

***Figure 12: Artemisia annua* Momundo extracts induce DNA-fragmentation in cancer cells.** MDA-MB-231 cells were treated with Momundo, Momundo-ACN (10, 100 µg/ml, each), or paclitaxel (100 nM), followed by propidium iodide staining and flow cytometry. The percentages of apoptotic cells with hypodiploid DNA-content are shown. Data are mean ± SEM, $n = 4$, *$p < 0.05$, **$p < 0.01$. Figure adapted with permission from our own publication (Lang et al., 2019), page 6, © 2019 The Authors, under a creative commons license, CC BY-NC-ND 4.0, creativecommons.org/licenses/by-nc-nd/4.0/.

Mitochondria promote apoptosis by the release of cytochrome c and additional pro-apoptotic molecules into the cytosol, which leads to activation of caspase 3 (Okada and Mak, 2004). Analysis of the mitochondrial membrane potential (ΔΨm) demonstrated significant loss of the mitochondrial integrity after treatment with 100 nM paclitaxel or 10 µg/ml Momundo after 48 and 72 h, respectively. The percentage of cells with reduced mitochondrial membrane potential after 72 h was increased from 4.0 % to 18.1 % after treatment with Momundo extract and to 43.4 % after paclitaxel treatment revealing permeabilization of the mitochondrial membrane (Figure 13) (Lang et al., 2019).

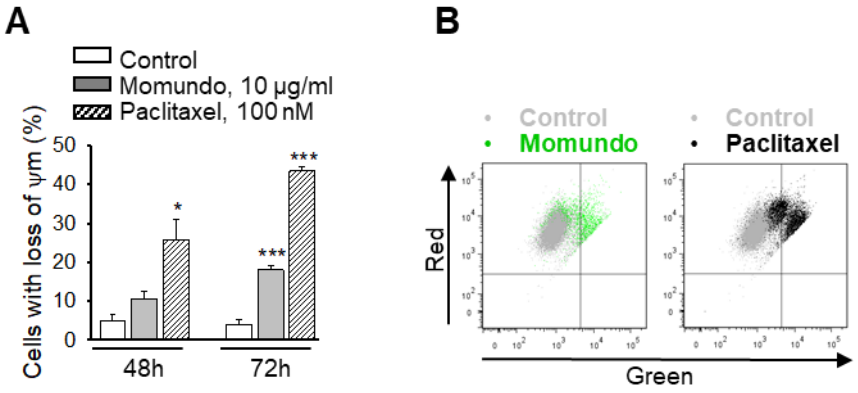

Figure 13: **Momundo extract treatment induces loss of mitochondrial integrity in cancer cells.** (A) MDA-MB-231 TNBC cells were treated with either 10 µg/ml Momundo extract or 100 nM paclitaxel for 48 and 72 h. Cells with reduced mitochondrial membrane potential (ΔΨm) were analyzed after incubation with JC-1 dye and flow cytometry. Percentage of cells with loss of ΔΨm is shown. (B) Representative dot blots of cells treated for 72 h are shown. Data are mean ± SEM, $n = 3$, $^{*}p < 0.05$, $^{***}p < 0.001$. Figure adapted with permission from our own publication (Lang et al., 2019), page 6, © 2019 The Authors, under a creative commons license, CC BY-NC-ND 4.0, creativecommons.org/licenses/by-nc-nd/4.0/.

Disruption of the mitochondrial function can result in cytochrome c release, followed by activation of Apaf-1 and caspase 3 (Wong, 2011). Hence, the activity of caspase 3 was analyzed. Treatment with Momundo extract (10 or 100 µg/ml) induced caspase 3 activation suggesting involvement of the intrinsic apoptotic pathway (Figure 14) (Lang et al., 2019).

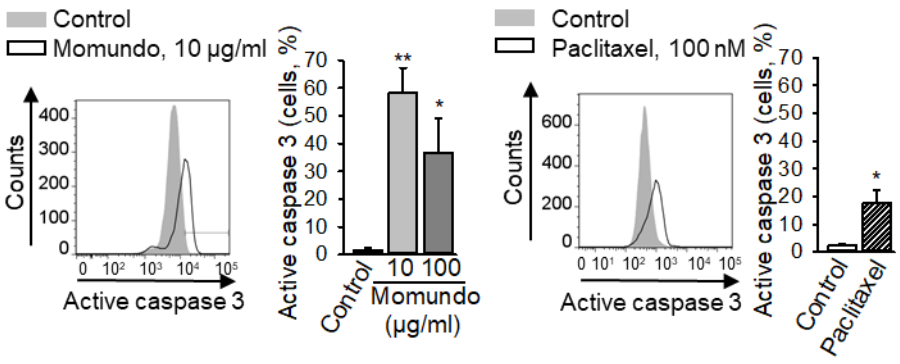

Figure 14: **Momundo extract treatment activates caspase 3 in cancer cells.** After treatment of MDA-MB-231 TNBC cells with Momundo (10 or 100 µg/ml) or paclitaxel (100 nM) for 48 h, the cells were incubated with the fluorogenic caspase 3 substrate Z-DEVD-R110 and were analyzed flow cytometrically. Data are mean ± SEM, $n = 3$, $*p < 0.05$, $**p < 0.01$. Figure adapted with permission from our own publication (Lang et al., 2019), page 6, © 2019 The Authors, under a creative commons license, CC BY-NC-ND 4.0, creativecommons.org/licenses/by-nc-nd/4.0/.

3.2.4 Momundo Extracts Inhibit Proliferation of Breast Cancer Xenografts *In Vivo* Grown on the CAM

To verify the antitumor activity *in vivo*, 3D breast cancer xenografts, grown on the chick chorioallantoic membrane of fertilized chick eggs, were analyzed (Skowron et al., 2017; Syrovets et al., 2005). Momundo and Momundo-ACN extracts dose-dependently inhibited tumor growth of breast cancer xenografts *in vivo*, as indicated by significantly reductions of the tumor volume from 13.2 mm^3 to 8 mm^3 and 4.3 mm^3 after treatment with Momundo (10 and 100 µg/ml) and from 14.5 mm^3 to 8.9 mm^3 and 2.8 mm^3 after treatment with Momundo-ACN (10 and 100 µg/ml), respectively (Figure 15) (Lang et al., 2019).

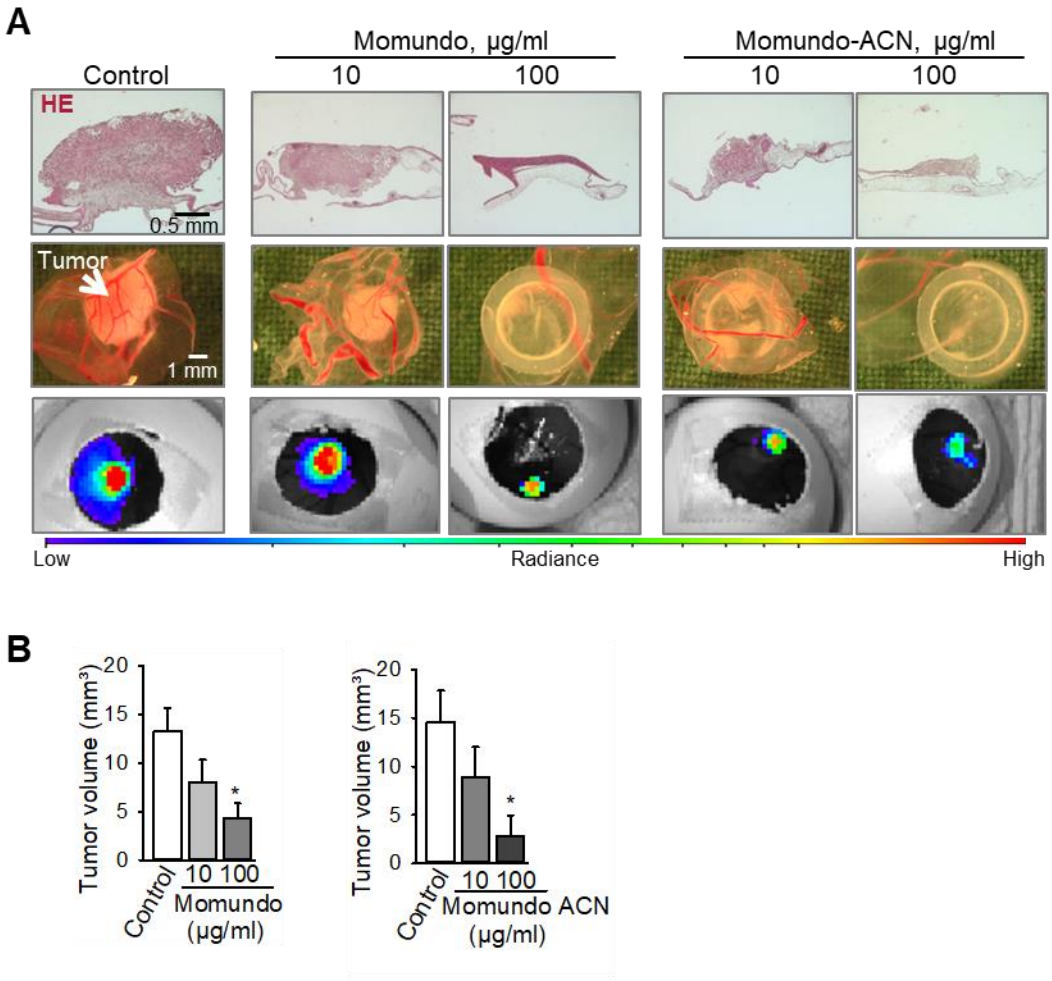

Figure 15: **Momundo *Artemisia annua* extracts inhibit the growth of MDA-MB-231 TNBC xenografts *in vivo*.** MDA-MB-231 xenografts grown on the chorioallantoic membranes (CAM) of fertilized chick eggs were treated with 20 µl of the respective extract (10 and 100 µg/ml) for three consecutive days. The xenografts were analyzed by life imaging using an IVIS system and immunohistochemistry on day four after treatment initiation. (A) Upper row: hematoxylin and eosin staining, center row: tumor images after extraction and bottom row: *in ovo* bioluminescence imaging of tumors after addition of D-luciferin. (B) Mean tumor volumes are shown. Results are expressed as mean ± SEM of $n \geq 7$ tumors/group, Kruskal-Wallis test, Dunn's post-hoc test, $*p < 0.05$. Figure adapted with permission from our own publication (Lang et al., 2019), page 7, © 2019 The Authors, under a creative commons license, CC BY-NC-ND 4.0, creativecommons.org/licenses/by-nc-nd/4.0/.

The inhibition of cell proliferation was further confirmed by immunohistochemical analysis of 5 µm tumor-slices indicating reduced expression of the proliferation marker Ki-67 (Figure 16A). Momundo 10 and 100 µg/ml reduced the Ki-67 expression from 21.2 % in the control group to 11.1 % and 8.5 %, respectively and Momundo-ACN 10 and 100 µg/ml from 18.5 % to 10.8 % and 1.3 %, respectively. Moreover, TUNEL-staining revealed DNA strand breaks and apoptotic

cell death *in vivo* (Figure 16B). Importantly, no overt toxic effects on the chick embryo could be observed (Lang et al., 2019).

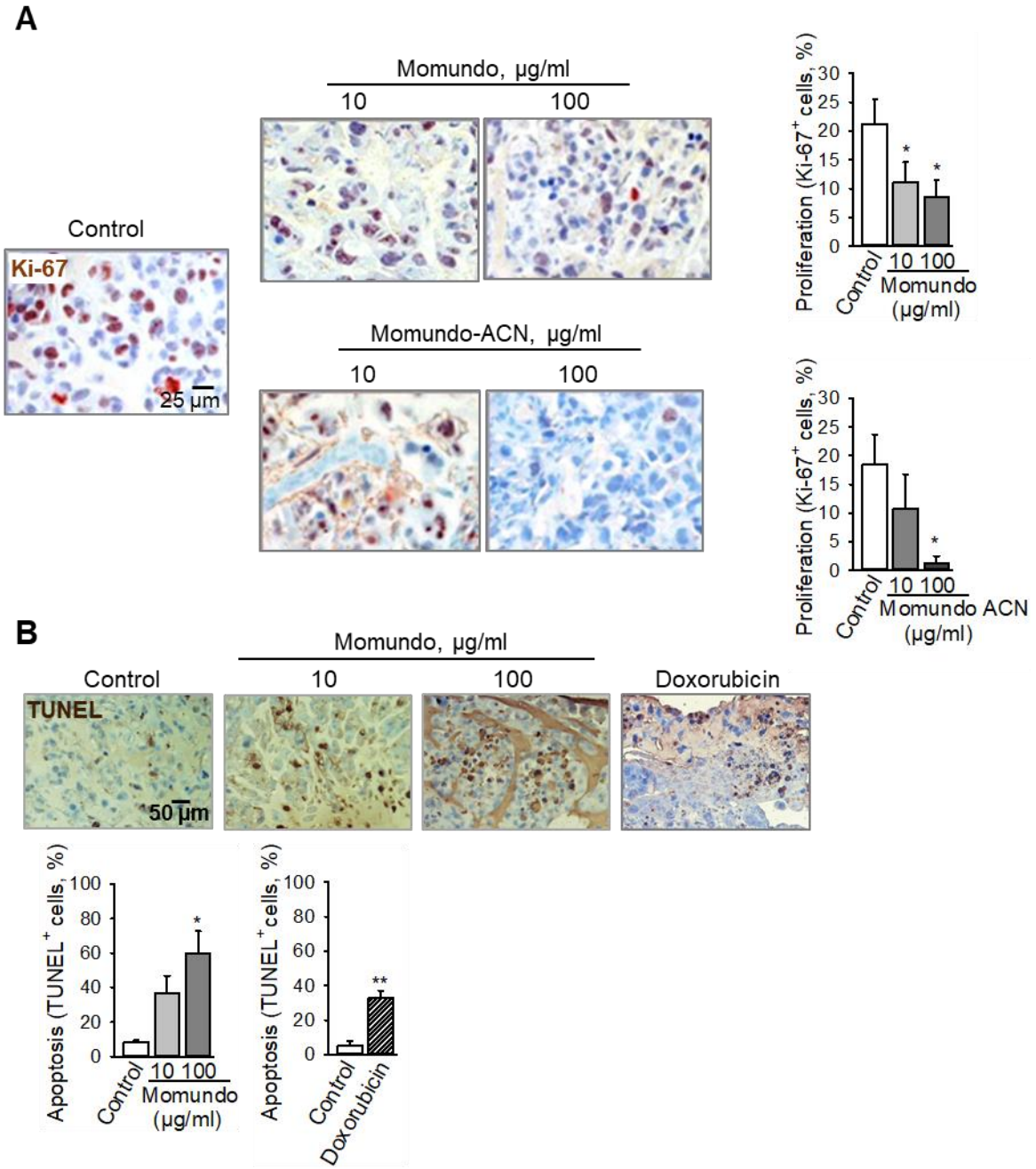

Figure 16: **Momundo extract treatment reduces the expression of the proliferation marker Ki-67 and induces apoptosis in breast cancer xenografts grown on the CAM *in vivo*.** (A) MDA-MB-231 xenografts were treated with 20 µl of the respective extracts (10 and 100 µg/ml) for three consecutive days and were analyzed immunohistochemically using antibodies against Ki-67. Representative pictures after staining of Ki-67 proliferation antigen (red-brown nuclear stain), original magnification 200x and quantification of Ki-67$^+$ are shown. (B) Representative pictures after TUNEL staining and quantification

of TUNEL$^+$ cells. Doxorubicin (1 µM) served as positive control. Data are mean ± SEM of $n \geq 5$ tumors/group, Kruskal-Wallis test and Dunn's post-hoc multi-group test, or Mann-Whitney rank sum test for 2 groups, $*p < 0.05$, $**p < 0.01$. Figure adapted with permission from our own publication (Lang et al., 2019), page 7, © 2019 The Authors, under a creative commons license, CC BY-NC-ND 4.0, creativecommons.org/licenses/by-nc-nd/4.0/.

3.2.5 Momundo Extract Treatment Inhibits Tumor Growth in Nude Mice

Since the extracts effectively inhibited tumor growth in the CAM assay (Figure 15 and Figure 16) and because of limitations of the CAM *in vivo* model (Nowak-Sliwinska et al., 2014), the effectiveness of the Momundo *Artemisia annua* extract was further evaluated in orthotopic breast cancer xenografts in athymic nude mice. The animals were treated with the Momundo-HP-β-CD complex daily over three weeks or the vehicle for the negative control (Figure 17A). Doxorubicin was administered once a week because of its high toxicity. Tumor growth was effectively retarded in mice treated with Momundo daily and doxorubicin weekly (Figure 17B). Body weight was monitored once a week and was significantly reduced in mice treated with doxorubicin. In contrast, the animals which had been treated with the Momundo *Artemisia annua* extract slightly gained some weight (Figure 17C). Moreover, doxorubicin significantly increased plasma levels of AST and ALT liver enzymes, revealing hepatic toxicity. Also, treatment with Momundo extract slightly increased AST and ALT liver enzymes but considerably less compared to doxorubicin-treated mice suggesting lower systemic toxicity (Figure 17D) (Lang et al., 2019).

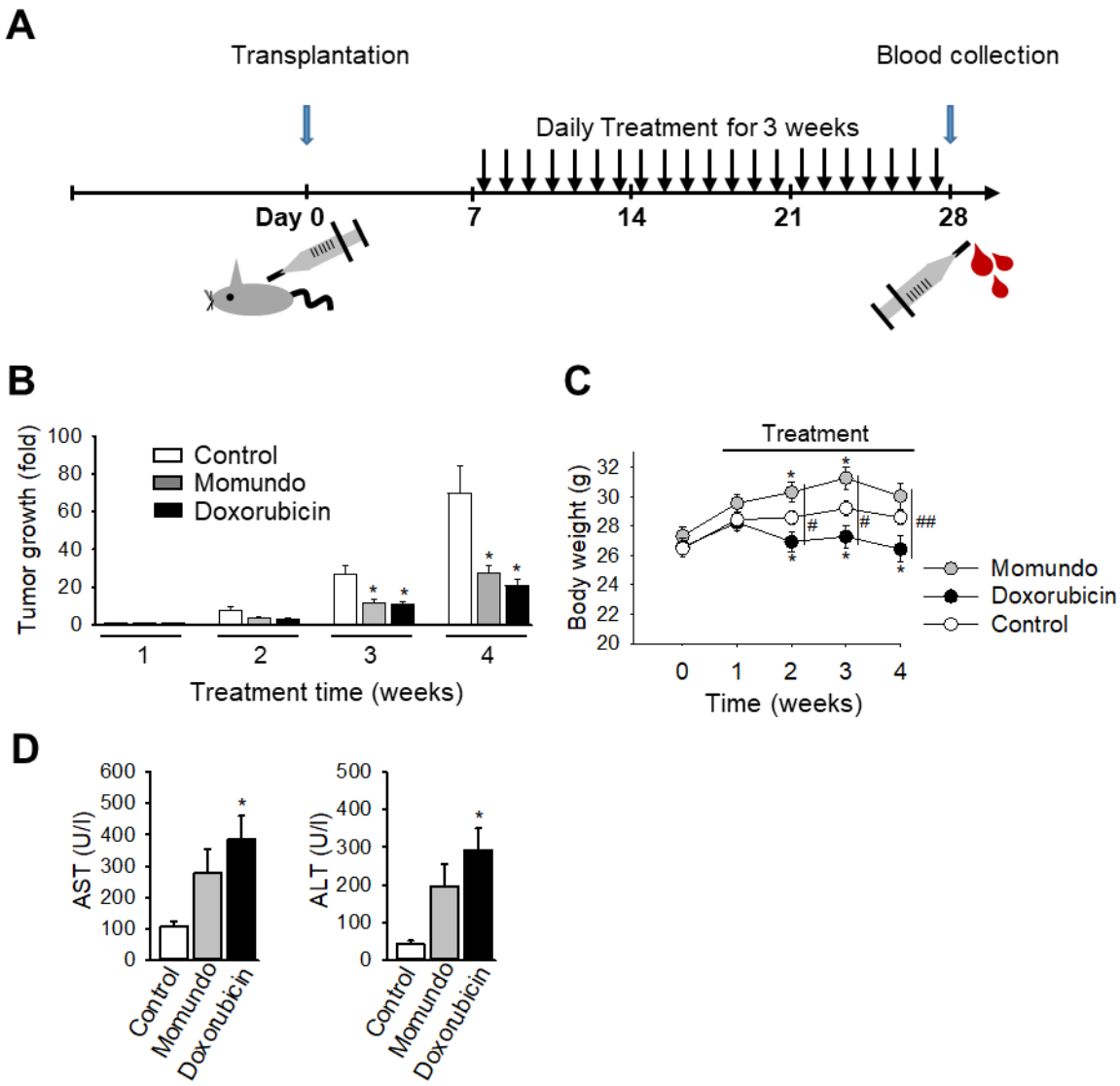

Figure 17: **Momundo *Artemisia annua* extract inhibits tumor growth in nude mice.** (A) Scheme of the treatment procedure. Mice with pre-established orthotopic MDA-MB-231 xenografts were treated with 100 mg kg^{-1} day^{-1} Momundo extract or cyclodextrin solvent daily, or with 2 mg kg^{-1} $week^{-1}$ doxorubicin for three consecutive weeks. (B) The x-fold tumor growth is shown. The tumor volume was normalized to the average tumor volume measured at treatment initiation. (C) The body weights of the mice were monitored weekly. (D) Momundo extract treatment slightly increased the hepatic liver enzymes AST and ALT. Data are mean ± SEM of $n = 8$ (B, C) and $n = 4$ (D) mice per group; Kruskal-Wallis and Dunn's post-hoc test (B), Newman-Keuls test (C), $*p < 0.05$ Momundo or doxorubicin vs. control, $\#p < 0.05$ and $\#\#p < 0.01$ Momundo vs. doxorubicin. Figure adapted with permission from our own publication (Lang et al., 2019), page 8, © 2019 The Authors, under a creative commons license, CC BY-NC-ND 4.0, creativecommons.org/licenses/by-nc-nd/4.0/.

3.3 Antitumor Activity of the Pure Compounds Identified in the Momundo *Artemisia annua* dietary supplement

3.3.1 Chrysosplenol D and Casticin Selectively Inhibit the Viability of Cancer Cells

To identify distinct ingredients with antiproliferative activity in the Momundo dietary supplement, the cytotoxity of pure compounds was examined next. Chrysosplenol D, casticin, and arteannuin B were identified as the most active ingredients of the Momundo *Artemisia annua* extract. These compounds effectively inhibited the proliferation of MDA-MB-231 breast cancer cells already after 24 h of treatment (Figure 18) (Lang et al., 2019).

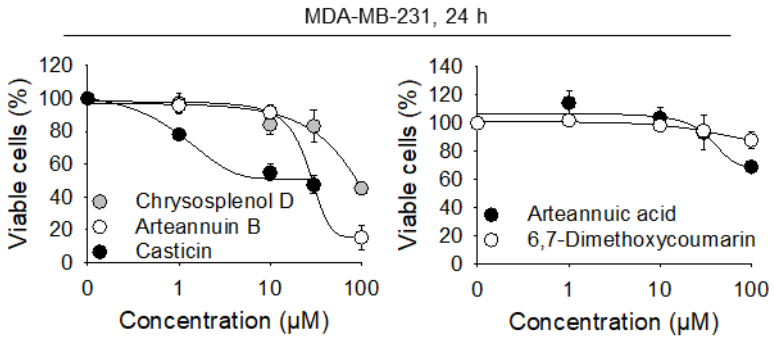

Figure 18: **Three out of five isolated main ingredients from Momundo extract effectively inhibit cancer cell proliferation.** MDA-MB-231 cells were treated with the isolated compounds for 24 h. Viability was analyzed by XTT assay, *n* = 3-5. Figure adapted with permission from our own publication (Lang et al., 2019), page 9, © 2019 The Authors, under a creative commons license, CC BY-NC-ND 4.0, creativecommons.org/licenses/by-nc-nd/4.0/.

The most abundant components of the extract, chrysosplenol D, casticin, 6,7-dimethoxycoumarin, and arteannuic acid, were additionally analyzed concerning their toxicity towards four treatment-resistant cancer cell lines of different origin. In contrast to chrysosplenol D and casticin, 6,7-dimethoxycoumarin and arteannuic acid demonstrated no toxicity towards all five cancer cell lines within 48 h (Figure 19A,B). Toxicity of the identified substances was also compared to the toxicity of artemisinin. Notably, artemisinin did not reveal any remarkable antiproliferative or toxic effect towards any cancer cell line tested exhibiting IC_{50} > 100 µM after 48 h (Figure 19A,B) (Lang et al., 2020).

The two flavonols, chrysosplenol D and casticin, exhibited remarkable toxicity towards all five cancer cell lines of different origin although with varying efficacies. The non-small-cell lung carcinoma (NSCLC) cell line A549 was the most sensitive one towards chrysosplenol D and casticin treatment exhibiting IC_{50} values of 7.3 and 1.8 µM, respectively. The androgen-independent prostate carcinoma cell line PC-3, was the most resistant one with IC_{50} values of 40.8

and 73.1 µM towards chrysosplenol D and casticin, respectively. The hormone-sensitive breast cancer cells MCF-7 were more sensitive to casticin treatment (IC_{50} = 16 µM) than to chrysosplenol D (IC_{50} = 36.4 µM). MIA PaCa-2 pancreas cancer cells were highly sensitive towards casticin, exhibiting an IC_{50} of 0.7 µM. Interestingly, despite the structural similarity of casticin and chrysosplenol D, the IC_{50} value of chrysosplenol D for MIA PaCa-2 cells was with 35.6 µM much higher (Figure 19A) (Lang et al., 2020).

The viability of triple-negative breast cancer cells MDA-MB-231 was inhibited after 48 h by chrysosplenol D and casticin with IC_{50} values of 11.6 and 19.5 µM, respectively. Similar to paclitaxel, casticin inhibited the proliferation of only a proportion of cells. In contrast, no viable cells could be detected after treatment with high concentrations of chrysosplenol D (Figure 19B). Noteworthy, both flavonols exhibited only little toxic effects on peripheral blood mononuclear cells (PBMC) demonstrating selectivity towards cancer cells (Figure 19B) (Lang et al., 2020).

Finally, the normalized growth rate inhibition (GR) was calculated. This method is insensitive to the duration of the viability assay and the doubling time of the cells (Hafner et al., 2016). Chrysosplenol D and casticin exhibited a GR_{50} value of 6.7 µM and 4.0 µM on MDA-MB-231 cells, respectively (Figure 19C). The GR_{max} value was positive for casticin demonstrating, similar to paclitaxel, rather cytostatic effects, whereas GR_{max} was negative for cells treated with chrysosplenol D indicating a cytotoxic molecular mode of action. Calculation of GR_{50} values of additional treatment-resistant cancer cells showed a significant correlation (p = 0.00009) of GR_{50} and IC_{50} values of the analyzed cancer cells treated with chrysosplenol D and casticin (Figure 19C).

The identified active flavonols chrysosplenol D and casticin were further analyzed regarding their potential antitumor efficacies and apoptosis-inducing properties. Chrysosplenol D was of particular interest, as nearly no data about its potential antitumor efficacy were available.

A

Tissue	Cell line	p53 status	IC_{50}, µM, 48h				
			Chrysosplenol D	Casticin	6,7-Dimethoxy-coumarin	Arteannuic acid	Artemisinin
Breast	MDA-MB-231	mut GOF	11.6 ± 4.1	19.5 ± 3.2	> 100	> 100	> 100
Breast	MCF7	wt	36.4. ± 2.7	16.0 ± 1.4	> 100	> 100	> 100
NSCLC	A549	wt	7.3 ± 0.3	1.8 ± 0.1	> 100	> 100	> 100
Pancreas	MIA PaCa-2	mut GOF	35.6 ± 11.6	0.7 ± 0.1	> 100	> 100	> 100
Prostate	PC-3	-	40.8 ± 6.1	73.1 ± 5.9	> 100	> 100	> 100

B

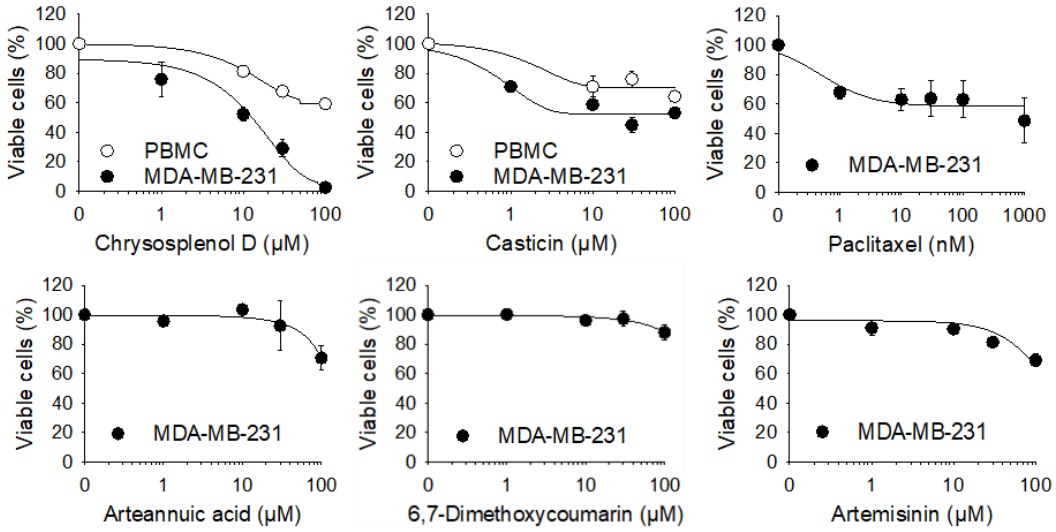

C

Tissue	Cell line	GR_{50}, µM	
		Chrysosplenol D	Casticin
Breast	MDA-MB-231	6.7	4.0
Breast	MCF7	24.3	6.8
NSCLC	A549	3.0	1.6
Pancreas	MIA PaCa-2	34.4	0.3
Prostate	PC-3	25.6	61.2

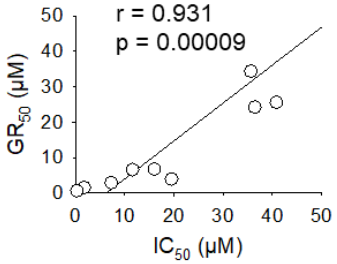

***Figure 19*: Chrysosplenol D and casticin inhibit the viability of a variety of treatment-resistant cancer cells, whereas 6,7-dimethoxycoumarin, arteannuic acid, and artemisinin show no remarkable toxicity.** (A) Cancer cell lines of different origin were treated with the respective compounds for 48 h, followed by analysis of cell viability by the XTT assay. NSCLC – non-small cell lung cancer. (B) MDA-MB-231 TNBC cells and PBMC were treated as in (A) and were analyzed by XTT. Paclitaxel served as positive control. PBMC are relatively resistant towards chrysosplenol D and casticin treatment. (C) GR_{50} (half maximal growth rate inhibition) of chrysosplenol D and casticin on different treatment resistant cancer cells. Cells were treated as in (A) and GR_{50} were analyzed as described by (Hafner et al., 2016). Pearson Moment Correlation of GR_{50} and IC_{50} values. Data are mean ± SEM of n = 3-5. Figure

3.3.2 Chrysosplenol D and Casticin Inhibit the Progression of the Cancer Cell Cycle

Cell cycle deregulation along with uncontrolled proliferation is a characteristic feature of cancer. Many types of neoplasias can be selectively targeted through inhibition of regulatory cell cycle proteins revealing an attractive target for anticancer therapeutics (Malumbres and Barbacid, 2009; Otto and Sicinski, 2017). The Momundo *Artemisia annua* extract treatment of MDA-MB-231 cells induced cell cycle perturbations and accumulation of the cells in the S-phase and G_2/M-phase (Figure 11). Therefore, effects of chrysosplenol D and casticin on the cancer cell cycle were analyzed next. Chrysosplenol D induced accumulation of the cells in the S-phase and increased the number of cells in the G_2/M-phase of the cell cycle. The percentage of cells in the G_1-phase was concentration-dependently reduced (Figure 20A). The accumulation of cells in the S-phase might be a result of cell death in G_2/M-phase, which could be particularly sensitive to chrysosplenol D and undergo apoptosis resulting in DNA-fragmentation and reduced DNA-contents (Lang et al., 2020). In contrast, the tubulin-binding agent casticin (Haidara et al., 2006) induced a strong, concentration-dependent accumulation of the cells in the G_2/M-phase and the number of cells in the G_1-phase was accordingly reduced. The induced accumulation of MDA-MB-231 cells in the G_2/M-phase was similar to cell cycle arrest induced by 100 nM paclitaxel (Figure 20B), a known inductor of M-phase-arrest due to its tubulin-binding efficacies (Morris and Fornier, 2008).

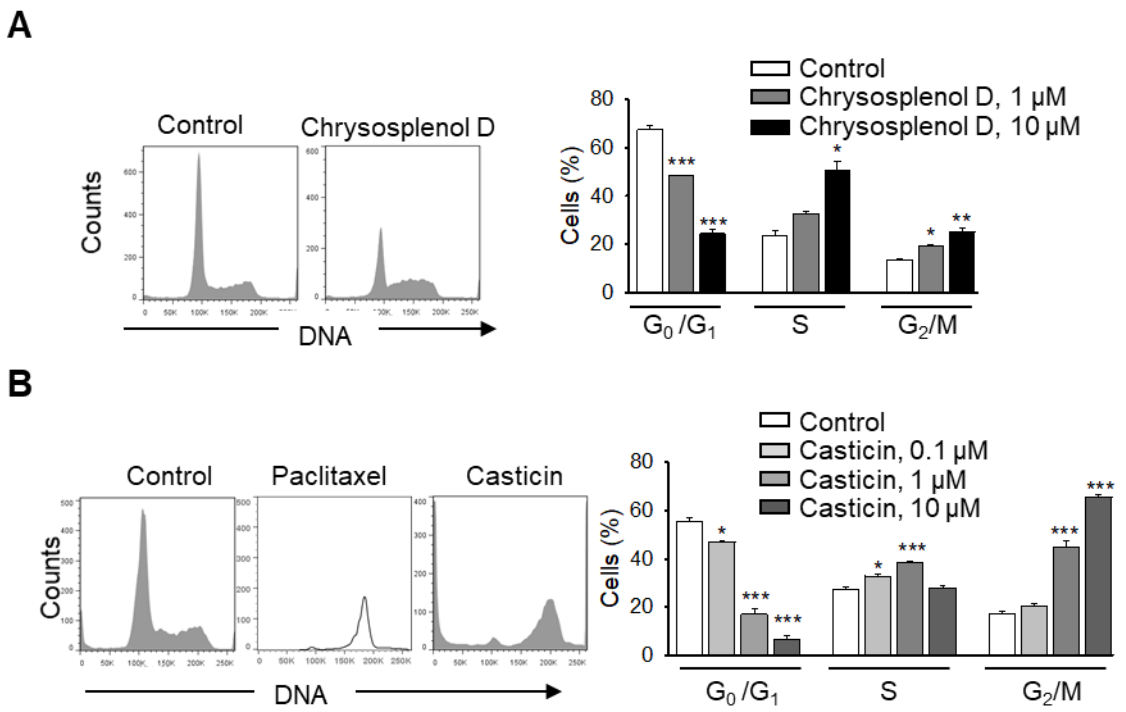

Figure 20: **Chrysosplenol D and casticin induce cell-cycle perturbations in treatment-resistant TNBC cells.** (A) MDA-MB-231 cells were incubated with chrysosplenol D (1 or 10 µM) for 48 h, followed by DNA-staining with propidium iodide and cell-cycle analysis by flow cytometry. Representative histograms are shown (left panel) after treatment with 1 µM chrysosplenol D. (B) MDA-MB-231 TNBC cells were incubated with casticin (0.1, 1 or 10 µM) for 48 h and were analyzed as described in (A). Representative histograms (left panel) are shown for casticin (1 µM, 48 h) and paclitaxel (100 nM, 24 h). Data are mean ± SEM, $n = 3$, $*p < 0.05$, $**p < 0.01$, $***p < 0.001$. Figure adapted with permission from our own publication (Lang et al., 2020), page 5, © 2020 The Authors, under a creative commons license, CC BY 4.0, http://creativecommons.org/licenses/by/4.0/.

3.3.3 Chrysosplenol D and Casticin Induce Apoptosis

In the scenario of cancer, apoptosis is suppressed and induction of apoptosis is therefore an important treatment strategy (Wong, 2011). Due to the fact that Momundo *Artemisia annua* extracts induced apoptotic cell death, it was further analyzed whether treatment with the identified active ingredients might induce apoptosis as well.

An early marker of apoptosis is the loss of the asymmetric distribution of phosphatidylserine (PS). Once apoptosis occurs, PS is exposed to the outer leaflet of the cell membrane, where it acts as recognition marker for macrophages (Taylor et al., 2008). FITC-coupled annexin V is a widely used indicator to detect PS-exposure. In the present study, propidium iodide (PI)/annexin V-FITC double staining was performed. This allows to distinguish between apoptotic and necrotic cell death, because the DNA-intercalating PI is excluded from cells with an intact plasma

membrane. A significant increase of early apoptotic cells (annexin V^+/PI^- cells) could be detected by flow cytometry after 48 h. Compared to the vehicle control, chrysosplenol D treatment for 48 h increased the percentage of early apoptotic cells from 6.7 % to 15.8 % and casticin to 16.8 %. The positive control paclitaxel likewise increased the percentage of annexin V^+/PI^- cells from 5.1 % to 15.7 % after 48 h (Figure 21) (Lang et al., 2020).

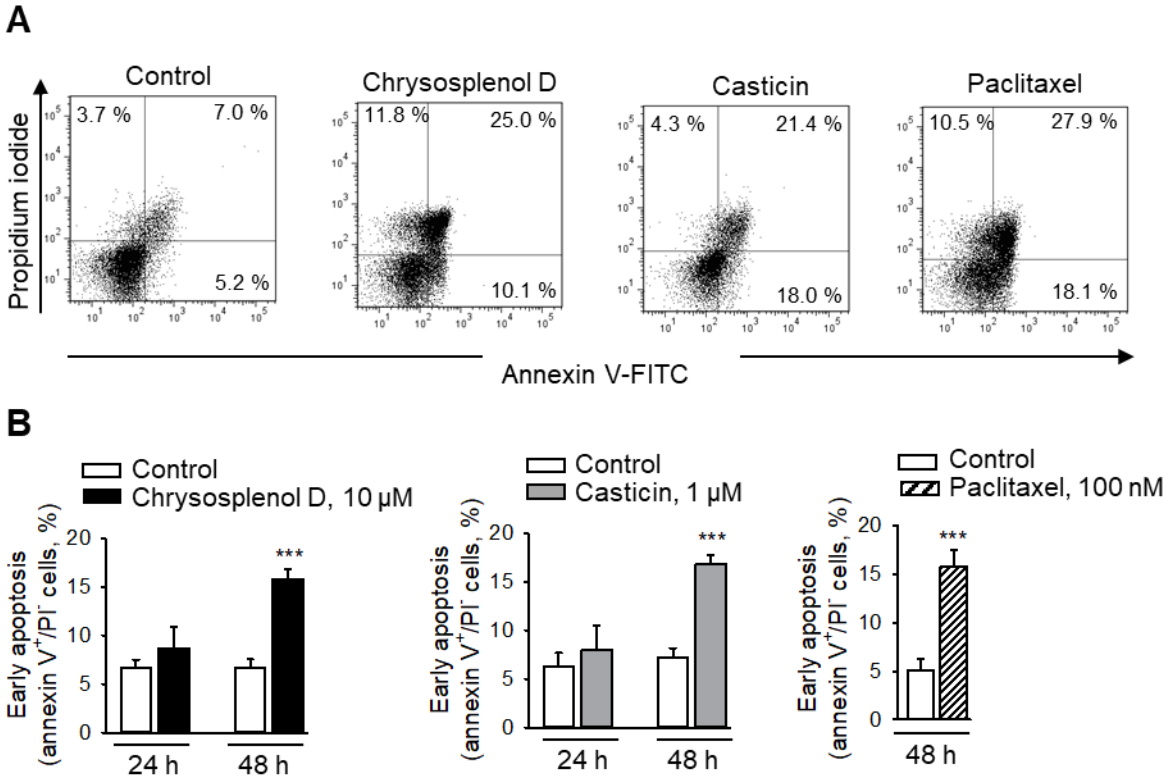

Figure 21: **Chrysosplenol D and casticin increase the number of early apoptotic MDA-MB-231 cells.** Cells were treated for 24 or 48 h with chrysosplenol D (10 µM), casticin (1 µM), or paclitaxel (100 nM), followed by staining with annexin V-FITC/propidium iodide and analysis by flow cytometry. (A) Representative dot blots after treatment for 48 h are shown. (B) Graphs show percentage of early apoptotic cells (annexin V^+/PI^- cells). Data are mean ± SEM, n = 3-5, ***p < 0.001. Figure adapted with permission from our own publication (Lang et al., 2020), page 6, © 2020 The Authors, under a creative commons license, CC BY 4.0, http://creativecommons.org/licenses/by/4.0/.

Another highly characteristic, late occurring feature of apoptosis is the fragmentation of DNA and the loss of nuclear DNA content due to the formation of apoptotic bodies (Riccardi and Nicoletti, 2006) as already described in section 3.2.3. Treatment with low concentrations of chrysosplenol D (1 µM) or casticin (0.1 µM) for 48 h induced DNA-fragmentation and significantly increased the percentage of cells with hypodiploid DNA contents (Figure 22). This increase was similar to that seen in MDA-MB-231 cells treated with paclitaxel (100 nM) (Lang et al., 2020).

These results reveal apoptosis induced by the *Artemisia annua* flavonols chrysosplenol D and casticin.

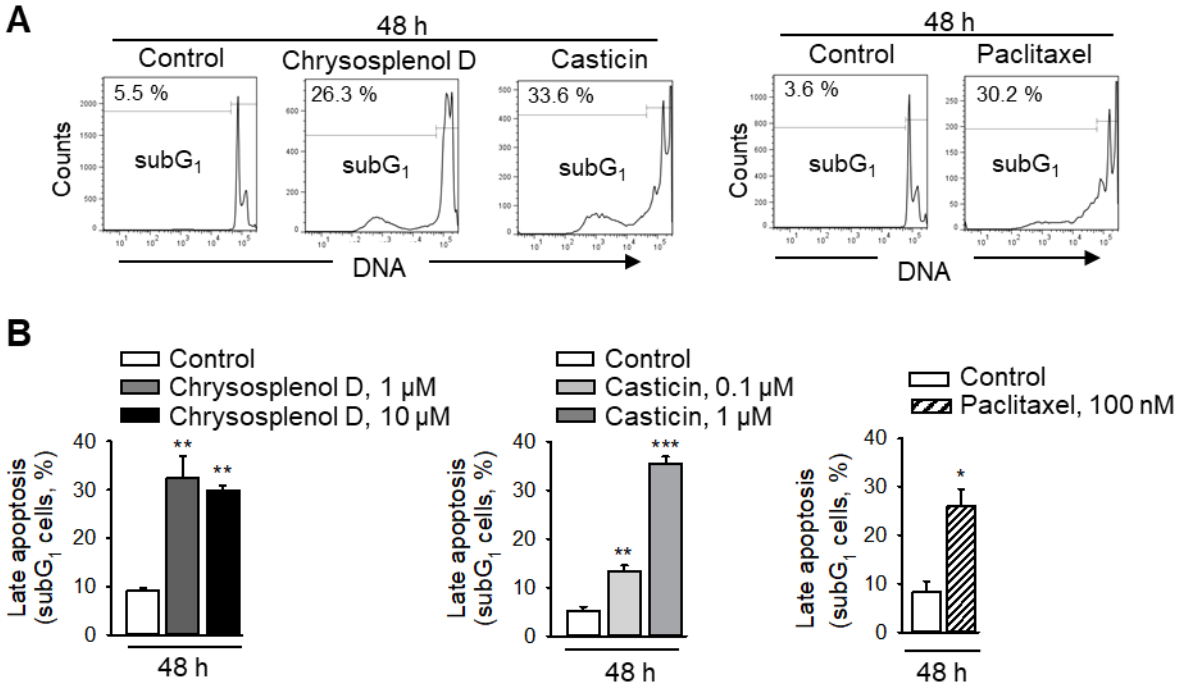

Figure 22: **Chrysosplenol D and casticin induce DNA fragmentation in cancer cells.** MDA-MB-231 cells were treated with chrysosplenol D (1 or 10 µM), casticin (0.1 or 1 µM), or paclitaxel (100 nM), followed by DNA-staining with propidium iodide in the presence of DNase-free RNase A and analysis by flow cytometry. (A) Representative histograms of chrysosplenol D (10 µM) and casticin (1 µM) are shown. (B) Quantification of $subG_1$ cells. Data are mean ± SEM, $n = 3$, $^*p < 0.05$, $^{**}p < 0.01$, $^{***}p < 0.001$. Figure adapted with permission from our own publication (Lang et al., 2020), page 6, © 2020 The Authors, under a creative commons license, CC BY 4.0, http://creativecommons.org/licenses/by/4.0/.

3.3.4 Chrysosplenol D and Casticin Inhibit Growth of Breast Cancer Xenografts *In Vivo*

Furthermore, antiproliferative efficacy of the identified components of the Momundo *Artemisia annua* extract with potent antiproliferative and apoptosis-inducing efficacy was analyzed *in vivo*. After chrysosplenol D and casticin treatment (both 30 µM), the tumor growth of MDA-MB-231 xenografts grown on the chorioallantoic membranes of fertilized chick eggs was effectively inhibited (Figure 23A). Quantification of Ki-67$^+$ cells demonstrated a significant reduction of proliferating cells. The percentage of these cells was reduced from 100 % proliferation in the control group to 40.7 % after three days of topical treatment with chrysosplenol D and to 8.3 % after treatment with casticin demonstrating potent antiproliferative efficacy *in vivo*. By contrast, the standard chemotherapeutic doxorubicin (1 µM) reduced the number of proliferating Ki-67$^+$ cells to 25.5 % (Figure 23B) (Lang et al., 2020).

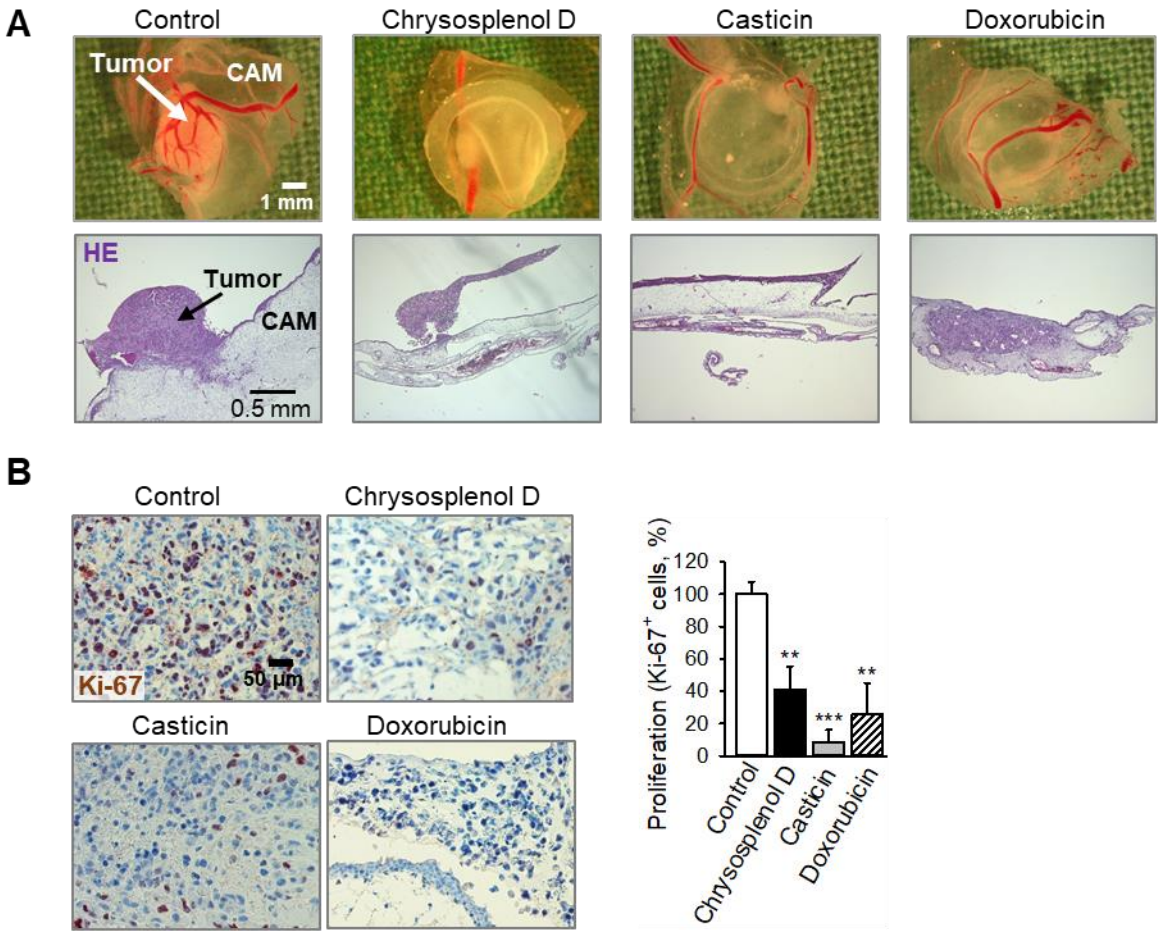

***Figure 23*: Chrysosplenol D and casticin inhibit tumor growth of MDA-MB-231 breast cancer xenografts grown on chick chorioallantoic membranes (CAM).** MDA-MB-231 xenografts grown on the CAM were treated with chrysosplenol D (30 µM), casticin (30 µM), or doxorubicin (1 µM) for three consecutive days. The compounds were applied topically in 0.9 % NaCl (final DMSO concentration 0.5 %). On day four after treatment initiation, tumors were collected, imaged, and embedded in paraffin for immunohistochemical analysis. (A) Representative pictures of tumor xenografts immediately after extraction are shown (upper row) and hematoxylin and eosin (HE) staining (bottom row, original magnification 50x). (B) Ki-67$^+$ cells (red nuclear stain) as analyzed by immunohistochemistry. Representative pictures are shown on the left hand side (original magnification 200x) and quantification of proliferating Ki-67-positive cells on the right hand side. Data are mean ± SEM, n = 4-7, $^{**}p < 0.01$, $^{***}p < 0.001$. Figure adapted with permission from our own publication (Lang et al., 2020), page 7, © 2020 The Authors, under a creative commons license, CC BY 4.0, http://creativecommons.org/licenses/by/4.0/.

3.3.5 Chrysosplenol D and Casticin Induce Loss of Mitochondrial Integrity

Since treatment with the Momundo *Artemisia annua* extract induced loss of the mitochondrial membrane integrity, the effect of chrysosplenol D and casticin on the mitochondrial integrity

was also analyzed using the lipophilic cationic JC-dye. Cells with reduced mitochondrial membrane potential can be detected by a fluorescence shift from red to green. Paclitaxel served as positive control.

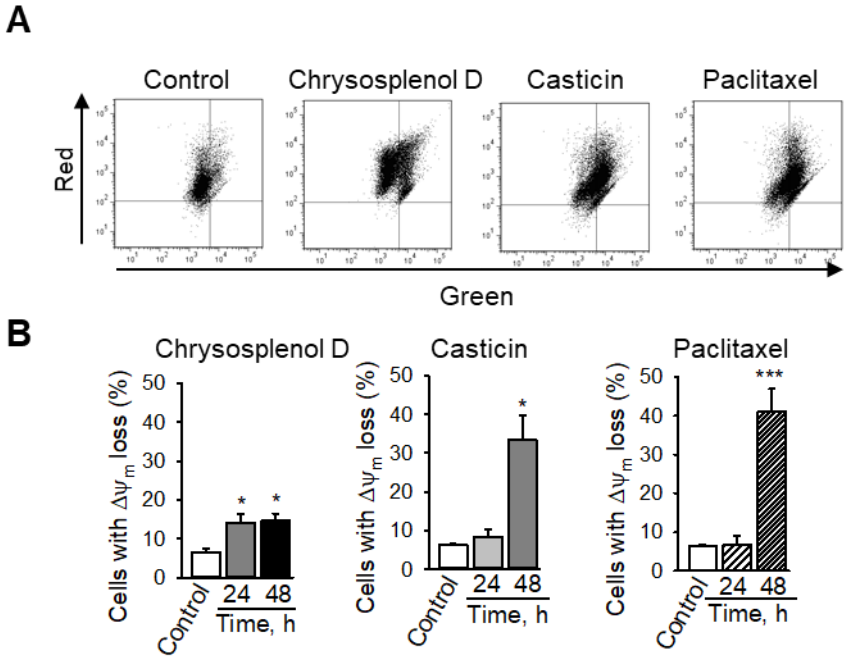

Figure 24: **Chrysosplenol D and casticin affect the mitochondrial membrane integrity in cancer cells.** (A) MDA-MB-231 breast cancer cells were treated with 10 µM chrysosplenol D, 1 µM casticin, or 100 nM paclitaxel. After 24 and 48 h, cells were stained with the mitochondrial potential sensor JC-1 and were analyzed by flow cytometry. Representative dot plots after 48 h are shown. (B) Cells were treated as in (A) and percentages of cells with loss of mitochondrial membrane potential (ΔΨm) were quantified. Data are mean ± SEM, n = 3-4, *p < 0.05, ***p < 0.001. Figure adapted with permission from our own publication (Lang et al., 2020), page 8, © 2020 The Authors, under a creative commons license, CC BY 4.0, http://creativecommons.org/licenses/by/4.0/.

Treatment with 10 µM chrysosplenol D significantly increased the number of cells with dissipation of the mitochondrial membrane potential already after 24 h from 6.5 % to 14.2 %. In contrast, treatment with 1 µM casticin, similar to treatment with 100 nM paclitaxel, induced loss of ΔΨm only after 48 h. The number of cells with mitochondrial membrane dissipation was increased from 6.3 % to 33.5 % after treatment with the tubulin-binding casticin (Haidara et al., 2006) and to 41.1 % after treatment with paclitaxel for 48 h. In chrysosplenol D-treated cells, loss of mitochondrial membrane potential takes place 24 h earlier (Figure 24) pointing to an active role of mitochondria in the induction of apoptotic cell death (Lang et al., 2020).

3.3.6 Chrysosplenol D and Casticin Induce Oxidative Stress in Breast Cancer Cells

Most cancer cells exhibit higher ROS levels than their healthy counterparts revealing a feature that can be used for the development of new selective cancer therapeutics. Cancer cells are usually more vulnerable towards ROS stress than healthy cells due to a lower threshold of ROS toleration, which can possibly result in apoptosis (Krishnaswamy and Sushil K., 2000; Trachootham et al., 2009).

Monitoring ROS levels in MDA-MB-231 cells after treatment with chrysosplenol D and casticin (both 30 µM) demonstrates that ROS levels increased significantly already within 1.5 h (Figure 25A). The ROS levels were sustained elevated during the whole treatment up to 48 h. Interestingly, mitochondrial superoxide levels were only elevated after 48 h after the same treatment (Figure 25A,B).

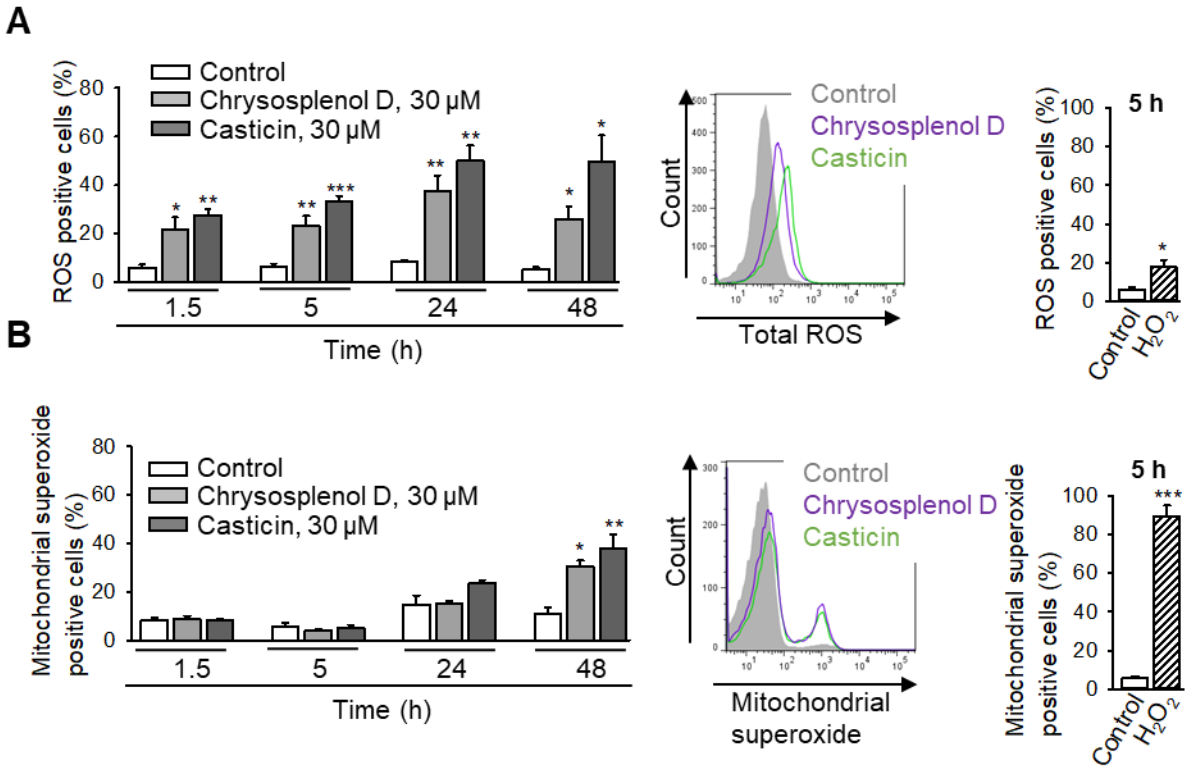

***Figure 25*: Chrysosplenol D and casticin induce sustained oxidative stress in MDA-MB-231 cells.** (A) Cells were treated with chrysosplenol D, casticin (both 30 µM), or H_2O_2 (100 µM, 5 h) for positive control. Then, cells were stained with H_2DCFDA and were analyzed flow cytometrically. (B) Cells were treated and analyzed as in (A), and stained with MitoSox™ red. Graphs show percentage of cells with increased ROS or superoxide levels compared to control. Representative histograms after 48 h are shown. Data are mean ± SEM, $n = 4$. Multi-group analysis was performed using the one-way ANOVA or Kruskal-Wallis one way analysis of variance, followed by Newman-Keuls test, $*p < 0.05$, $**p < 0.01$, $***p < 0.001$.

3.3.7 Chrysosplenol D and Casticin Activate ERK1/2

With the intention to identify possible molecular targets involved in inhibition of cell growth and cytotoxicity mediated by chrysosplenol D and casticin, the phosphorylation profiles of 43 kinases and their protein substrates were analyzed. Treatment with chrysosplenol D or casticin (both 30 µM) for 3 h significantly activated ERK1/2 by phosphorylation on threonine-202/tyrosine-204 and threonine-185/tyrosine-187 (Figure 26A). These findings were further confirmed by western immunoblotting and treatment with lower concentrations of the compounds (10 µM chrysosplenol D and 1 µM casticin) (Figure 26B). Chrysosplenol D and casticin increased the high basal ERK1/2 activation in MDA-MB-231 cells. U0126 (10 µM), a MEK-inhibitor was used as control. Contrary, neither chrysosplenol D nor casticin induced changes in AKT phosphorylation (Figure 26) (Lang et al., 2020).

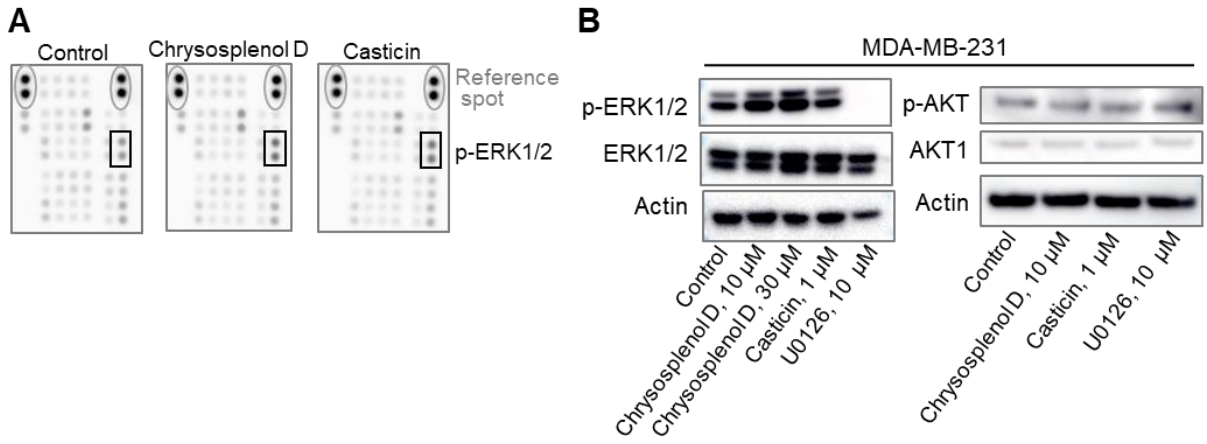

Figure 26: **Chrysosplenol D and casticin induce sustained ERK1/2 activation in MDA-MB-231 breast cancer cells.** (A) MDA-MB-231 cells were serum starved for 12 h, followed by treatment with chrysosplenol D or casticin (both 30 µM) for 3 h. Analysis of protein phosphorylation in whole cell lysates was analyzed by human phospho-kinase array. Representative membranes out of two independent experiments are shown. (B) Increased ERK1/2 phosphorylation was confirmed by western immunoblotting. Cells were treated as in (A) but with lower concentrations of chrysosplenol D (10 µM or 30 µM), casticin (1 µM) or the MEK-inhibitor U0126 (10 µM) for 3 h. Equal amounts of protein were analyzed by western blotting and by using antibodies against p-ERK1/2, ERK1/2, p-AKT (S473), AKT1, and actin (loading control). Representative blots out of two independent experiments are shown. Figure adapted with permission from our own publication (Lang et al., 2020), page 10, © 2020 The Authors, under a creative commons license, CC BY 4.0, http://creativecommons.org/licenses/by/4.0/.

3.3.8 Chrysosplenol D-Induced Cell Death Is Mediated by ERK1/2

To provide evidence for the implication of ERK1/2 activation in cell death induced by chrysosplenol D and casticin, the MEK-inhibitor U0126 was introduced. MEK inhibition consequently

resulted in inhibition of ERK1/2 activation (Figure 26B). The specificity of U0126 was controlled by its inactive analogue U0124 (Favata et al., 1998). Proliferation of MDA-MB-231 cells was slightly affected by treatment with U0126, whereas U0124 did not affect the cell viability (Figure 27). Pretreatment with 5 µM U0126 for 1 h followed by additional 48 h of treatment with casticin even slightly reduced viability of MDA-MB-231 cells. In contrast, toxicity of chrysosplenol D was abolished when MDA-MB-231 were pretreated with the MEK-inhibitor U0126 (Figure 27). These results demonstrate the involvement of ERK1/2 in cell death induced by chrysosplenol D, whereas ERK1/2 is not involved in casticin-induced toxicity (Lang et al., 2020).

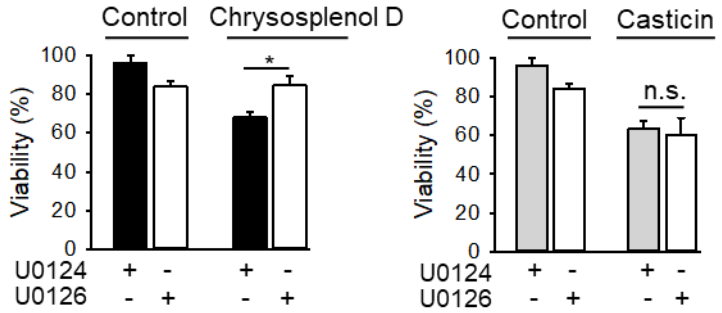

Figure 27: **Chrysosplenol D-induced cytotoxicity is mediated by ERK1/2 activation**. Pretreatment with the MEK-inhibitor U0126, but not with the inactive analogue U0124 (both 5 µM, 1 h) attenuated chrysosplenol D-induced toxicity, but not casticin-induced toxicity (both 10 µM). Viability was analyzed after 48 h by XTT assay. Data are mean ± SEM, $n = 3$, $*p < 0.05$, n.s. – not significant. Figure adapted with permission from our own publication (Lang et al., 2020), page 10, © 2020 The Authors, under a creative commons license, CC BY 4.0, http://creativecommons.org/licenses/by/4.0/.

3.3.9 ERK1/2 and AKT Activation Patterns in Different Cancer Cells

ERK1/2 and AKT activity was further examined in different cell lines and correlation with sensitivity to chrysosplenol D and casticin was explored. Figure 28A demonstrates high basal ERK1/2 activity in MDA-MB-231 cells and low basal AKT activity. The most resistant cancer cell line towards chrysosplenol D treatment was the androgen-independent prostate cancer cell line PC-3 (Figure 19A). It exhibited no ERK1/2 activity but high activation of the AKT1 pathway (Figure 28A). Equally, the more resistant MCF-7 breast cancer cells (Figure 19A,C) exhibited higher AKT activity but lower ERK1/2 activity (Figure 28A). The more sensitive A549 and MDA-MB-231 cells exhibited low AKT activation (Figure 19A,C and Figure 28A). Remarkably, the basal ERK1/2 activity in MDA-MB-231, MCF-7, MIA PaCa-2, and PC-3 cells but not in A549 cells inversely correlated with the IC_{50} values of chrysosplenol D (Lang et al., 2020).

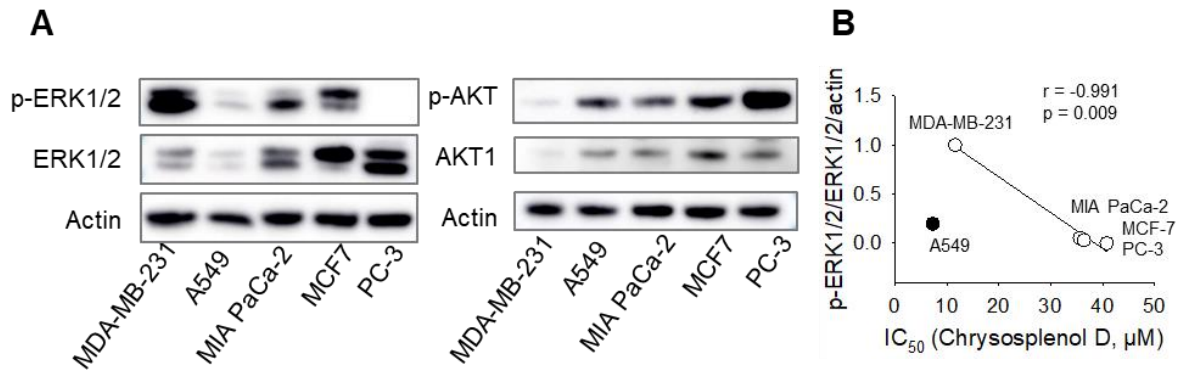

Figure 28: **ERK1/2 and AKT activation profile in different cancer cell lines.** (A) Cells were serum-starved for 12 h, followed by incubation for 2 h with medium containing 10 % FCS. ERK1/2 and AKT phosphorylation were analyzed by western immunoblotting. Equal amounts of protein from whole cell extracts were analyzed with antibodies against p-ERK1/2, ERK1/2, p-AKT (S473), AKT1, and actin (loading control). One representative blot out of two experiments is shown. (B) Basal ERK1/2 activity, analyzed as in (A) inversely correlates with the IC_{50} values of MDA-MB-231, MIA PaCa-2, MCF-7, and PC-3 cells (open symbols), treated with chrysosplenol D for 48 h. A549 cells – closed symbols. Data were analyzed by Pearsons's correlation. Figure adapted with permission from our own publication (Lang et al., 2020), page 10, © 2020 The Authors, under a creative commons license, CC BY 4.0, http://creativecommons.org/licenses/by/4.0/.

4 Discussion

In early times already, leading physicians like Hippocrates and Dioscurides used herbal remedies for cancer treatment (Karpozilos and Pavlidis, 2004), pointing to the important role of naturally occurring compounds. Still today, natural products are and will also be in the future a fundamental source for the discovery of new lead compounds for the development of new drugs. Important structural characteristics such as aromatic rings, complex ring systems, chiral centers, number and ratio of heteroatoms, as well as saturation of the molecule are often essential features for biological activity of compounds (Balunas and Kinghorn, 2005). During the long history of medicinal plants, their use was always empirically based without existing knowledge about the mechanistic basis of their pharmacological activity (Atanasov et al., 2015). Currently, almost 80 % of all drugs approved by the FDA during the last three decades for cancer therapy are of natural origin or based on natural compounds (Bishayee and Sethi, 2016). Thus, compounds from natural origin have become fundamental for cancer therapy, e.g. vinca alkaloids, taxanes, epipodophyllotoxins, as well as camptothecins and derivatives (Mehta et al., 2010). Natural products are still considered as very interesting compounds for new strategies regarding treatment and prevention of cancer because of multimodal actions and possibly, distinct lower toxicity (Srivastava et al., 2016). In addition, bioactive phytochemicals have been shown to target diverse signaling molecules and pathways and might be valuable chemopreventive and chemotherapeutic drugs. Actually, high flavonoid consumption is reported to inversely correlate with cancer occurrence (Ferreira et al., 2010; Kashyap et al., 2019). A few of these natural occurring substances were subjected to clinical trials showing promising results (Bishayee and Sethi, 2016).

Herbal dietary supplements, such as *Artemisia annua* extracts, are widely used by people suffering from cancer. Countless people are likely to use *Artemisia annua* preparations because of low costs, apparent effectivity, and missing faith in Western medicine (van der Kooy and Sullivan, 2013). However, the pharmaceutical content, therapeutic effectivity and possible risks of these preparations have been inadequately studied. Pharmacokinetic and pharmacodynamic interactions with herbal preparations and conventional anticancer drugs can seriously affect the patients' health (Sparreboom et al., 2004). Thus, more research is required in particular for different *Artemisia annua* formulations, preparation methods, active ingredients and comparison of their efficacy and safety (Alsanad et al., 2016; Michaelsen et al., 2015; van der Kooy and Sullivan, 2013).

In recent years, artemisinin and its semisynthetic derivatives came into the focus of intense investigations regarding their potential anticancer activity (Efferth, 2017a). The anticancer activity of artemisinin is controversely discussed and closely linked to the iron metabolism of cancer cells (Efferth et al., 2004; Michaelsen et al., 2015; Nakase et al., 2009). Though, the artemisinin derivatives artesunate and dihydroartesunate are already subjected to clinical trials (Efferth, 2017b; Michaelsen et al., 2015). However, existing evidence proposes, that the medicinal plant contains additional and more active ingredients than the better investigated artemisinin. Indeed,

Artemisia annua contains a large number of biologically active substances and is considered as a source for new herbal anticancer therapeutics (Breuer and Efferth, 2014; Efferth et al., 2011; Ferreira et al., 2010). Thus, further research concerning novel active ingredients is of particular interest. During the analysis of different *Artemisia annua* dietary supplements, the Momundo *Artemisia annua* extract was identified as one with the highest potential antitumor activity. Hence, in the present study, the Momundo *Artemisia annua* extract was analyzed.

For the assessment of the cytotoxicity of the *Artemisia annua* extract as well as of identified ingredients different treatment resistant cancer cell lines were used. However, the focus of the present study was on highly metastatic TNBC cells. TNBC represents a heterogeneous breast cancer subtype with poor prognosis and aggressive behavior (Collignon et al., 2016; Jitariu et al., 2017). Currently, no targeted therapies are available and chemotherapies based on anthracyclines, cyclophosphamide, taxanes, and platinum salts remain the mainstay of treatment, although they are associated with serious long-term adverse effects, (Collignon et al., 2016; S3-Leitlinie-Mammakarzinom, 2018; Tao et al., 2015a). Hence, only limited treatment options are available. Thus, the identification of effective novel lead compounds with potential activity against TNBC as well as the understanding of their molecular mechanisms is of particular interest.

4.1 Analytical Characterization of the *Artemisia annua* Extract

For quantification of the artemisinin content in Momundo, a highly sensitive HPLC-MS/MS method was developed with an artemisinin LOD of 0.2 ng/mg Momundo extract. Despite the high sensitivity of the detection method, artemisinin remained undetectable in the *Artemisia annua* dietary supplement. Nevertheless, the Momundo extracts strongly reduced the number of viable TNBC cells indicating that besides artemisinin, *Artemisia annua* must contain additional active ingredients. The toxicity of the Momundo extract was considerably increased when the capsule content was macerated in ACN, a more lipophilic solvent, and the yielded extract was used for biomedical experiments after solvent evaporation. This finding points to the existence of lipophilic extract constituents with substantial cytotoxicity in the Momundo extract. Moreover, this finding is in accordance with the result from another study demonstrating that a methylene chloride extract of *Artemisia annua* containing more lipophilic ingredients, was more toxic towards HeLa cancer cells than the more hydrophilic methanol extract (Efferth et al., 2011). By chemical analysis, the most abundant ingredients of the extract were identified to be: 6,7-dimethoxycoumarin, chrysosplenol D, casticin, arteannuin B, and arteannuic acid.

4.2 Selective Cytotoxicity of the Extract and Identified Compounds

The Momundo-ACN extract inhibited the viability of a variety of treatment-resistant cancer cells of diverse tissue origin but with varying efficacies as indicated by different IC_{50} values. PC-3 prostate cancer cells and MCF-7 estrogen responsive breast cancer cells were identified

as the most resistant cancer cells when treated with the Momundo-ACN extract, whereas A549 NSCLC cells and MDA-MB-231 TNBC cells were identified as the most sensitive cell lines. In the present thesis it is shown that cytotoxicity induced by Momundo extracts is mediated by apoptosis. Different responsiveness of the cancer cells towards extract treatment might be because of variations in apoptotic signaling pathways (Lang et al., 2019). MCF-7 cells are caspase-3-deficient, which is considered as a causative reason for their resistance against chemotherapeutic treatment (Yang et al., 2001). Ideally, a chemotherapeutic drug should selectively target cancer cells with a minimum of collateral damage to adjacent cells (Srivastava et al., 2016). Remarkably, Momundo-ACN extract treatment in concentrations, which drastically inhibited the viability of cancer cells, did not exhibit any remarkable effect on the viability of normal mammary breast epithelial cells or PBMC. Non-stimulated PBMC do not proliferate under cell culture conditions, which might be an explanation for their resistance towards treatment with the *Artemisia annua* extract, which obviously targets the cell cycle progression. But the viability of proliferating lymphocytes remained also unaffected by Momundo extract treatment (Lang et al., 2019). These findings reveal no tissue specificity of the *Artemisia annua* extract because the viability of cancer cells from different tissues was reduced. However, the extract exhibited differential cytotoxicity between cancer cells and healthy blood and epithelial cells.

The ability to selectively target cancer cells by the Momundo-ACN extract encouraged further analysis of the cytotoxicity of the most abundant ingredients. 6,7-Dimethoxycoumarin and arteannuic acid exhibited no toxicity towards any of the cell lines tested. In contrast, arteannuin B, casticin, and chrysosplenol D effectively reduced the number of viable MDA-MB-231 breast cancer cells and might synergistically contribute to the growth inhibition of cancer cells mediated by the *Artemisia annua* extract (Lang et al., 2019). Of note, artemisinin exhibited also no toxicity to any of the cancer cell lines tested supporting the hypothesis that artemisinin might not be the most effective ingredient of the medicinal plant (Efferth et al., 2011; Ferreira et al., 2010; Lang et al., 2019; van der Kooy and Sullivan, 2013). A cytotoxicity of casticin has previously been reported in MDA-MB-231 and MCF-7 breast cancer, H1299 lung cancer, and HCT116 colon carcinoma cells (Haidara et al., 2006; Liu et al., 2014). Beyond that, our results demonstrate that the viability of A549 NSCLC cells, MIA PaCa-2 pancreatic cancer cells, and PC-3 prostate cancer cells was also effectively inhibited by casticin albeit with varying efficacy. The viability of PBMC after chrysosplenol D and casticin treatment was only slightly affected. Whereas various studies already reported the potential anticancer activity of casticin, almost no data are available about the structurally related flavonol chrysosplenol D. Here, it is shown that treatment of MDA-MB-231, MCF-7, A549, MIA PaCa-2, and PC-3 cells with chrysosplenol D also effectively inhibited the viability of cancer cells. When MDA-MB-231 cells were treated with casticin and paclitaxel almost 50 % of the cells remained resistant after 48 h of treatment, whereas no resistant cells occurred after 48 h of treatment with chrysosplenol D demonstrating that its toxicity is cell cycle-independent.

Of interest, the flavonol quercetin, structurally related to chrysosplenol D and casticin, was also in the focus of intense studies for its potential anticancer activity in recent years. In MDA-MB-

231 cells, the toxicity of chrysosplenol D and casticin was considerably higher than the toxicity reported for quercetin (Chien et al., 2009). After treatment of MDA-MB-231 cells with 200 µM quercetin, which is an unrealistically high concentration for *in vivo* studies, around 80 % of the cells were still viable after 48 h (Chien et al., 2009). The reason for the higher toxicity of chrysosplenol D and casticin could be, on the one hand, the methoxylated flavonol structure resulting in a more lipophilic molecule with possible better membrane permeability. On the other hand, it was reported, that for the high antiproliferative activity the following structural criteria are important: the *ortho*-catechol moiety of ring B, the C2-C3 double bond, the C-3 hydroxyl, as well as the C-8 methoxyl groups (Chan et al., 2018; Ferreira et al., 2010; Kawaii et al., 1999). Chrysosplenol D and casticin exhibit some of these features revealing a possible explanation for the high cytotoxicity.

An innovative tool to compare cancer cell sensitivity to treatment with a respective compound, is the calculation of the GR_{50} value instead of the IC_{50} value. This drug-response parameter is in contrast to calculation of IC_{50} values independent of the cell division number that takes place during the assay (Hafner et al., 2016), therefore representing a suitable tool for the comparison of treatment sensitivity of cells with different genetic background and different doubling times. Nevertheless, the present data demonstrate significant correlation of GR_{50} and IC_{50} values for MDA-MB-231, A549, PC-3, MCF-7, and MIA PaCa-2 cells, treated with chrysosplenol D and casticin (Lang et al., 2020).

4.3 Antitumor Activity of the Extracts and Active Ingredients *In Vivo*

For analysis of the antitumor activity of the Momundo extracts and of therein contained flavonols casticin and chrysosplenol D, the CAM model was used to analyze tumor growth of MDA-MB-231/Luc xenografts *in vivo*. The Momundo extracts, chrysosplenol D and casticin significantly inhibited tumor growth, whilst no systemic toxic effects on the chick embryo could be observed. The CAM model provides an attractive model to investigate tumorigenesis in 3D. Fertilized chick eggs are naturally immunodeficient allowing xenografting of human cancer cells. Additionally, the CAM allows direct physical accessibility to the xenotransplantats growing in an *in vivo* environment (Jefferies et al., 2017; Nowak-Sliwinska et al., 2014). However, the topical instead of systemic application of the test compounds and the lack of a drug metabolism comparable to mammals represent limitations of the model (Jefferies et al., 2017; Nowak-Sliwinska et al., 2014).

For this reason, the antitumor activity of the Momundo extract was further explored in athymic nude mice. Mice were treated with Momundo-HP-β-CD complexes daily allowing good solubility in aqueous medium and *i.p.* administration of the extract. Also in this experimental setting, the tumor growth was effectively inhibited. Compared to doxorubicin, which, based on its adverse effects, was only applied once a week, lower hepatic toxicity, as indicated by the plasma levels of the hepatic enzymes AST and ALT, was observed (Lang et al., 2019). On top of that, mice treated with doxorubicin exhibited an increased aggressive behavior and suffered from

significant weight loss. By contrast, in Momundo-extract-treated mice, even a slight increase of body weight could be observed. This could be beneficial for cancer patients who are often suffering from severe cachexia. Likewise, in another study in which HCT116 colon cancer cells were xenografted in nude mice, followed by daily intratumoral treatment with 40 mg/kg of an ethanolic *Artemisia annua* extract for 21 days, demonstrated that the extract reduced tumor volume whilst no decrease in mice body weight was observed (Kim et al., 2017). Moreover, no biochemical and hematological toxicity could be observed when an ethanolic *Artemisia annua* extract in high doses up to 300 mg/kg/d for 28 days was orally administered to male Wistar rats (Eteng et al., 2013). In addition, in a case report of an 80 years old patient with metastatic prostate cancer, an initially good therapeutic response to treatment with *Artemisia annua* capsules was described. After treatment with bicalitumide for two weeks, a long-term treatment with *Artemisia annua* capsules followed and resulted in initial regression. During the therapy neither toxicity nor adverse effects known from chemotherapeutic regimes were observed and the treatment with *Artemisia annua* capsules was accompanied by an improved life quality (Michaelsen et al., 2015). Similarly, a cat and three dogs had been treated with herbal extracts of *Artemisia annua* after surgical extirpation of a sarcoma and the cat and one dog survived 40 and 37 month without relapse. The two other dogs showed complete remission and were 39 and 26 month later still alive whilst no adverse effects could be observed (Breuer and Efferth, 2014). These findings point to a seemingly good tolerability of *Artemisia annua* extracts but, of course, large-scaled investigations are needed. In contrast, chemotherapy-related toxicities seriously affect the patients' quality of life and eventually result in patients' death (Tao et al., 2015a). Early toxicities such as cytopenias, fatigue, alopecia, musculoskeletal pain, peripheral neuropathy, and neurocognitive dysfunction but also chronic and late effects like cardiomyopathy, secondary cancers, early menopause, and affected fertility are very serious adverse effects cancer patients are exposed to (Tao et al., 2015a). Anthracyclines, as components of the standard chemotherapy regimens for TNBC are inducers of cardiotoxicity, in particular in high cumulative doses. Neurotoxicity is commonly observed in taxane-based regimens (Tao et al., 2015a). Obviously a high price, considering the overall poor survival response of patients with TNBC (Bianchini et al., 2016; Hudis and Gianni, 2011). Hence, novel therapeutic compounds with potent anticancer activity but low systemic toxicity are urgently needed.

4.4 Targeting the Cell Cycle as an Anticancer Treatment Strategy

Uncontrolled proliferation caused by altered protein expression, involved in the progression of the cell cycle and control mechanisms, is a hallmark of most neoplasias (Hanahan and Weinberg, 2011; Otto and Sicinski, 2017). Hence, the inhibition of the cell cycle progression, which can subsequently result in apoptosis, has been recognized as an important therapeutic strategy (Otto and Sicinski, 2017).

Treatment with Momundo and Momundo-ACN extracts induced concentration-dependent cell cycle perturbations in MDA-MB-231 cells. Already after 24 h treatment with both extracts an

accumulation of polyploid cells, with multi-nucleated morphology after was observed, which was similar to that induced by paclitaxel or a synthetic analogue of halogenated monoterpenes from *Plocamium* red algae (El Gaafary et al., 2019). Accordingly, this could either indicate cytokinesis failure (Fujiwara et al., 2005; Lens and Medema, 2019), or the cells exit from mitosis and enter interphase without chromosome separation or cell division. This scenario is termed mitotic slippage resulting in cells with higher ploidy and has been shown for microtubule-binding drugs like paclitaxel (de Leeuw et al., 2015; Denisenko et al., 2016; Riffell et al., 2009). Considering that casticin, one of the most abundant Momundo *Artemisia annua* extract components inhibits tubulin polymerization and induces mitotic catastrophe with its various outcomes (cell death during mitosis or slippage and polyploidy) in K562 leukemic cells (Blagosklonny, 2007; Shen et al., 2009), this could explain the induction of polyploid cells by the Momundo *Artemisia annua* extracts. MDA-MB-231 cells express non-functional p53 (Berglind et al., 2008; Vogiatzi et al., 2016). In fact, mitotic catastrophe is independent of p53 and might be regarded as a response mechanism to DNA-damaging drugs of p53-mutant tumor cells (Portugal et al., 2009).

It was also shown, that casticin, similar to paclitaxel induces a strong G_2/M-phase cell accumulation in leukemic K562 cells, in MCF-7 breast cancer cells, and H1299 lung carcinoma cells (Haidara et al., 2006; Shen et al., 2009). In our study, these results have been confirmed by using MDA-MB-231 TNBC cells, in which casticin equally induced a strong dose-dependent cell accumulation in the G_2/M-phase. In contrast to casticin and paclitaxel, chrysosplenol D increased the proportion of cells in both, the S- and G_2/M-phases (Lang et al., 2020). Similar effects have been described for the structurally related flavonol quercetin interacting with DNA and inducing cell cycle arrest in the S-phase (Srivastava et al., 2016). However, the increase in the S-phase might also be caused by apoptotic 4N cells loosing DNA content.

4.5 Induction of Apoptosis

Cancer cells often exhibit dysregulations in apoptotic pathways promoting uncontrolled proliferation and therapy resistance (Igney and Krammer, 2002). For this reason, the activation of the apoptotic cell death machinery by plant-derived compounds has become a promising treatment strategy (Fulda, 2010; Pfeffer and Singh, 2018). Triggering apoptosis in highly metastatic TNBC cells without affecting neighboring cells might improve the patient's prognosis.

Analysis of several apoptotic parameters, provided compelling evidence that the Momundo extracts induce apoptosis. The results demonstrate that treatment of TNBC cells with Momundo extract resulted in strong activation of the effector caspase 3, induced dissipation of the mitochondrial membrane potential $\Delta\Psi m$, and DNA-fragmentation as indicated by the formation of an apoptotic subG_1 cell population (Riccardi and Nicoletti, 2006). These findings suggest the involvement of the intrinsic apoptotic pathway. Likewise, treatment with the Momundo extract induced apoptosis *in vivo* as analyzed by DNA strand breaks of breast cancer xenografts grown on the CAM (Lang et al., 2019).

Equally, the flavonols chrysosplenol D and casticin effectively increased the number of cells with loss of ΔΨm. In casticin- and paclitaxel-treated MDA-MB-231 cells, loss of ΔΨm coincidences with apoptosis, in compliance with the fact that both compounds have the same intracellular target, tubulin (Haidara et al., 2006). In chrysosplenol D-treated cells dissipation of ΔΨm occurs 24 h earlier suggesting an active role of mitochondria in induction of apoptosis mediated by chrysosplenol D.

Mitochondria are important for the orchestration of apoptosis. Intracellular cell stress can result in opening of the mitochondrial permeability transition (MPT) pore and disruption of ΔΨm. Mitochondria contain pro-apoptotic molecules activating the intrinsic pathway of apoptosis by the release of cytochrome c, which activates apoptotic caspases (Okada and Mak, 2004). Also, chrysosplenol D and casticin significantly increased the number of early apoptotic cells, characterized by phosphatidylserine exposure on the outer leaflet of the cell membrane without affected plasma membrane integrity (Galluzzi et al., 2009).

Casticin and chrysosplenol D significantly increased cellular ROS levels already after 90 min of treatment. Interestingly, the mitochondrial superoxide levels were only increased after 48 h, the time point when cells started to undergo apoptosis. Cancer cells are reported to be selectively vulnerable towards ROS stress (Panieri and Santoro, 2016). ROS can activate the intrinsic apoptotic pathway in various ways. High levels of ROS can induce p53 activation and the activation of the c-Jun N-terminal kinase (JNK), which can in turn activate pro-apoptotic Bcl-family proteins (Redza-Dutordoir and Averill-Bates, 2016). On top of that, it was reported that ROS is able to activate intrinsic apoptosis by oxidation of cardiolipin and promoting cytochrome c release. Moreover, ROS can cause mitochondrial membrane permeabilization and opening of BAX/BAK transition pores promoting the release of apoptosis-inducing mitochondrial factors (Redza-Dutordoir and Averill-Bates, 2016). In addition, high ROS levels can also activate ERK1/2 by inhibition of ERK1/2 specific phosphatases (DUSP) (Cagnol and Chambard, 2010). This is in accordance with our findings, because chrysosplenol D-induced cell death is mediated by ERK1/2 (Lang et al., 2020).

4.6 Chrysosplenol D-Induced Cell Death is Mediated by ERK1/2

Extracellular signal-regulated kinases (ERK1/2) are mediators of cell proliferation, growth, survival, differentiation, and transformation. ERK1/2 kinases as a part of the pro-oncogenic Ras/Raf/MEK/ERK signaling pathway are often activated in cancer cells because of the frequently observed mutations of *Ras* and *B-Raf* genes promoting proliferation and apoptosis resistance (De Luca et al., 2012). However, available evidence indicates that ERK1/2 kinases might also trigger antiproliferative pathways and apoptosis. Under specific conditions depending on the type of the cell and the stimuli, ERK1/2 kinases are implicated in the initiation of senescence, apoptosis or autophagy (Mebratu and Tesfaigzi, 2009). Hence, the role of ERK1/2 in cancer treatment is very complex (Deschenes-Simard et al., 2014). ERK1/2 activation is in-

volved in cell death induced by different antitumor agents as described for flavonoids like quercetin or apigenin, but also for DNA-damaging agents, such as doxorubicin, cisplatin or etoposid (Cagnol and Chambard, 2010; Kim et al., 2008; Llorens et al., 2004; Tang et al., 2002).

MDA-MB-231 cells exhibit significant high levels of phosphorylated ERK1/2, because of mutated *K-ras* (Hoeflich et al., 2009; Hollestelle et al., 2007; von Lintig et al., 2000). These results were confirmed by western blot analysis demonstrating high basal ERK1/2 activation in MDA-MB-231 cells. Both flavonols, chrysosplenol D and casticin, augmented already increased basal activation of ERK1/2 in MDA-MB-231 cells. For analysis of the involvement of ERK1/2 activation in cell death induction by chrysosplenol D and casticin, the MEK inhibitor U0126 and its inactive analogue U0124 were used. The MEK inhibitor U0126 effectively inhibited the phosphorylation and activation of ERK1/2. Treatment only with U0126 slightly inhibited the viability of MDA-MB-231 cells, an effect in line with the role of ERK1/2 activity in MDA-MB-231 proliferation (Hoeflich et al., 2009). When cells were treated with U0126 and additionally with casticin, cell viability was even slightly reduced. In contrast, the inhibition of ERK1/2 activation by U0126 abolished the toxicity of chrysosplenol D. These findings clearly demonstrate that ERK1/2 activation is important for cell death induction by chrysosplenol D. Differently, casticin-induced cell death is independent of ERK1/2 activation (Lang et al., 2020). Inhibition of ERK1/2 similarly abolished cisplatin-induced cell death in Saos-2 osteosarcoma and Kelly neuroblastoma cells (Woessmann et al., 2002) and camptothecin-induced cell death in MDA-MB-231 cells (Mirzoeva et al., 2009) demonstrating the divalent role of ERK1/2 in cell death and proliferation.

The mechanisms and conditions for cell death mediated by ERK1/2 are still not fully understood. DNA-damaging agents are reported to activate ERK1/2 independently of p53 and downstream of the ATM kinase (Mebratu and Tesfaigzi, 2009). Such compounds are often described to activate the intrinsic, mitochondrial pathway of apoptosis. Hence, phosphorylated ERK1/2, reported to be localized to mitochondrial membranes, was shown to target mitochondrial function disrupting the mitochondrial membrane potential ($\Delta\Psi m$) and to trigger cytochrome c release. Furthermore, ERK1/2 activation can induce pro-apoptotic gene expression of Bcl-2 family proteins (Cagnol and Chambard, 2010). In the present study, the inhibition of ERK1/2 was initiated 1 h before chrysosplenol D treatment, possibly not sufficient for new protein synthesis (Bacus et al., 2001). ERK1/2 can directly activate caspase 8 or potentiate activation of death receptors by various mechanisms (Cagnol and Chambard, 2010).

Furthermore, ERK1/2 can stabilize and activate p53 by different mechanisms and under distinct conditions ERK-mediated expression of p53 is required for induction of apoptosis (Cagnol and Chambard, 2010). Respectively, NSCLC A549 cells expressing wild type p53 ($p53^{wt}$) (Berglind et al., 2008) were exceptionally sensitive to chrysosplenol D treatment. By contrast, PC-3 cells with a lack of the functional p53 gene (Berglind et al., 2008) were the most resistant cells among the five tested cell lines. It appears, that considering only the p53 status might not suffice to

explain the differing sensitivity of different cancer cells to treatment with chrysosplenol D. Indeed, MCF-7 breast cancer cells express wild type p53 ($p53^{wt}$) and remain still comparatively resistant against treatment with chrysosplenol D. On the contrary, MDA-MB-231 breast cancer cells harbor a gain of function mutation of p53, which actively drives tumor progression and metastasis autonomously of downstream targets of p53 (Berglind et al., 2008; Vogiatzi et al., 2016) but are, after the A549 cells, the most sensitive cells to chrysosplenol D. The pancreatic MIA PaCa-2 cells also carry a gain of function mutation of p53 (Yan et al., 2008) and were rather resistant to chrysosplenol D treatment. Therefore, the p53 status alone is not a sufficient explanation for sensitivity to chrysospelnol D and casticin (Lang et al., 2020), but can contribute to apoptotic cell death induction by these compounds. Therefore, involvement of different pathways also needs to be considered.

The chrysosplenol D-resistant PC-3 cells are additionally characterized by the lack of the phosphatase PTEN, which induces unusually high activity of the PI3K/AKT pathway (El Gaafary et al., 2015; Estrada et al., 2010). Likewise, the comparatively resistant MCF-7 cells exhibited high basal AKT activation, whilst MDA-MB-231 cells and A459 cells, which are very sensitive to chrysosplenol D, are characterized by low PI3K/AKT activity. Therefore, the AKT activation profile in the analyzed cells correlates inversely to chrysosplenol D sensitivity. Thus, higher PI3K/AKT activity is associated with higher resistance to chrysosplenol D treatment.

The PI3K and MAPK pathways can interact in various ways and co-regulate their activity (De Luca et al., 2012). Different studies demonstrated this, because the inhibition of ERK1/2 activity was compensated by increased activation of the PI3K/AKT pathway (Deschenes-Simard et al., 2014). Furthermore, negative feedback signaling of ERK1/2 can affect upstream activators of RAS/ERK1/2 which also mediate pro-survival PI3K/AKT/mTOR signaling (Deschenes-Simard et al., 2014). This is also supported by our results demonstrating that the chrysosplenol D-resistant PC-3 cell line exhibits high PI3K/AKT activation and no basal ERK1/2 activity. MDA-MB-231 cells exhibiting high sensitivity to chrysosplenol D on the contrary demonstrate high basal ERK1/2 activity. The basal ERK1/2 activity in MDA-MB-231 and MCF-7 breast cancer cells, in MIA PaCa-2 pancreatic cancer cells, and in PC-3 prostate cancer cells, but not in NSCLC A549 cells, strongly inversely correlated with the IC_{50} values of chrysosplenol D. In summary, low basal AKT pathways activation yet high basal ERK1/2 activity might be predictive indicators for the sensitivity of malignant cells to treatment with chrysosplenol D (Lang et al., 2020).

An important feature affecting the outcome of ERK1/2 signaling might be the kinetics and the duration of ERK1/2 activation (Mebratu and Tesfaigzi, 2009). The kinetics and duration of sustained high aberrant ERK1/2 activity can induce the proteasome-dependent degradation of numerous phosphoproteins, which are required for growth of the cell and progression of the cell-cycle (Deschenes-Simard et al., 2014). The degradation of these phosphoproteins induces cell stresses, which are associated with mitochondrial dysfunction (Deschenes-Simard et al., 2014). Aberrant ERK1/2 activity can be recognized by tumor-suppressor pathways initiating apoptotic

cell death (Deschenes-Simard et al., 2014). These findings can be supported by chrysosplenol D treatment of MDA-MB-231 cells, elevated ERK1/2 activity followed by loss of mitochondrial membrane potential ($\Delta\Psi m$), and induction of apoptosis.

Furthermore, the pro-apoptotic activity of ERK1/2 should also be considered for the evaluation of the use of pharmacologic inhibitors targeting the MAPK pathway. Inhibition of the Ras/Raf/MEK/ERK pathway should only be considered for application when ERK1/2 kinases are oncogenic (Deschenes-Simard et al., 2014). However, more studies are required to analyze the exact conditions allowing ERK1/2 activation to propagate the death of a cell or its proliferation (Mebratu and Tesfaigzi, 2009).

Taken together, the present data provide evidence that an *Artemisia annua* extract, marketed as a dietary supplement, exhibits antitumor activity. Further active ingredients beside artemisinin with activity against TNBC and a variety of other treatment-resistant cancer cells have been identified and could synergistically contribute to the antitumor efficacy of the analyzed *Artemisia annua* extract. The flavonols chrysosplenol D and casticin were identified as compounds with potential anticancer activity with different mechanisms of action and are worth of further exploration. Different to casticin, chrysosplenol D induced cell death is mediated by ERK1/2.

5 Summary

In the past few years, the Chinese medicinal plant *Artemisia annua* L., and in particular semi-isynthetic derivatives of artemisinin, have gained increasing attention for their potential anti-cancer activity. However, only little is known about *Artemisia annua* extracts and numerous bioactive compounds therein, beside the better explored artemisinin.

Therefore, chemical characterization of an *Artemisia annua* extract was conducted. The extract is devoid of detectable artemisinin but exhibits remarkable antiproliferative efficacies on highly metastatic triple negative human breast cancer (TNBC) MDA-MB-231 cells and other treatment-resistant cancer cells. The most abundant components of the *Artemisia annua* extract are 6,7-dimethoxy-coumarin, chrysosplenol D, casticin and arteannuic acid. The *Artemisia annua* extract inhibits the viability of breast (MDA-MB-231 and MCF-7), pancreas (MIA PaCa-2), prostate (PC-3) and non-small cell lung cancer (A549) cells, whereas the viability of normal mammary epithelial cells and peripheral blood mononuclear cells remains unaffected at equal concentrations. Similarly, the extract ingredients chrysosplenol D and casticin exhibit selective cytotoxicity to cancer cells, whereas 6,7-dimethoxycoumarin and arteannuic acid exhibit no toxicity to any other of the analyzed cancer cell lines. The *Artemisia annua* extract and the flavonols chrysosplenol D and casticin inhibit the cell cycle progression and induce apoptosis. To examine the *in vivo* antiproliferative efficacy of the extract, chrysosplenol D, and casticin, their effects on TNBC MDA-MB-231 xenografts grown on the chick chorioallantoic membrane (CAM) and in nude mice were analyzed. The *Artemisia annua* extract effectively inhibits tumor growth in nude mice and on the CAM. Likewise, chrysosplenol D and casticin inhibit the MDA-MB-231 proliferation in the CAM assay. Notably, no systemic toxicity on the chicken embryos could be observed after treatment with the *Artemisia annua* extract, chrysosplenol D, or casticin. The systemic administration of the *Artemisia annua* extract to nude mice reveals good tolerability.

Chrysosplenol D induces ERK1/2 activation. Although ERK1/2 kinases are often activated in cancer promoting cell proliferation, under certain conditions upregulated ERK1/2 kinases can also mediate apoptosis. In contrast to casticin, the toxicity induced by chrysosplenol D in MDA-MB-231 cells is mediated by ERK1/2.

To sum up, this work provides evidence for an antitumor activity of an *Artemisia annua* extract, that is marketed as a dietary supplement, against highly metastatic TNBC. Active extract ingredients have been identified and it is shown for the first time that the flavonol chrysosplenol D exhibits antitumor activity against TNBC and inhibits the proliferation of a variety of treatment-resistant cancer cells. This work might contribute to further successful investigations of *Artemisia annua*-derived compounds and their potential therapeutic use.

6 References

1. Aarts, M., Linardopoulos, S., Turner, N.C., 2013. Tumour selective targeting of cell cycle kinases for cancer treatment. Curr Opin Pharmacol 13, 529-535.
2. Alsanad, S.M., Howard, R.L., Williamson, E.M., 2016. An assessment of the impact of herb-drug combinations used by cancer patients. BMC Complement Altern Med 16, 393.
3. Asati, V., Mahapatra, D.K., Bharti, S.K., 2016. PI3K/Akt/mTOR and Ras/Raf/MEK/ERK signaling pathways inhibitors as anticancer agents: Structural and pharmacological perspectives. Eur J Med Chem 109, 314-341.
4. Atanasov, A.G., Waltenberger, B., Pferschy-Wenzig, E.M., Linder, T., Wawrosch, C., Uhrin, P., Temml, V., Wang, L., Schwaiger, S., Heiss, E.H., Rollinger, J.M., Schuster, D., Breuss, J.M., Bochkov, V., Mihovilovic, M.D., Kopp, B., Bauer, R., Dirsch, V.M., Stuppner, H., 2015. Discovery and resupply of pharmacologically active plant-derived natural products: A review. Biotechnol Adv 33, 1582-1614.
5. Bacus, S.S., Gudkov, A.V., Lowe, M., Lyass, L., Yung, Y., Komarov, A.P., Keyomarsi, K., Yarden, Y., Seger, R., 2001. Taxol-induced apoptosis depends on MAP kinase pathways (ERK and p38) and is independent of p53. Oncogene, 147-155.
6. Balunas, M.J., Kinghorn, A.D., 2005. Drug discovery from medicinal plants. Life Sci 78, 431-441.
7. Behrend, L., Henderson, G., Zwacka, R.M., 2003. Reactive oxygen species in oncogenic transformation. Biochem Soc Trans 31, 1441-1444.
8. Berglind, H., Pawitan, Y., Kato, S., Ishioka, C., Soussi, T., 2008. Analysis of p53 mutation status in human cancer cell lines: a paradigm for cell line cross-contamination. Cancer Biol Ther 7, 699-708.
9. Bianchini, G., Balko, J.M., Mayer, I.A., Sanders, M.E., Gianni, L., 2016. Triple-negative breast cancer: challenges and opportunities of a heterogeneous disease. Nature Reviews Clinical Oncology 13, 674-690.
10. Bishayee, A., Sethi, G., 2016. Bioactive natural products in cancer prevention and therapy: Progress and promise. Semin Cancer Biol 40-41, 1-3.
11. Blagosklonny, M.V., 2007. Mitotic arrest and cell fate: why and how mitotic inhibition of transcription drives mutually exclusive events. Cell Cycle 6, 70-74.
12. Breuer, E., Efferth, T., 2014. Treatment of Iron-Loaded Veterinary Sarcoma by Artemisia annua. Nat Prod Bioprospect 4, 113-118.
13. Brisibe, E.A., Umoren, U.E., Brisibe, F., Magalhäes, P.M., Ferreira, J.F.S., Luthria, D., Wu, X., Prior, R.L., 2009. Nutritional characterisation and antioxidant capacity of different tissues of Artemisia annua L. Food Chemistry 115, 1240-1246.
14. Brown, G.D., 2010. The biosynthesis of artemisinin (Qinghaosu) and the phytochemistry of Artemisia annua L. (Qinghao). Molecules 15, 7603-7698.

15. Cagnol, S., Chambard, J.C., 2010. ERK and cell death: mechanisms of ERK-induced cell death--apoptosis, autophagy and senescence. FEBS J 277, 2-21.
16. Cagnol, S., Van Obberghen-Schilling, E., Chambard, J.C., 2006. Prolonged activation of ERK1,2 induces FADD-independent caspase 8 activation and cell death. Apoptosis 11, 337-346.
17. Chan, E.W.C., Wong, S.K., Chan, H.T., 2018. Casticin from Vitex species: a short review on its anticancer and anti-inflammatory properties. Journal of Integrative Medicine 16, 147-152.
18. Chien, S.Y., Wu, Y.C., Chung, J.G., Yang, J.S., Lu, H.F., Tsou, M.F., Wood, W.G., Kuo, S.J., Chen, D.R., 2009. Quercetin-induced apoptosis acts through mitochondrial- and caspase-3-dependent pathways in human breast cancer MDA-MB-231 cells. Hum Exp Toxicol 28, 493-503.
19. Collignon, J., Lousberg, L., Schroeder, H., Jerusalem, G., 2016. Triple-negative breast cancer: treatment challenges and solutions. Breast Cancer (Dove Med Press) 8, 93-107.
20. Cortazar, P., Zhang, L., Untch, M., Mehta, K., Costantino, J.P., Wolmark, N., Bonnefoi, H., Cameron, D., Gianni, L., Valagussa, P., Swain, S.M., Prowell, T., Loibl, S., Wickerham, D.L., Bogaerts, J., Baselga, J., Perou, C., Blumenthal, G., Blohmer, J., Mamounas, E.P., Bergh, J., Semiglazov, V., Justice, R., Eidtmann, H., Paik, S., Piccart, M., Sridhara, R., Fasching, P.A., Slaets, L., Tang, S., Gerber, B., Geyer, C.E., Pazdur, R., Ditsch, N., Rastogi, P., Eiermann, W., von Minckwitz, G., 2014. Pathological complete response and long-term clinical benefit in breast cancer: the CTNeoBC pooled analysis. The Lancet 384, 164-172.
21. Cowan, A.E., Jun, S., Gahche, J.J., Tooze, J.A., Dwyer, J.T., Eicher-Miller, H.A., Bhadra, A., Guenther, P.M., Potischman, N., Dodd, K.W., Bailey, R.L., 2018. Dietary Supplement Use Differs by Socioeconomic and Health-Related Characteristics among U.S. Adults, NHANES 2011(-)2014. Nutrients 10, 1114.
22. de Leeuw, R., Berman-Booty, L.D., Schiewer, M.J., Ciment, S.J., Den, R.B., Dicker, A.P., Kelly, W.K., Trabulsi, E.J., Lallas, C.D., Gomella, L.G., Knudsen, K.E., 2015. Novel actions of next-generation taxanes benefit advanced stages of prostate cancer. Clin Cancer Res 21, 795-807.
23. De Luca, A., Maiello, M.R., D'Alessio, A., Pergameno, M., Normanno, N., 2012. The RAS/RAF/MEK/ERK and the PI3K/AKT signalling pathways: role in cancer pathogenesis and implications for therapeutic approaches. Expert Opin Ther Targets 16 Suppl 2, S17-27.
24. Denisenko, T.V., Sorokina, I.V., Gogvadze, V., Zhivotovsky, B., 2016. Mitotic catastrophe and cancer drug resistance: A link that must to be broken. Drug Resist Updat 24, 1-12.
25. Denkert, C., Liedtke, C., Tutt, A., von Minckwitz, G., 2017. Molecular alterations in triple-negative breast cancer—the road to new treatment strategies. The Lancet 389, 2430-2442.

26. Denton, D., Nicolson, S., Kumar, S., 2012. Cell death by autophagy: facts and apparent artefacts. Cell Death Differ 19, 87-95.
27. Deschenes-Simard, X., Kottakis, F., Meloche, S., Ferbeyre, G., 2014. ERKs in cancer: friends or foes? Cancer Res 74, 412-419.
28. Diana, A., Franzese, E., Centonze, S., Carlino, F., Della Corte, C.M., Ventriglia, J., Petrillo, A., De Vita, F., Alfano, R., Ciardiello, F., Orditura, M., 2018. Triple-Negative Breast Cancers: Systematic Review of the Literature on Molecular and Clinical Features with a Focus on Treatment with Innovative Drugs. Curr Oncol Rep 20, 76.
29. Dominguez-Brauer, C., Thu, K.L., Mason, J.M., Blaser, H., Bray, M.R., Mak, T.W., 2015. Targeting Mitosis in Cancer: Emerging Strategies. Mol Cell 60, 524-536.
30. Efferth, T., 2017a. Cancer combination therapies with artemisinin-type drugs. Biochem Pharmacol 139, 56-70.
31. Efferth, T., 2017b. From ancient herb to modern drug: Artemisia annua and artemisinin for cancer therapy. Semin Cancer Biol 46, 65-83.
32. Efferth, T., Benakis, A., Romero, M.R., Tomicic, M., Rauh, R., Steinbach, D., Hafer, R., Stamminger, T., Oesch, F., Kaina, B., Marschall, M., 2004. Enhancement of cytotoxicity of artemisinins toward cancer cells by ferrous iron. Free Radic Biol Med 37, 998-1009.
33. Efferth, T., Herrmann, F., Tahrani, A., Wink, M., 2011. Cytotoxic activity of secondary metabolites derived from Artemisia annua L. towards cancer cells in comparison to its designated active constituent artemisinin. Phytomedicine 18, 959-969.
34. El Gaafary, M., Buchele, B., Syrovets, T., Agnolet, S., Schneider, B., Schmidt, C.Q., Simmet, T., 2015. An alpha-acetoxy-tirucallic acid isomer inhibits Akt/mTOR signaling and induces oxidative stress in prostate cancer cells. J Pharmacol Exp Ther 352, 33-42.
35. El Gaafary, M., Ezzat, S.M., El Sayed, A.M., Sabry, O.M., Hafner, S., Lang, S., Schmiech, M., Syrovets, T., Simmet, T., 2017. Acovenoside A induces mitotic catastrophe followed by apoptosis in non-small-cell lung cancer cells. J Nat Prod 80, 3203-3210.
36. El Gaafary, M., Hafner, S., Lang, S.J., Jin, L., Sabry, O.M., Vogel, C.V., Vanderwal, C.D., Syrovets, T., Simmet, T., 2019. A Novel Polyhalogenated Monoterpene Induces Cell Cycle Arrest and Apoptosis in Breast Cancer Cells. Mar Drugs 17, 437.
37. Estrada, A.C., Syrovets, T., Pitterle, K., Lunov, O., Büchele, B., Schimana-Pfeifer, J., Schmidt, T., Morad, S.A., Simmet, T., 2010. Tirucallic acids are novel pleckstrin homology domain-dependent Akt inhibitors inducing apoptosis in prostate cancer cells. Mol Pharmacol 77, 378-387.
38. Eteng, M.U., Abolaji, A.O., Ebong, P.E., Brisibe, E.A., Dar, A., Kabir, N., Iqbal Choudhary, M., 2013. Biochemical and haematological evaluation of repeated dose

exposure of male Wistar rats to an ethanolic extract of Artemisia annua. Phytother Res 27, 602-609.

39. Favata, M.F., Horiuchi, K.Y., Manos, E.J., Daulerio, A.J., Stradley, D.A., Feeser, W.S., Van Dyk, D.E., Pitts, W.J., Earl, R.A., Hobbs, F., Copeland, R.A., Magolda, R.L., Scherle, P.A., Trzaskos, J.M., 1998. Identification of a Novel Inhibitor of Mitogen-activated Protein Kinase Kinase. Journal of Biological Chemistry 273, 18623-18632.
40. Ferreira, J.F., Luthria, D.L., Sasaki, T., Heyerick, A., 2010. Flavonoids from Artemisia annua L. as antioxidants and their potential synergism with artemisinin against malaria and cancer. Molecules 15, 3135-3170.
41. Fink, S.L., Cookson, B.T., 2005. Apoptosis, pyroptosis, and necrosis: mechanistic description of dead and dying eukaryotic cells. Infect Immun 73, 1907-1916.
42. Flores, M.L., Castilla, C., Avila, R., Ruiz-Borrego, M., Saez, C., Japon, M.A., 2012. Paclitaxel sensitivity of breast cancer cells requires efficient mitotic arrest and disruption of Bcl-xL/Bak interaction. Breast Cancer Res Treat 133, 917-928.
43. Fujiwara, T., Bandi, M., Nitta, M., Ivanova, E.V., Bronson, R.T., Pellman, D., 2005. Cytokinesis failure generating tetraploids promotes tumorigenesis in p53-null cells. Nature 437, 1043-1047.
44. Fulda, S., 2010. Modulation of apoptosis by natural products for cancer therapy. Planta Med 76, 1075-1079.
45. Galluzzi, L., Aaronson, S.A., Abrams, J., Alnemri, E.S., Andrews, D.W., Baehrecke, E.H., Bazan, N.G., Blagosklonny, M.V., Blomgren, K., Borner, C., Bredesen, D.E., Brenner, C., Castedo, M., Cidlowski, J.A., Ciechanover, A., Cohen, G.M., De Laurenzi, V., De Maria, R., Deshmukh, M., Dynlacht, B.D., El-Deiry, W.S., Flavell, R.A., Fulda, S., Garrido, C., Golstein, P., Gougeon, M.L., Green, D.R., Gronemeyer, H., Hajnoczky, G., Hardwick, J.M., Hengartner, M.O., Ichijo, H., Jaattela, M., Kepp, O., Kimchi, A., Klionsky, D.J., Knight, R.A., Kornbluth, S., Kumar, S., Levine, B., Lipton, S.A., Lugli, E., Madeo, F., Malomi, W., Marine, J.C., Martin, S.J., Medema, J.P., Mehlen, P., Melino, G., Moll, U.M., Morselli, E., Nagata, S., Nicholson, D.W., Nicotera, P., Nunez, G., Oren, M., Penninger, J., Pervaiz, S., Peter, M.E., Piacentini, M., Prehn, J.H., Puthalakath, H., Rabinovich, G.A., Rizzuto, R., Rodrigues, C.M., Rubinsztein, D.C., Rudel, T., Scorrano, L., Simon, H.U., Steller, H., Tschopp, J., Tsujimoto, Y., Vandenabeele, P., Vitale, I., Vousden, K.H., Youle, R.J., Yuan, J., Zhivotovsky, B., Kroemer, G., 2009. Guidelines for the use and interpretation of assays for monitoring cell death in higher eukaryotes. Cell Death Differ 16, 1093-1107.
46. Giacinti, C., Giordano, A., 2006. RB and cell cycle progression. Oncogene 25, 5220-5227.
47. Glick, D., Barth, S., Macleod, K.F., 2010. Autophagy: cellular and molecular mechanisms. J Pathol 221, 3-12.

48. Hafner, M., Niepel, M., Chung, M., Sorger, P.K., 2016. Growth rate inhibition metrics correct for confounders in measuring sensitivity to cancer drugs. Nature Methods 13, 521-527.
49. Haidara, K., Zamir, L., Shi, Q.W., Batist, G., 2006. The flavonoid Casticin has multiple mechanisms of tumor cytotoxicity action. Cancer Lett 242, 180-190.
50. Hanahan, D., Weinberg, R.A., 2011. Hallmarks of cancer: the next generation. Cell 144, 646-674.
51. Hengartner, M.O., 2000. The biochemistry of apoptosis. Nature 407, 770-776.
52. Hoeflich, K.P., O'Brien, C., Boyd, Z., Cavet, G., Guerrero, S., Jung, K., Januario, T., Savage, H., Punnoose, E., Truong, T., Zhou, W., Berry, L., Murray, L., Amler, L., Belvin, M., Friedman, L.S., Lackner, M.R., 2009. In vivo antitumor activity of MEK and phosphatidylinositol 3-kinase inhibitors in basal-like breast cancer models. Clin Cancer Res 15, 4649-4664.
53. Hollestelle, A., Elstrodt, F., Nagel, J.H., Kallemeijn, W.W., Schutte, M., 2007. Phosphatidylinositol-3-OH kinase or RAS pathway mutations in human breast cancer cell lines. Mol Cancer Res 5, 195-201.
54. Hudis, C.A., Gianni, L., 2011. Triple-negative breast cancer: an unmet medical need. Oncologist 16 Suppl 1, 1-11.
55. Igney, F.H., Krammer, P.H., 2002. Death and anti-death: tumour resistance to apoptosis. Nat Rev Cancer 2, 277-288.
56. Jefferies, B., Lenze, F., Sathe, A., Truong, N., Anton, M., von Eisenhart-Rothe, R., Nawroth, R., Mayer-Kuckuk, P., 2017. Non-invasive imaging of engineered human tumors in the living chicken embryo. Sci Rep 7, 4991.
57. Jitariu, A., Cîmpean, a., Ribatti, D., Raica, M., 2017. Triple negative breast cancer: the kiss of death. Oncotarget 8, 46652-46662.
58. Karpozilos, A., Pavlidis, N., 2004. The treatment of cancer in Greek antiquity. Eur J Cancer 40, 2033-2040.
59. Kashyap, D., Garg, V.K., Tuli, H.S., Yerer, M.B., Sak, K., Sharma, A.K., Kumar, M., Aggarwal, V., Sandhu, S.S., 2019. Fisetin and Quercetin: Promising Flavonoids with Chemopreventive Potential. Biomolecules 9, 174.
60. Kawaii, S., Tomono, Y., Katase, E., Ogawa, K., Yano, M., 1999. Antiproliferative activity of flavonoids on several cancer cell lines. Biosci Biotechnol Biochem 63, 896-899.
61. Kim, E.J., Kim, G.T., Kim, B.M., Lim, E.G., Kim, S.Y., Kim, Y.M., 2017. Apoptosis-induced effects of extract from Artemisia annua Linne by modulating PTEN/p53/PDK1/Akt/ signal pathways through PTEN/p53-independent manner in HCT116 colon cancer cells. BMC Complement Altern Med 17, 236.
62. Kim, Y.H., Lee, D.H., Jeong, J.H., Guo, Z.S., Lee, Y.J., 2008. Quercetin augments TRAIL-induced apoptotic death: involvement of the ERK signal transduction pathway. Biochem Pharmacol 75, 1946-1958.

63. Koehn, F.E., Carter, G.T., 2005. The evolving role of natural products in drug discovery. Nat Rev Drug Discov 4, 206-220.
64. Koff, J., Ramachandiran, S., Bernal-Mizrachi, L., 2015. A Time to Kill: Targeting Apoptosis in Cancer. International Journal of Molecular Sciences 16, 2942-2955.
65. Krishnaswamy, K., Sushil K., J., 2000. Oxidative stress and apoptosis. Pathophysiology 7, 153-163.
66. Lang, S.J., Schmiech, M., Hafner, S., Paetz, C., Steinborn, C., Huber, R., Gaafary, M.E., Werner, K., Schmidt, C.Q., Syrovets, T., Simmet, T., 2019. Antitumor activity of an Artemisia annua herbal preparation and identification of active ingredients. Phytomedicine 62, 152962.
67. Lang, S.J., Schmiech, M., Hafner, S., Paetz, C., Werner, K., El Gaafary, M., Schmidt, C.Q., Syrovets, T., Simmet, T., 2020. Chrysosplenol d, a Flavonol from Artemisia annua, Induces ERK1/2-Mediated Apoptosis in Triple Negative Human Breast Cancer Cells. Int J Mol Sci 21, 4090.
68. Lapenna, S., Giordano, A., 2009. Cell cycle kinases as therapeutic targets for cancer. Nat Rev Drug Discov 8, 547-566.
69. Lawen, A., 2003. Apoptosis-an introduction. Bioessays 25, 888-896.
70. Lee, E.R., Kang, Y.J., Kim, J.H., Lee, H.T., Cho, S.G., 2005. Modulation of apoptosis in HaCaT keratinocytes via differential regulation of ERK signaling pathway by flavonoids. J Biol Chem 280, 31498-31507.
71. Lens, S.M.A., Medema, R.H., 2019. Cytokinesis defects and cancer. Nat Rev Cancer 19, 32-45.
72. Liu, L.P., Cao, X.C., Liu, F., Quan, M.F., Sheng, X.F., Ren, K.Q., 2014. Casticin induces breast cancer cell apoptosis by inhibiting the expression of forkhead box protein M1. Oncol Lett 7, 1711-1717.
73. Liu, Y., Levine, B., 2015. Autosis and autophagic cell death: the dark side of autophagy. Cell Death Differ 22, 367-376.
74. Llorens, F., Miro, F.A., Casanas, A., Roher, N., Garcia, L., Plana, M., Gomez, N., Itarte, E., 2004. Unbalanced activation of ERK1/2 and MEK1/2 in apigenin-induced HeLa cell death. Exp Cell Res 299, 15-26.
75. Malumbres, M., Barbacid, M., 2009. Cell cycle, CDKs and cancer: a changing paradigm. Nat Rev Cancer 9, 153-166.
76. Mayer, I.A., Arteaga, C.L., 2016. The PI3K/AKT Pathway as a Target for Cancer Treatment. Annu Rev Med 67, 11-28.
77. Mebratu, Y., Tesfaigzi, Y., 2009. How ERK1/2 activation controls cell proliferation and cell death is subcellular localization the answer? Cell Cycle 8, 1168-1175.
78. Mehta, R.G., Murillo, G., Naithani, R., Peng, X., 2010. Cancer chemoprevention by natural products: how far have we come? Pharm Res 27, 950-961.
79. Michaelsen, F.W., Saeed, M.E., Schwarzkopf, J., Efferth, T., 2015. Activity of Artemisia annua and artemisinin derivatives, in prostate carcinoma. Phytomedicine 22, 1223-1231.

80. Mirzoeva, O.K., Das, D., Heiser, L.M., Bhattacharya, S., Siwak, D., Gendelman, R., Bayani, N., Wang, N.J., Neve, R.M., Guan, Y., Hu, Z., Knight, Z., Feiler, H.S., Gascard, P., Parvin, B., Spellman, P.T., Shokat, K.M., Wyrobek, A.J., Bissell, M.J., McCormick, F., Kuo, W.L., Mills, G.B., Gray, J.W., Korn, W.M., 2009. Basal subtype and MAPK/ERK kinase (MEK)-phosphoinositide 3-kinase feedback signaling determine susceptibility of breast cancer cells to MEK inhibition. Cancer Res 69, 565-572.
81. Moloney, J.N., Cotter, T.G., 2018. ROS signalling in the biology of cancer. Seminars in Cell & Developmental Biology 80, 50-64.
82. Morris, P.G., Fornier, M.N., 2008. Microtubule active agents: beyond the taxane frontier. Clin Cancer Res 14, 7167-7172.
83. Nabeyrat, E., Jones, G.E., Fenwick, P.S., Barnes, P.J., Donnelly, L.E., 2003. Mitogen-activated protein kinases mediate peroxynitriteinduced cell death in human bronchial epithelial cells. American Journal of Physiology-Lung Cellular and Molecular Physiology 284, L1112-L1120.
84. Nakase, I., Gallis, B., Takatani-Nakase, T., Oh, S., Lacoste, E., Singh, N.P., Goodlett, D.R., Tanaka, S., Futaki, S., Lai, H., Sasaki, T., 2009. Transferrin receptor-dependent cytotoxicity of artemisinin-transferrin conjugates on prostate cancer cells and induction of apoptosis. Cancer Lett 274, 290-298.
85. Nowak-Sliwinska, P., Segura, T., Iruela-Arispe, M.L., 2014. The chicken chorioallantoic membrane model in biology, medicine and bioengineering. Angiogenesis 17, 779-804.
86. Okada, H., Mak, T.W., 2004. Pathways of apoptotic and non-apoptotic death in tumour cells. Nat Rev Cancer 4, 592-603.
87. Otto, T., Sicinski, P., 2017. Cell cycle proteins as promising targets in cancer therapy. Nat Rev Cancer 17, 93-115.
88. Ouyang, L., Shi, Z., Zhao, S., Wang, F.T., Zhou, T.T., Liu, B., Bao, J.K., 2012. Programmed cell death pathways in cancer: a review of apoptosis, autophagy and programmed necrosis. Cell Prolif 45, 487-498.
89. Panieri, E., Santoro, M.M., 2016. ROS homeostasis and metabolism: a dangerous liason in cancer cells. Cell Death Dis 7, e2253.
90. Pfeffer, C.M., Singh, A.T.K., 2018. Apoptosis: A Target for Anticancer Therapy. Int J Mol Sci 19, 448.
91. Portugal, J., Mansilla, S., Bataller, M., 2009. Mechanisms of Drug-Induced Mitotic Catastrophe in Cancer Cells. Current Pharmaceutical Design 16, 69-78.
92. Redza-Dutordoir, M., Averill-Bates, D.A., 2016. Activation of apoptosis signalling pathways by reactive oxygen species. Biochim Biophys Acta 1863, 2977-2992.
93. Rhind, N., Russell, P., 2012. Signaling pathways that regulate cell division. Cold Spring Harb Perspect Biol 4, a005942.
94. Riccardi, C., Nicoletti, I., 2006. Analysis of apoptosis by propidium iodide staining and flow cytometry. Nat Protoc 1, 1458-1461.

95. Riffell, J., Zimmerman, C., Khong, A., McHardy, L., Roberge, M., 2009. Effects of chemical manipulation of mitotic arrest and slippage on cancer cell survival and proliferation. Cell Cycle 8, 3029-3042.
96. Rodriguez-Garcia, C., Sanchez-Quesada, C., J, J.G., 2019. Dietary Flavonoids as Cancer Chemopreventive Agents: An Updated Review of Human Studies. Antioxidants 8, 137.
97. S3-Leitlinie-Mammakarzinom, 2018. Leitlinienprogramm Onkologie (Deutsche Krebsgesellschaft, Deutsche Krebshilfe, AWMF): S3-Leitlinie Früherkennung, Diagnose, Therapie und Nachsorge des Mammakarzinoms, Kurzversion 4.1 , 2018, AWMF Registernummer: 032-045OL, http://www.leitlinienprogramm-onkologie.de/leitlinien/mammakarzinom/ , (accessed: 07-03-2019).
98. Sabharwal, S.S., Schumacker, P.T., 2014. Mitochondrial ROS in cancer: initiators, amplifiers or an Achilles' heel? Nat Rev Cancer 14, 709-721.
99. Schmiech, M., Lang, S.J., Werner, K., Rashan, L.J., Syrovets, T., Simmet, T., 2019. Comparative Analysis of Pentacyclic Triterpenic Acid Compositions in Oleogum Resins of Different Boswellia Species and Their In Vitro Cytotoxicity against Treatment-Resistant Human Breast Cancer Cells. Molecules 24, 2153.
100. Schwartz, G.K., Shah, M.A., 2005. Targeting the cell cycle: a new approach to cancer therapy. J Clin Oncol 23, 9408-9421.
101. Shen, B., 2015. A New Golden Age of Natural Products Drug Discovery. Cell 163, 1297-1300.
102. Shen, J.K., Du, H.P., Yang, M., Wang, Y.G., Jin, J., 2009. Casticin induces leukemic cell death through apoptosis and mitotic catastrophe. Ann Hematol 88, 743-752.
103. Siegel, R.L., Miller, K.D., Jemal, A., 2019. Cancer statistics, 2019. CA Cancer J Clin 69, 7-34.
104. Skowron, M.A., Sathe, A., Romano, A., Hoffmann, M.J., Schulz, W.A., van Koeveringe, G.A., Albers, P., Nawroth, R., Niegisch, G., 2017. Applying the chicken embryo chorioallantoic membrane assay to study treatment approaches in urothelial carcinoma. Urol Oncol 35, 544.e511–544.e523.
105. Son, Y., Cheong, Y.K., Kim, N.H., Chung, H.T., Kang, D.G., Pae, H.O., 2011. Mitogen-Activated Protein Kinases and Reactive Oxygen Species: How Can ROS Activate MAPK Pathways? J Signal Transduct 2011, 792639.
106. Sparreboom, A., Cox, M.C., Acharya, M.R., Figg, W.D., 2004. Herbal remedies in the United States: potential adverse interactions with anticancer agents. J Clin Oncol 22, 2489-2503.
107. Srivastava, S., Somasagara, R.R., Hegde, M., Nishana, M., Tadi, S.K., Srivastava, M., Choudhary, B., Raghavan, S.C., 2016. Quercetin, a Natural Flavonoid Interacts with DNA, Arrests Cell Cycle and Causes Tumor Regression by Activating Mitochondrial Pathway of Apoptosis. Sci Rep 6, 24049.
108. Syrovets, T., Gschwend, J.E., Buchele, B., Laumonnier, Y., Zugmaier, W., Genze, F., Simmet, T., 2005. Inhibition of IkappaB kinase activity by acetyl-boswellic acids

promotes apoptosis in androgen-independent PC-3 prostate cancer cells in vitro and in vivo. J Biol Chem 280, 6170-6180.

109. Tang, D., Wu, D., Hirao, A., Lahti, J.M., Liu, L., Mazza, B., Kidd, V.J., Mak, T.W., Ingram, A.J., 2002. ERK activation mediates cell cycle arrest and apoptosis after DNA damage independently of p53. J Biol Chem 277, 12710-12717.
110. Tao, J.J., Visvanathan, K., Wolff, A.C., 2015a. Long term side effects of adjuvant chemotherapy in patients with early breast cancer. Breast 24 Suppl 2, S149-153.
111. Tao, Z., Shi, A., Lu, C., Song, T., Zhang, Z., Zhao, J., 2015b. Breast Cancer: Epidemiology and Etiology. Cell Biochem Biophys 72, 333-338.
112. Taylor, R.C., Cullen, S.P., Martin, S.J., 2008. Apoptosis: controlled demolition at the cellular level. Nat Rev Mol Cell Biol 9, 231-241.
113. Trachootham, D., Alexandre, J., Huang, P., 2009. Targeting cancer cells by ROS-mediated mechanisms: a radical therapeutic approach? Nat Rev Drug Discov 8, 579-591.
114. van der Kooy, F., Sullivan, S.E., 2013. The complexity of medicinal plants: the traditional Artemisia annua formulation, current status and future perspectives. J Ethnopharmacol 150, 1-13.
115. Vitale, I., Galluzzi, L., Castedo, M., Kroemer, G., 2011. Mitotic catastrophe: a mechanism for avoiding genomic instability. Nat Rev Mol Cell Biol 12, 385-392.
116. Vogiatzi, F., Brandt, D.T., Schneikert, J., Fuchs, J., Grikscheit, K., Wanzel, M., Pavlakis, E., Charles, J.P., Timofeev, O., Nist, A., Mernberger, M., Kantelhardt, E.J., Siebolts, U., Bartel, F., Jacob, R., Rath, A., Moll, R., Grosse, R., Stiewe, T., 2016. Mutant p53 promotes tumor progression and metastasis by the endoplasmic reticulum UDPase ENTPD5. Proc Natl Acad Sci USA 113, E8433-E8442.
117. von Lintig, F.C., Dreilinger, A.D., Varki, N.M., Wallace, A.M., Casteel, D.E., Boss, G.R., 2000. Ras activation in human breast cancer. Breast cancer research and treatment 62, 51-62.
118. Woessmann, W., Chen, X., Borkhardt, A., 2002. Ras-mediated activation of ERK by cisplatin induces cell death independently of p53 in osteosarcoma and neuroblastoma cell lines. Cancer Chemother Pharmacol 50, 397-404.
119. Wong, R.S., 2011. Apoptosis in cancer: from pathogenesis to treatment. J Exp Clin Cancer Res 30, 87.
120. Yan, W., Liu, G., Scoumanne, A., Chen, X., 2008. Suppression of inhibitor of differentiation 2, a target of mutant p53, is required for gain-of-function mutations. Cancer Res 68, 6789-6796.
121. Yang, X.-H., Sladek, T.L., Liu, X., Butler, B.R., Froelich, C.J., Thor, A.D., 2001. Reconstitution of Caspase 3 Sensitizes MCF-7 Breast Cancer Cells to Doxorubicin- and Etoposide-induced Apoptosis. Cancer Research 61, 348-354.

Appendix

Validation Data of the Quantification Method of the Major Ingredients contained in Momundo *Artemisia annua* extracts

Table 2: **Validation data of the quantification method of the major ingredients contained in the Momundo *Artemisia annua* extracts.** Regression of calibration curves, limit of detection and limit of quantification, precision and accuracy of the method are shown. Figure adapted with permission from our own publication (supplementary material) (Lang et al., 2019), © 2019 The Authors, under a creative commons license, CC BY-NC-ND 4.0, creativecommons.org/licenses/by-nc-nd/4.0/.

		6.7-Dimethoxycoumarin	Chrysosplenol D	Casticin	Arteannuin B	Arteannuic acid
Regression	linear range [ng/ml]	5000 - 10	5000 - 10	5000 - 10	5000 - 10	5000 - 100
	correlation coefficient	0.9992	0.9999	0.9996	0.9999	0.9994
	LOD[a] [ng/mg]	2.9	1.0	1.0	0.5	15.0
	LOQ[a] [ng/mg]	11.0	3.7	3.8	2.0	58.0
Precision	low level intraday variation (RSD [%])	2.1	9.8	7.5	5.3	3.6
	low level interday variation (RSD [%])	4.4	10.6	8.9	3.9	4.0
	high level intraday variation (RSD [%])	1.1	8.0	4.0	3.5	5.2
	high level interday variation (RSD [%])	5.1	10.4	6.1	4.3	2.6
Accuracy	Recovery mean (± SD) [%]	94.6 (4.9)	103.2 (4.0)	102.2 (1.8)	100.3 (3.7)	98.7 (2.2)

[a] LOD and LOQ with a corresponding sample concentration of 10 mg/ml

List of Figures

List of Tables

Acknowledgements

This work arose at the Institute of Pharmacology of Natural Products and Clinical Pharmacology during the years 2017 till 2019. Completing a doctoral thesis is a real challenge and would not have been possible without the support of numerous people and a great team.

Firstly, I would like to express my sincere gratitude to my supervisor Prof. Dr. Thomas Simmet, former head of the institute, for giving me the opportunity to work on this very interesting and challenging project. I am very grateful for his continuous support of my research, his trust in me and my work, his patience, encouragement, valuable advice and immense knowledge.

Special thanks are given to Prof. Dr. Tatiana Syrovets for her great expertise, supervision, insightful comments and motivation. She supported me and my work with her wide experience all the time and provided expert guidance with experimental and technical problems, writing papers and reports. I am very grateful that I got the opportunity to learn so much from her.

Also, I express my gratitude to the members of the dissertation committee for reviewing my manuscript, constructive comments and challenging questions.

I wish to thank M.Sc. Michael Schmiech for the analytical characterization of the *Artemisia annua* extracts and for his successful guidance with the extract fractionation and isolation of the respective components. Through him I was able to gain a lot of new analytical insights and knowledge. Also, during the last three years I found a good friend in him.

Furthermore, I gratefully want to acknowledge Dr. Susanne Hafner, Felicitas Genze and Eva Winkler for their support and advice with the *in vivo* experiments. At this point I also want to express special thanks to Dr. Susanne Hafner for her support and guidance during my starting time at this institute.

I also want to thank Dr. Christian Paetz from the Max-Planck-Institute in Jena for the excellent collaboration regarding the structure determination by NMR spectroscopy.

Special thanks go to the whole institute and all my colleagues and former members of the institute for constant support, stimulating discussions and for the very nice time we had together. I gratefully want to acknowledge Dr. Menna El Gaafary, Dr. Ann-Kathrin Gaiser and Dr. Monica Rubio Ayala for their support when I was a new member of the institute.

Last but not least I would like to thank my parents, Markus, my sister and all my friends for their support during my whole studies and their confidence in my work.

This work was financed and supported by the Academic Center for Complementary and Integrative Medicine (AZKIM), State Ministry of Baden-Württemberg for Sciences, Research and Arts.

CV

Sophia Lang

Curriculum vitae (CV) has been removed for data privacy protection reasons.